REPORT DOCUMENTATION PAGE

Public Reporting burden for this collection of information is estimated to average 1 hour per response, including the time for reviewing instructions, searching existing data sources, gathering and maintaining the data needed, and completing and reviewing the collection of information. Send comment regarding this burden estimates or any other aspect of this collection of information, including suggestions for reducing this burden, to Washington Headquarters Services, Directorate for information Operations and Reports, 1215 Jefferson Davis Highway, Suite 1204, Arlington, VA 22202-4302, and to the Office of Management and Budget, Paperwork Reduction Project (0704-0188,) Washington, DC 20503.

1. AGENCY USE ONLY (Leave Blank)	2. REPORT DATE 18 July 2007	3. REPORT TYPE AND DATES COVERED Final Report 1 June 2001 – 31 August 2006
4. TITLE AND SUBTITLE Intelligent Luminescence for Communication Display and Identification		5. FUNDING NUMBERS G DAAD19-01-1-0603
6. AUTHOR(S) C. J. Summers, N. Farhat, I. C. Khoo, J. Wager and P. Holloway.		
7. PERFORMING ORGANIZATION NAME(S) AND ADDRESS(ES) Georgia Institute of Technology, School of Material Science & Engineering – 771 Ferst Dr. NW, 30332-0245		8. PERFORMING ORGANIZATION REPORT NUMBER
9. SPONSORING / MONITORING AGENCY NAME(S) AND ADDRESS(ES) U. S. Army Research Office P.O. Box 12211 Research Triangle Park, NC 27709-2211		10. SPONSORING / MONITORING AGENCY REPORT NUMBER 42250.4 - PH-MUR
11. SUPPLEMENTARY NOTES The views, opinions and/or findings contained in this report are those of the author(s) and should not be construed as an official Department of the Army position, policy or decision, unless so designated by other documentation.		
12 a. DISTRIBUTION / AVAILABILITY STATEMENT Approved for public release: distribution unlimited.		12 b. DISTRIBUTION CODE

13. ABSTRACT (Maximum 200 words)

MURI Final Report Abstract

A highly integrated, cross-disciplinary research program was conducted to establish the scientific and technological basis for intelligent luminescent materials, devices and systems. Novel luminescent and optical systems were researched to realize a new intelligence modeling methodology: corticonics. Specific achievements include low threshold organic quantum dot emitters, luminescence modification by 3D photonic crystals, beam steering based on a superlattice photonic crystal, optimization of liquid crystal properties, development of optically transparent n- and p-type wide band gap materials and transparent transistors for display applications. It was demonstrated that emissive and active infiltrated photonic crystals, highly transparent conductive materials and nano-structured materials offer the potential for initiating many new device functions. For example, low-threshold tunable sources and detectors, optically and electronically controlled optical switching, beam steering, and bi-stable elements for logic and threshold computing decisions. Also new family of highly nonlinear liquid crystals that exhibit, bi-stability, self-oscillations and bifurcation were identified as a promising class of materials for implementing and testing the corticonic paradigm. A novel, transparent, thin-film enhancement-mode transistor was reported with ~ 90% visible transparency and an on/off ratio of 10^6 for integration into display and identification systems.

14. SUBJECT TERMS	15. NUMBER OF PAGES
Luminescence Dynamical Pattern Recognition: Corticonics Nonlinear & Photosensitive Nematic Liquid Crystals Active and Emissive Photonic Crystals Transparent Electronic/Opto-electronic Materials Electroluminescence Nanoparticles	
	16. PRICE CODE

17. SECURITY CLASSIFICATION OR REPORT	18. SECURITY CLASSIFICATION ON THIS PAGE	19. SECURITY CLASSIFICATION OF ABSTRACT	20. LIMITATION OF ABSTRACT
UNCLASSIFIED	**UNCLASSIFIED**	**UNCLASSIFIED**	**UL**

GENERAL INSTRUCTIONS FOR COMPLETING SF 298

The Report Documentation Page (RDP) is used for announcing and cataloging reports. It is important that this information be consistent with the rest of the report, particularly the cover and title page. Instructions for filling in each block of the form follow. It is important to **stay within the lines** to meet *optical scanning requirements.*

Block 1. Agency Use Only (Leave blank)

Block 2. Report Date. Full publication date including day, month, and year, if available (e.g. 1 Jan 88). Must cite at least year.

Block 3. Type of Report and Dates Covered. State whether report is interim, final, etc. If applicable enter inclusive report dates (e.g. 10 Jun 87 - 30 Jun 88).

Block 4. Title and Subtitle. A title is taken from the part of the report that provides the most meaningful and complete information. When a report is prepared in more than one volume, repeat the primary title, and volume number, and include subtitle for the specific volume. On classified documents enter the title classification in parentheses.

Block 5. Funding Numbers. To include contract and grant numbers; may include program element number(s) project number(s), task number(s), and work unit number(s). Use the following labels:

C -	Contract	PR -	Project
G -	Grant	TA -	Task
PE -	Program Element	WU -	Work Unit Accession No.

Block 6. Author(s). Name(s) of person(s) responsible for writing the report, performing the research, or credited with the content of the report. If editor or compiler, this should follow the name(s).

Block 7. Performing Organization Name(s) and Address(es). Self-explanatory.

Block 8. Performing Organization Report Number. Enter the unique alphanumeric report number(s) assigned by the organization performing the report.

Block 9. Sponsoring/Monitoring Agency Name(s) and Address(es) Self-explanatory.

Block 10. Sponsoring/Monitoring Agency Report Number. (*if known*)

Block 11. Supplementary Notes. Enter information not included elsewhere such as; prepared in cooperation with....; Trans. of...; To be published in.... When a report is revised, include a statement whether the new report supersedes or supplements the older report.

Block 12a. Distribution/Availability Statement. Denotes public availability or limitations. Cite any availability to the public. Enter additional limitations or special markings in all capitals (e.g. NORFORN, REL, ITAR).

DOD	-	See DoDD 4230.25, "Distribution Statements on Technical Documents."
DOE	-	See authorities.
NASA	-	See Handbook NHB 2200.2.
NTIS	-	Leave blank.

Block 12b. Distribution Code.

DOD	-	Leave Blank
DOE	-	Enter DOE distribution categories from the Standard Distribution for unclassified Scientific and Technical Reports
NASA	-	Leave Blank.
NTIS	-	Leave Blank.

Block 13. Abstract. Include a brief (*Maximum 200 words*) factual summary of the most significant information contained in the report.

Block 14. Subject Terms. Keywords or phrases identifying major subject in the report.

Block 15. Number of Pages. Enter the total number of pages.

Block 16. Price Code. Enter appropriate price code (NTIS *only*).

Block 17. - 19. Security Classifications. Self-explanatory. Enter U.S. Security Regulations (i.e., UNCLASSIFIED). If form contains classified information, stamp classification on the top and bottom of the page.

Block 20. Limitation of Abstract. This block must be completed to assign a limitation to the abstract. Enter either UL (Unlimited) or SAR (same as report). An entry in this block is necessary if the abstract is to be limited. If blank, the abstract is assumed to be unlimited.

MEMORANDUM OF TRANSMITTAL

U.S. Army Research Office
ATTN: AMSRL-RO-BI (TR)
P.O. Box 12211
Research Triangle Park, NC 27709-2211

☐ Reprint (Orig + 2 copies)   ☐ Technical Report (Orig + 2 copies)

☐ Manuscript (1 copy)   X Final Progress Report (Orig + 2 copies)

                                     ☐ Related Materials, Abstracts, Theses (1 copy)

CONTRACT/GRANT NUMBER: G DAAD19-01-1-0603

REPORT TITLE: Intelligent Luminescence for Communication, Display and Identification

is forwarded for your information.

SUBMITTED FOR PUBLICATION TO (applicable only if report is manuscript):

                         Sincerely,

                                Christopher J. Summers

MURI FINAL REPORT

Multi-University Research Initiative

Intelligent Luminescence for Communication, Display and Identification

Final Report
June 1, 2001 - August 31, 2006

Prepared for:

Dr. Rich Hammond
US Army Research Office

Department of The Army
U.S. Army Robert Morris Acquisition Center
Research Triangle Park Contracting Division
P. O. Box 12211
Research Triangle Park
NC 27709-2211

Grant Number: DAAD19-01-1-0603(ARO)

Prepared by:

Christopher J. Summers, Ph.D.

School of Materials Science and Engineering
Georgia Institute of Technology
Atlanta, GA 30332-0245

Table of Contents

1. FOREWORD

This report briefly reviews the many activities, accomplishments and publications of the MURI program on "Intelligent Luminescence for Communication, Display and Identification". The team members and affiliations were:

- **Professor Christopher J. Summers, Georgia Institute of Technology**

- **Professor I. C. Khoo, Pennsylvania State University**

- **Professor Paul H. Holloway, University of Florida**

- **Professor John F. Wager, Oregon State University**

- **Professor Nabil H. Farhat, University of Pennsylvania.**

The goal of this MURI team was to discover intelligent luminescent materials and devices that can perform innovative methods of data assessment, communication, identification/recognition and display. As implied by the title, this MURI program has the following directions: development of new Opto-Electronic and optical materials and devices for on-chip and pixel-to-pixel communication, the ability of these devices to act as display devices with memory, and to accomplish local data processing with potential to impact situations such as those calling for camouflage or identification of threats.

For more information, contact: **Professor Christopher J. Summers**

404/385-0697
chris.summers@mse.gatech.edu

1

2. EXECUTIVE SUMMARY

This report summarizes the progress made during the MURI program "Intelligent Luminescence for Communication, Display and Identification". The contributing program team members were: the Georgia Institute of Technology, Oregon State University, University of Florida, Pennsylvania State University and The University of Pennsylvania. The principal program objectives were to discover intelligent luminescent materials and devices to perform innovative methods of data assessment, communication, identification/recognition and display. Specifically, this included the development of new optoelectronic and optical materials and devices for on-chip and pixel-to-pixel communication: the ability of these devices to act as display devices with memory, and to accomplish local data processing with the potential to impact situations such as those calling for camouflage or identification of threats.

To guide the research in intelligent processing, a corticonic model that emulates many of the features of the brain was developed. This formulation was demonstrated to be very robust in reproducibly identifying common features that can be buried within complex scenes. By identifying the computation mechanisms, practical routes to testing these algorithms, both electrically and optically, were devised. From these analyses it becomes apparent that although many background functions can be added to a pixel to improve its processing capability, to produce, or enable "intelligence", requires a series of feedback mechanisms between pixels, as schematically shown in Figure 1. Thus, strong feedback and interplay between neighboring and next neighbor pixels within a pixel array is required to establish an intelligent platform. Additionally, it is required that an individual pixel only output data and communicate when excited above a threshold signal that is generally determined by a summed input. The output from each pixel (actuator) thus depends not only on the stimulus it receives directly, but also on the sum of weighted signals from its nearest neighbors. The method of extracting invariant features has been shown to be of critical importance and is greatly improved by random frequency firing that depends on the detail of the signal levels in neighboring pixels. This "randomization" emulates the method used by biological systems in which both short and very long-range feedback mechanisms are used to establish the running trigger level. To reduce the complexity of the simulations, edge detecting algorithms were also developed. These studies complemented the more complete analysis and both were used to define the range of device and material functionalities that are required to implement these concepts. A test–bed electro-optical implementation was demonstrated at the end of the program.

A full consideration of these concepts shows that to enable the fast and efficient computation of the corticonic algorithms it is essential to develop optical devices with new functionalities. In this program, specific optical and optoelectronic material and device functionalities that would provide different avenues for these goals to be reached were defined. For example; extremely intense, zero threshold emitters are necessary to perform optical signal processing at low energies, as well as, devices for optical signal (beam) steering and combining, and for efficient out-coupling from a slab waveguide. Optical signal processing also require threshold and on/off switches that can produce nonlinear functions, such as bistablity and hysteresis. Finally, to implement these functions and address the desire to embed such technologies into display applications requires a supportive electro-optic and conductive transparent materials technology.

As seen from Figure 1, the ability to freely steer light within a plane makes it possible to spatially address different pixels within a chip and to combine beams. Additionally, being able to

out-couple this radiation is important for providing a trigger signal to another circuit component and possibly for providing a display characteristic. For optical computing it is also necessary to switch light and to perform bistable operations, i.e. the ability for a transient signal to switch a device from one state to another, without the need for a continuing "hold" pulse: thus providing an additional freedom of action in signal processing.
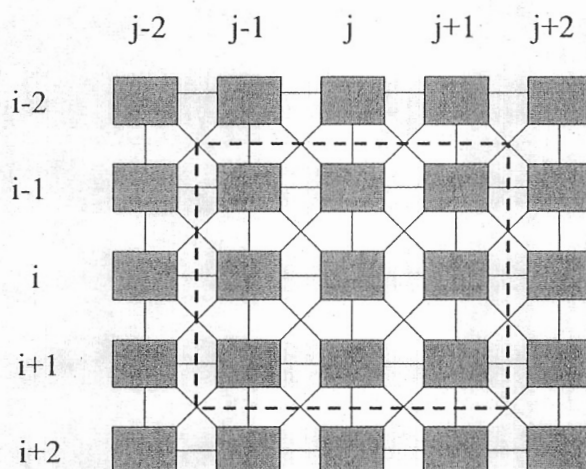

Figure 1. Concept for an intelligent pixel array. Pixel [i, j], is strongly connected to its nearest neighbors, shown within the dotted box, that are in turn connected to their nearest neighbors in the same way. For each connection the signals are weighted by different amounts.

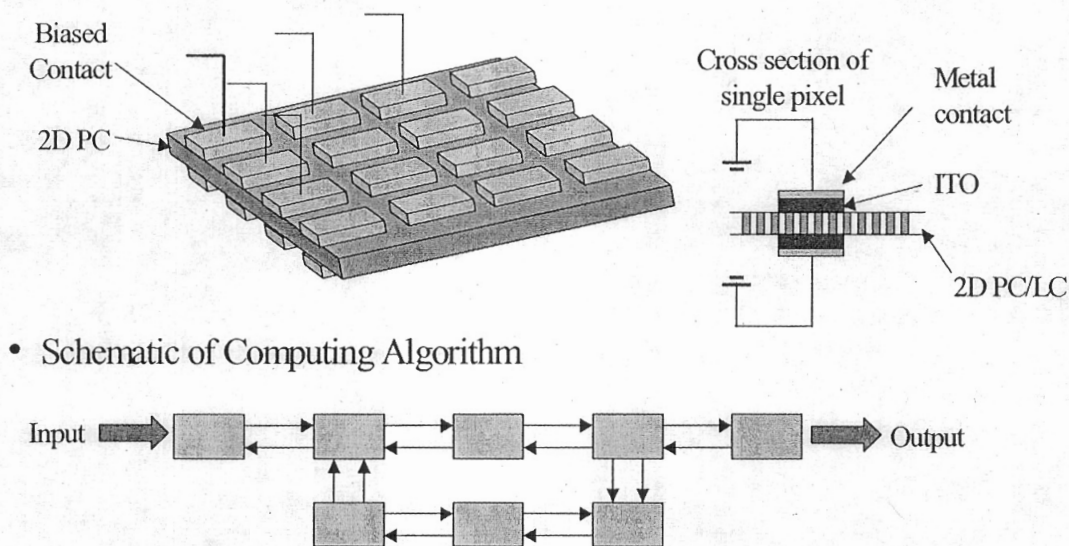- Schematic of Computing Algorithm

Figure 2. 2D photonic crystal electro-optic array showing a proposed optical circuit scheme in which light can be steered from one element to another and thus folded back on itself and in which light can be generated or down- or, up-converted in frequency. Insert demonstrates the ability to bias individual elements, so as to modulate, generate and detect light.

3

In all cases, these device specifications defined a need to demonstrate new materials properties. For example, to develop sources with low threshold properties and tunable characteristics research activities were focused on the development of conjugated polymers for low voltage electroluminescence; nanocrystalline phosphors, and microcavity photonic crystals. Additionally, theoretical models were developed to predict the optical properties (absorption and emission) of these materials, and to guide the development of composite and periodic structures. Also, it should be noted that the work on developing low threshold emitters and very efficient luminescent materials directly impacts devices for camouflage and displays, and that the beam steering devices will enable a simple alarm or friend/foe identification scheme to be realized. To perform the addressing scheme envisaged in Figure 1, a crucial need was the development of highly transparent and conductive n- and p-type doped materials to enable detector and source elements to be integrated with an optical structure and allow electrical and optical functions to be performed in the same material, or a material architecture. In this respect the use of these materials in a photonic crystal offers a way to perform both electrical and optical 3D localization for novel devices. Thus, a very important accomplishment was the invention and demonstration of highly transparent (75% transmission) n-channel accumulation mode thin film transistors and p-type doping techniques for wide band gap materials, such as, ZnO and K-doped BaCuSF. These developments have produced optically transparent bipolar transistor devices that can have a significant technological impact by enabling advanced display functions and new schemes for identification.

Mid-way through the program at the request of the Advisory Board several projects with high potential were down selected for continued study and development. In the first project it was decided to fully explore the potential of optical-electrical, or optical-optical tuning of opal properties such as reflectivity, transmission and potentially luminescence. This study was based on the advances made in designing and fabricating new opal structures, such as the non-close packed geometry, whose open structure enables considerable design flexibility; coupled with the optimization of liquid crystal properties and processes achieved at Penn State University. This GIT – PSU interaction was very successful in achieving dynamical tuning of the opal reflectance as outlined in this report and described in various papers.

The second activity was to investigate the potential of dynamically tuning the free propagation properties of light in both photonic crystal slabs and slab waveguides. This work was centered on a new superlattice photonic crystal geometry that was theoretically shown to exhibit giant refraction, dispersion and a very significant degree of tuning, when nonlinear elements (liquid crystal) can be incorporated into the holes of the structures, or if the structure is made from a nonlinear or electro-optical material. To practically demonstrate this concept waveguide structures were designed and fabricated at Georgia Tech and the University of Florida. These studies involve a GIT – UF – UPenn interaction – and a good start was made in demonstrating the potential of this approach to beam steering. In a related activity, a virtual wave guiding scheme for routing optical beam in a circuit was investigated and experimentally demonstrated.

The third project was to demonstrate the efficient computation of the Opto-electronic Nonlinear Coupling Coefficient that is central to the Corticonic Model, developed at University of Pennsylvania. Despite the fact that this algorithm requires a very complex circuit, circuit elements were isolated that could be used to demonstrate a viable pathway to performing the complete calculation on a chip. The main activity of this program was shared between the

University of Florida and the University of Pennsylvania. A electrical circuit design was also completed and submitted to the DARPA fab line.

The fourth activity was to continue to demonstrate and expand the family of inorganic materials that can be used as Transparent Transistors and to integrate this work into the electro-optical sources being developed at the University of Florida and Pennsylvania State University. This work was based on the pioneering studies and advances made at the Oregon State University, which attracted considerable industrial interest and support. This activity was coordinated between OSU – UF – PSU.

The final activity was for Oregon State University to demonstrate with an industrial partner the application of their Transparent Transistor technology in a display demonstration, and this activity was on going at the end of the program.

In summary, this program has invented/discovered a wide variety of novel materials, material structures and device designs that offer new approaches to achieve the optical signal processing and the display goals of the program so as enable the development of "intelligent" optical processing systems. The highlights covered in this summary are more fully covered in the individual PI campus reports that follow and in the many papers that have been accepted for publication. Information has also been disseminated to the DoD scientific community in many reviews and presentations.

Some important program highlights are:

156   **Publications in peer reviewed journals**

82   **Invited Conference presentation**

65   **Contributed conference publications**

14   **Invention-disclosures and patents**

55   **Ph. Ds granted and fully supported**

2   **MS degrees granted**

4   **Post Doctoral Fellows Supported**

3. SCIENTIC AND TECHNOLOGY REPORTS

The following reports briefly review the many activities, accomplishments and publications of the MURI program on "Intelligent Luminescence for Communication, Display and Identification". The open literature and patent literature describes in detail the specifics of each activity. The team members and affiliations were:

- **Professor Christopher J. Summers, Georgia Institute of Technology**

- **Professor I. C. Khoo, Pennsylvania State University**

- **Professor Paul H. Holloway, University of Florida**

- **Professor John F. Wager, Oregon State University**

- **Professor Nabil H. Farhat, University of Pennsylvania.**

For more information please contact: **Professor Christopher J. Summers**

404/385-0697

chris.summers@mse.gatech.edu

MURI Intelligent Luminescence for Communication, Display, and Identification
Active and Emissive 2D and 3D Photonic Crystal Structures
C. J. Summers
Georgia Institute of Technology
Atlanta, Georgia 30332-0245
31 August 2006

1. Introduction

During this program our activities were concentrated into two areas:

1) The optimization of 3D photonic crystal (PC) structures to realize enhanced and controllable luminescent characteristics, (currently based on the opal fcc lattice because of its simplicity), and

2) The development of new 2D PC designs for controlling the flow of light on a chip.

Photonic crystals have the ability to control light not only by use of their photonic band gap (PBG) property, but also by the unique dispersion properties that they display outside of the forbidden, or restricted propagation region. The above two projects exploit the first and second properties, respectively. The goal of the first project was to develop intelligent sources "photonic crystal phosphors" that will have very narrow line widths, high luminosity and potentially, tunability. The concept is based on the dielectric doping of a PC to create a luminescent defect state within the band gap. Spectral tunability can then be realized by the infiltration of liquid crystals into the structure and appropriate biasing. In the second project, several new 2D PC structures were developed that can enhance beam collimation and enable beam steering between pixels on a chip. These structures are based on fine-tuning the dispersion surfaces in a PC and the modifications that results when optically active materials, such as liquid crystals and electro-optic materials, are incorporated into the structure; or alternately, the slab waveguide is fabricated from an electro-optic or optically active material. Specific details of both investigations are given below. In both projects, strong interactions were maintained with Professor Khoo at Pennsylvania State University and Professor Holloway at the University of Florida.

This program produced 42 peer reviewed papers, 10 conference papers, 4 invention disclosures, 25 invited presentation, 30 contributed presentations, and 19 Conference/Session Chairs. Most importantly 7 Ph. D students and 1 MS student were graduated (2 minorities) and 2 Post Doctoral Fellows supported. Of these researchers 7 currently have academic appointments and 2 are in industry.

2. Luminescent and Tunable 3D Photonic Crystal Structures
2.1 Overview

In a PC the width of the photonic band gap is strongly dependent on both the refractive index contrast that can be obtained between the high and low dielectric regions of the PC, and the actual structure and geometry of the PC lattice. Also the placement of the dielectric material in the structure is very important, and for obtaining both luminescent and tunable properties, the integration of different classes of materials are crucial. Very large band gaps can be obtained in diamond-like lattices, and methods to form these are being developed. However, our major

emphasis was on developing simpler structures that can be manufactured by a "bottom-up" self-assembly approach. Thus, the focus of our current work is on the development of dielectric placement techniques by atomic layer deposition using derivatives of the basic opal technology as the template. The specific steps involved were the development of structures with a wide photonic band gap that also exhibit luminescent behavior, the incorporation of a "defect doping" technology into these structures and then the extension of these concepts to other lattice structures. These techniques can then be extended to other lattice geometries at the appropriate time.

The proposed PC phosphor requires a large photonic crystal band gap, and so we have theoretically modeled and developed experimental methods whereby we can realize the fullest potential of opal based structures. The theoretical work enabled us to fully understand the effects that limit the PBG formation in the inverse opal structure and to design improved structures. Thus we have demonstrated:

1. Non-close packed opals that can increase the PBGs by a factor of two, up to 11% of the average gap wavelength.
2. That the relatively simple opal structure can be significantly enhanced by non-close packed geometries in which the air volume is reduced by collapsing the interlocking network of spheres and the structure becomes a collection of dumb-bell connections.
3. Multi-layered depositions for tunability and luminescent modification.
4. A sacrificial layer technique that enables the basis of a lattice to be significantly altered, so as to considerable enhance the optical properties of the lattice. This technique also allows the precise fabrication of non-close packed inverse opals and, when combined with the multilayered growth of high refractive index and luminescent materials, to obtain novel structures.
5. The backing filling of inverse opals to add measured thicknesses of dielectric material to the structure to statically tune the Bragg peak position and to enhance the width of the photonic band gap.
6. Tunable devices by the incorporation of liquid crystals into large pore inverse opals.
7. That the low temperature deposition capabilities of atomic layer deposition can be used to deposit titania on polystyrene opal templates and photo-lithographically developed structures in SU-8. This latter technique enables the design, and fabrication a wide range of complex 3D structures.

2.2 Results

As is well documented in many papers the optical properties of a photonic crystal depends on lattice structure, the basis geometry and the dielectric contrast. For example, theoretical studies show that full PBGs can be formed in dielectric diamond lattices for a dielectric contrast greater than 2.0, whereas higher symmetry lattices, such as the FCC require a dielectric contrast of 3.3. At the beginning of this program there were few ways to form 3D lattice networks, and so synthetically formed opals were used as a template. Furthermore, a key development of the study on 3D photonic crystals was not only the adoption of inverse opal structures as a viable test bed for technique development, but the realization and subsequent demonstration that atomic layer deposition could be used to conformally infiltrate these highly porous structures. Following deposition, the removal of the original template by etching leads to both the physical and dielectric inversion of the structure. The structural – optical property relationships of these structures was first demonstrated by the ALD deposition of ZnS:Mn (with

support from the Army Research Laboratories) and the correlation of the lattice constant of the structure (sphere size) with the Bragg peak position. Additionally, the observation of photoluminescence from these same structures demonstrated further functionality.

Later using low-temperature ALD to conformally deposit TiO_2, excellent agreement was found between structural properties and the Bragg peak reflection position for the original silica opal, the silica opal infiltrated with TiO_2 up to the maximum conformal filling faction of 86%, and the inverse TiO_2 opal after the silica template had been etched out: as shown sequentially in Figure 1. An extension of this technique to multilayer depositions of $TiO_2/ZnS:Mn/TiO_2$ led to the observation of photoluminescence modification as the dielectric constant and Bragg peak position, or PPBG was tuned into and off the emission wavelength of Mn, by the sequential deposition of TiO_2 in one nm steps. An example of these developments is given in Figure 2, which demonstrates the control that can be achieved over luminescence.
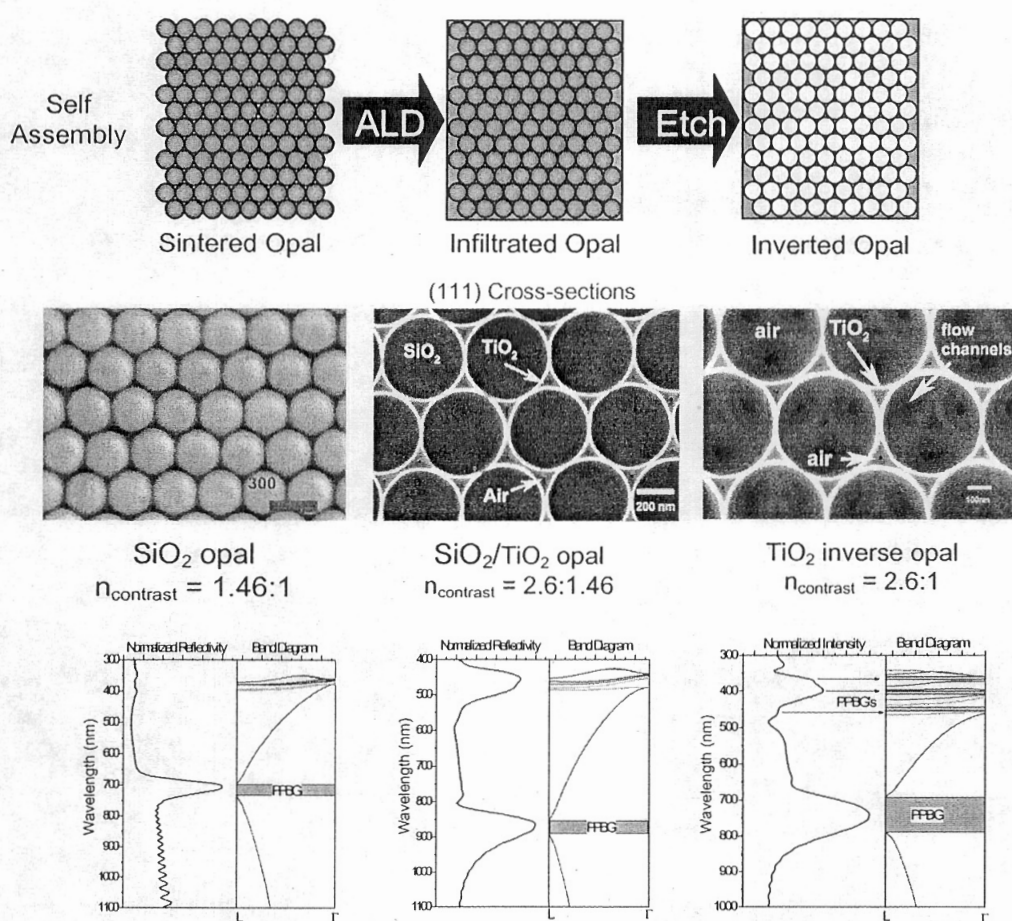

Figure 1. Inverse shell opal fabrication by: opal self-assembly; low-temperature ALD of TiO_2, selective etching to remove opal template. Corresponding SEM images and reflectance spectra are shown for each step. The shifts of the pseudo photonic bands indicates ~95% infiltration.
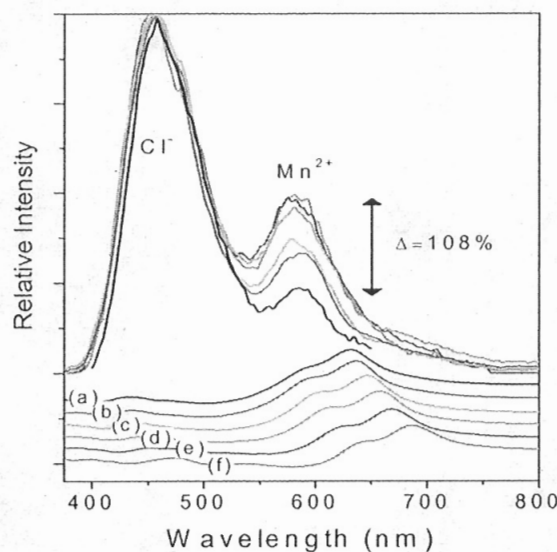
Figure 2. Photoluminescence (upper curves) compared with specular reflectivity (lower curves) as measured for (a, black) TiO_2 (14 nm)/ ZnS:Mn (20 nm)/air 433 nm inverse opal and after backfilling with (b, red) 1 (c, orange) 2, (d, green) 3, (e, blue) 4, and (f, magenta) 5 nm of TiO_2.

A further and very important development in the study on inverse opals was the invention of the sacrificial layer technique. In this method a two layer deposition technique was used to adjust the basis of the structure, such as to achieve large pore opals. This led to backfilling (a conformal coating of the inside of the opal structure) and the discovery that backfill could lead to dramatic adjustments in optical properties, a static tuning of the Bragg peak and an increase in the pseudo-directional photonic band gap along the (111) direction. The sequence of these steps and their impact is shown in Figures 3 and 4. These experimental studies were complemented by comprehensive modeling studies with the purpose to define the most optimum opal based structures for enhancing the magnitude of the photonic band gap and also to assess their potential for dynamic tuning by the incorporation of liquid crystal. The modeling studies of inverse opals led to the development of large pore opals whose extremely fine skeleton features (< 5% volume) provide excellent templates for spectral tuning structures as well as for structure replication and transformation into high index refraction materials or optically active electro-optical and luminescent materials.
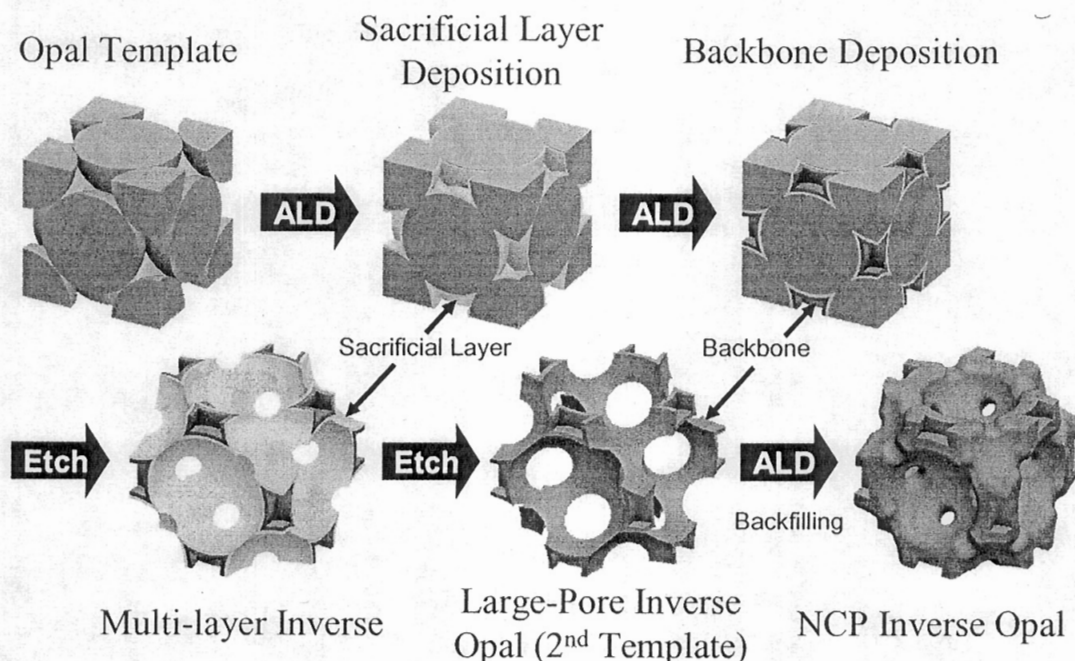
4

Figure 3. Fabrication schemes using ALD. From top left: unit cell of opal, deposition of sacrificial layer, deposition of backbone dielectric layer, removal of opal template to form multi-layer inverse opal, etching of sacrificial layer to form large pore inverse opal, backfilling of structure to form non-close packed inverse opal.
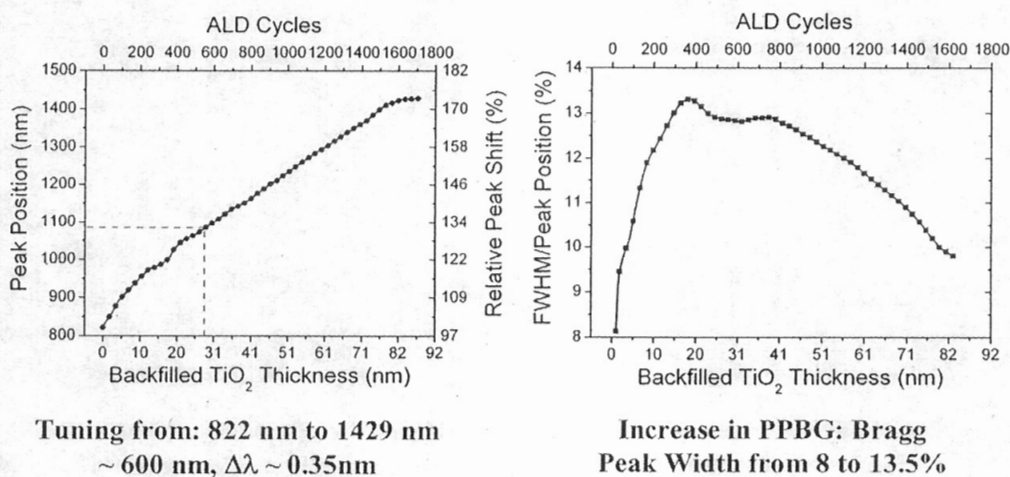

Tuning from: 822 nm to 1429 nm
~ 600 nm, Δλ ~ 0.35nm

Increase in PPBG: Bragg
Peak Width from 8 to 13.5%

Figure 4. Bragg peak position and width as a function of backfill thickness and number of ALD cycles for conformal deposition of TiO$_2$. Red line indicates the limited tuning range obtained with a simple inverse opal structure.

Figures 5 and 6 show simulations of the dynamic tuning predicted for LC infiltrated inverse opals upon the application of an applied electric field. This study shows that high dielectric constant templates provide the greatest tuning range and widest PBG because they allow the PBG to be sustained for a wider excursion in the magnitude of refractive index of the

LC infiltrated into the structure. Experimental studies of these structures are in excellent agreement with predictions and the properties of the LC used in these studies. The simulations for notch filters predict that the application of LCs exhibiting higher birefringence ($\Delta n = 0.6$) have the potential to produce a tuning range >300 nm in the visible. In a new development, the incorporation of dual frequency LC has produced both positive and negative shifts in frequency, which has been experimentally verified.
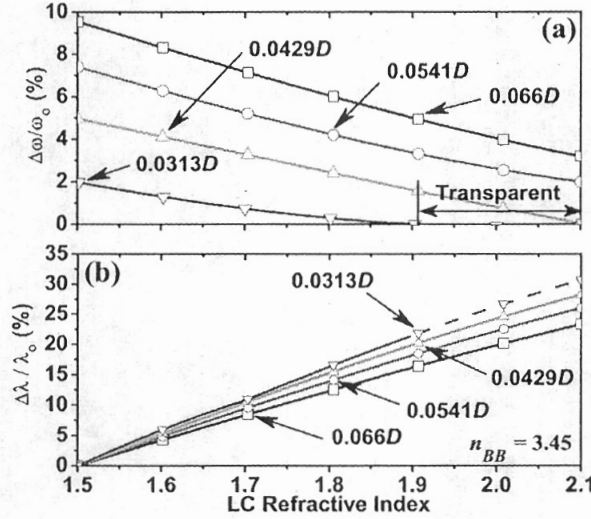
Figure 5. Bragg peak response of tuned silicon/gallium phosphide large-pore inverse opals (n_{BB} = 3.45) for backbone thickness, t_{BB} between 0.066D and 0.0313D, where D is sphere diameter. (a) Dependence of Bragg peak width on LC refractive index. (b) Dependence of the relative tuning ratio. For a backbone thickness $t_{BB}/D < 0.0429$, the structure becomes transparent for a range of LC index values, as indicated for example with $t_{BB}/D = 0.0313$ and LC index values ranging between ~ 1.9 and 2.1.
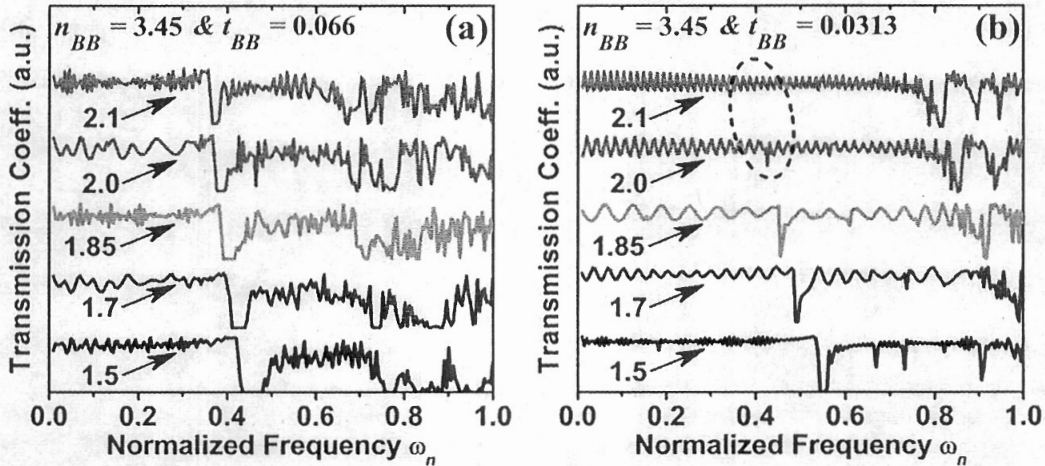

Figure 6. Transmission spectra of tuned silicon/gallium phosphide large-pore inverse opals (n_{BB} = 3.45) for LC refractive index values between 1.5 and 2.1. The spectra have been vertically translated for clarity. (a) Large-pore structure with a backbone thickness of 0.066D. (b) Large-pore structure with a backbone thickness of 0.0313D. The dashed circle indicates structures for which the Bragg peak has collapsed.

Following the successful development of these new techniques and because of the limited control that opals provide over lattice geometry, studies were performed on holographically derived structures formed in SU8 by a four-laser beam interference pattern. As shown in Figure 7 a SU8 polymer template (provided by the Turberfield group at Oxford University) was successfully coated and inverted and shown to exhibited model optical properties. The high fidelity of these structures dramatically demonstrated the versatility of the ALD technique and its capability to produce structures with extremely high finesse.
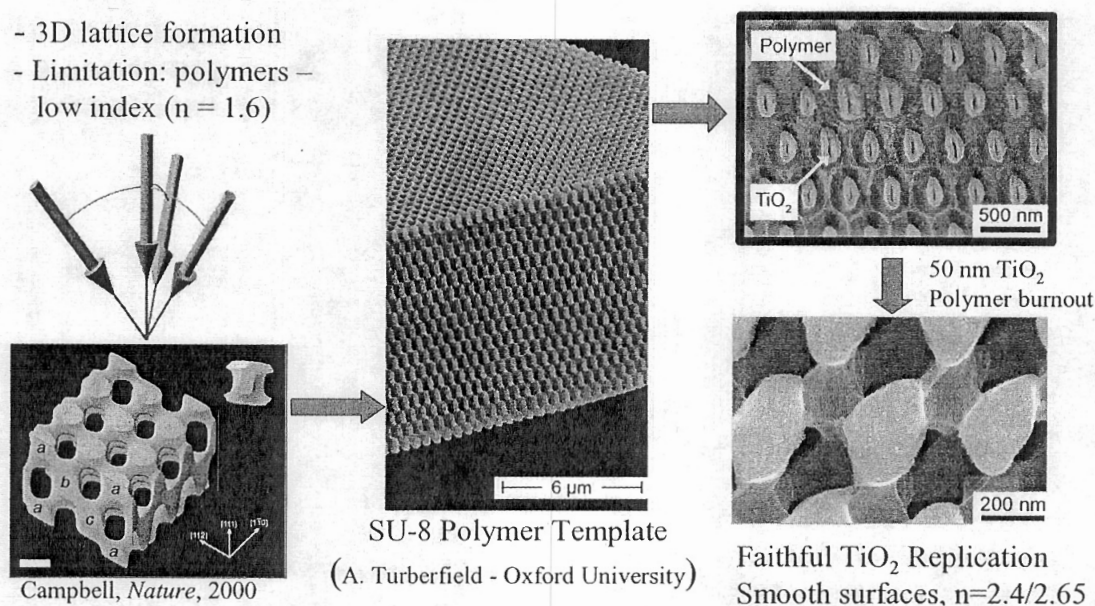

Figure 7. Demonstration of conversion of polymer structures by ALD: Formation of the physical template, infiltration with TiO_2 and inversion after the removal of the SU8.

The success of these structures led to the realization that ALD can be an important fabrication tool for nano-structures and a number of scenarios were envisaged. For example the role of ALD coupled with complementary etching processes can be used to invert, replicate and modify 3D nano structures. Figure 8 shows the potential of ALD to form inverted structures from a given template, to form precise topographical replicas of a structure by a double deposition process, and to perform these functions with a range of different material compositions, multilayers, or range of material structures. Thus, a low index structure can be replicated in a higher index material. Additionally, this process enables temperature-sensitive polymer structures to be inverted by low temperature ALD into a material that then serves as a high temperature template (double templating). An important consequence of this flexibility is that ALD enables a wide range of structures to be inverted, from opals to biological structures, and to be made from a range of different materials – including multilayered materials or a combination of materials so as to optimize the structure to achieve a higher level of functionality. In order to support this technology it is necessary to have a range of complementary etching protocols that enable the selective removal of one material with respect to another. These can range from conventional wet chemical solution etches, dissolving solutions and reactive gas plasma etching. For example, for the titania infiltration of silica opals it is possible to remove the silica by a HF etch, but only if the TiO_2 has been transformed from the amorphous state to either the anatase or

rutile phases by a mild anneal. Thus, we believe that the coupling of ALD to new techniques to form nanoscale lattices promises to contribute to the realization of true 3D PCs with large and tunable photonic band gaps.
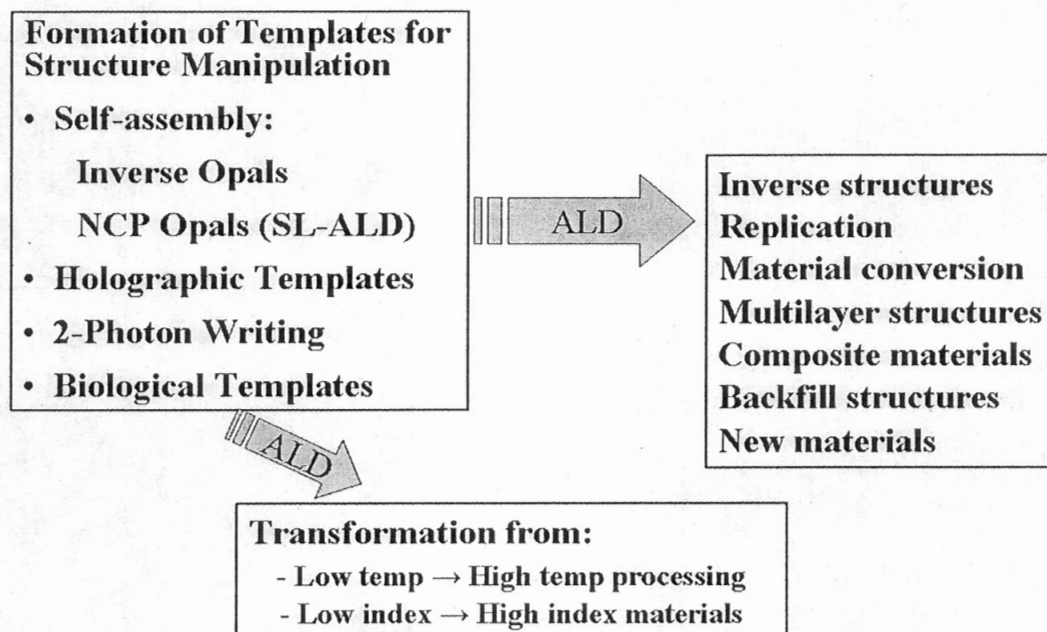
Formation of Templates for Structure Manipulation

- **Self-assembly:**

  Inverse Opals

  NCP Opals (SL-ALD)

- **Holographic Templates**
- **2-Photon Writing**
- **Biological Templates**

ALD →

Inverse structures
Replication
Material conversion
Multilayer structures
Composite materials
Backfill structures
New materials

ALD ↘

Transformation from:
- **Low temp → High temp processing**
- **Low index → High index materials**

Figure 8. Photonic Crystal Fabrication Strategies by Atomic Layer Deposition: Examples of how templates formed by a variety of technologies can be manipulated by atomic layer deposition.

In another study we have we achieved the ALD of GaP, a high index (n = 3.35) optoelectronic material and have infiltrated and inverted conventional opals structures. As shown in Figure 9 the inverse GaP opal showed a well formed directional band gap corresponding to the (111) direction and strong evidence of a full photonic band gap at higher energies of 1.72 eV, corresponding to a wavelength of 726 nm. This wavelength lies just within the red part of the spectrum and is one of very few reports of a photonic band gap in the visible.

Finally we have recently applied the ALD technique to modify the photonic band structure of 2D PCs. The resulting composite/multilayer waveguide structures demonstrate that the ALD-technique provides a method to precisely control and as well as to obtain unique band structure properties, as discussed in the following section.
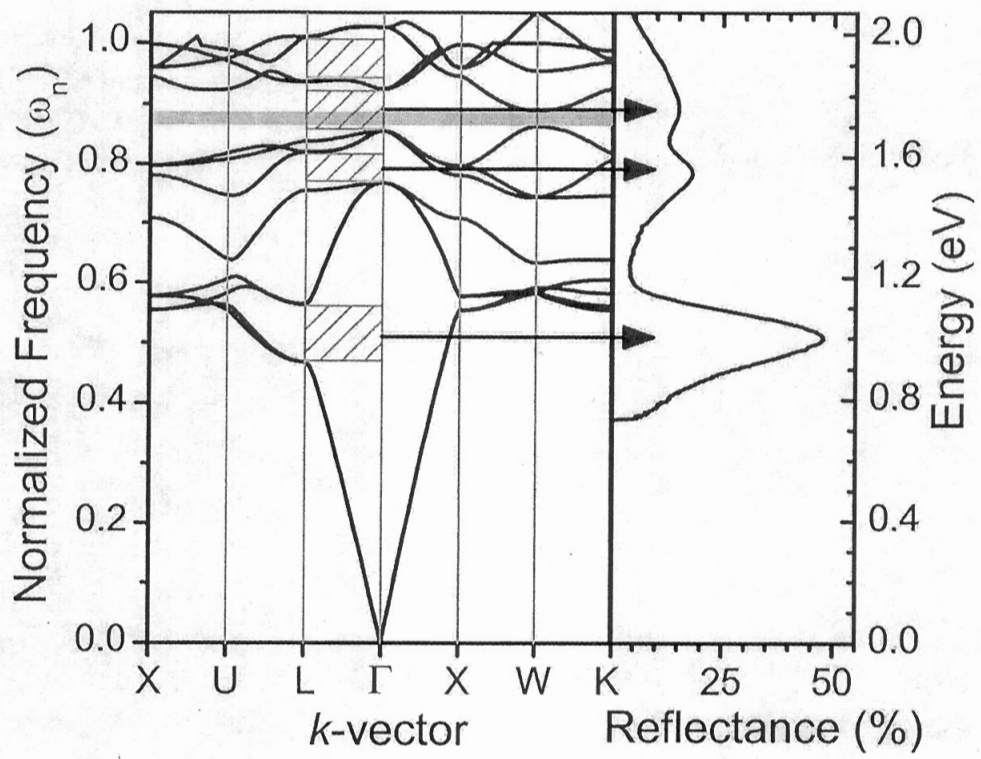
Figure 9. Correspondence between photonic band structure and reflectance spectra for a GaP inverse opal.

3. Two-Dimensional Photonic Crystals for Controlling the Flow of Light on a Chip

In this program thrust new material and device structures were developed for dynamically steering, dispersing, guiding, collimating, focusing and switching light propagating within, or across a chip. These devices include the superlattice photonic crystal structure, a "virtual waveguide" to improve beam collimation (also now called the super-collimation effect), negative index lens and Fabry-Perot resonator structures for bi-stability. Initially, to implement these designs a 2D laser photolithography tool was developed. However, the timely acquisition and commissioning of an electron beam tool in the Georgia Tech Microelectronics Facility during the last year of this program enabled these structures to be laid out by e-beam. New etching protocols were developed and an example of a typical fabrication run is shown later in Figure 11. At the end of the program we also demonstrated the effectiveness of ALD to modify the photonic band structure of 2D PC devices and to provide a new mechanism for tuning and also obtaining new photonic crystal properties.

3.1 On-Chip Optical Beam Processing: The Superlattice Photonic Crystal

A two-dimensional superlattice photonic crystal structure was invented in which the holes of a triangular lattice are either filled with LC and alternate rows biased to give different refractive indices, or the rows alternate between two different radii. Figure 10(a) shows the model for this SL-PC structure. The imposition of a superlattice on a triangular lattice was shown to reduce the photonic bandgap, introduce band splitting around high symmetry points, and change the dispersion contours so that dramatic effects occur in the propagation, refraction, and dispersion properties of the structure. For example, for single mode propagation, this structure is found to introduce a variety of unique optical phenomena such as positive *and* negative refraction at a *single excitation wavelength,* normal incidence refraction and high dispersion: an order of magnitude greater than that predicted for the triangular lattice.

The physical mechanisms responsible for these effects are directly related to Brillouin Zone folding effects on the triangular lattice that lowers the lattice symmetry and introduces anisotropy in the lattice. The unit cell definition of the SL now consists of two holes per lattice point so that the basis vectors are orthogonal as opposed to being inclined at 60°, as in the triangular lattice. This new structure lowers the crystal symmetry through BZ folding and creates a strong interaction between the photonic dispersion surfaces. As a result the dispersion response becomes highly asymmetrical, thereby introducing significantly different phenomena than can be observed in conventional triangular or square lattices.

Figures 10(a) and 10(b) respectively, show an illustration of the SL-PC waveguide structure and a schematic that describes the parameters of the structure. The structure consists of a triangular lattice of circular holes (dotted triangle) of two different radii such that adjacent rows, i and j, consist of a single radius, r_1 or r_2, respectively. The $[i, j]$ rows introduce an additional periodicity in the lattice in the y-direction. To incorporate this additional periodicity, a Bravais lattice with a two-point basis is used so that the new basis vectors $\mathbf{a}_1 = a(0,\sqrt{3})$ and $\mathbf{a}_2 = a(1,0)$ define a rectangular unit cell, where a is the lattice constant of the underlying triangular lattice. This converts the hexagonal reciprocal lattice of a triangular lattice which is indicated by the dotted lines in Fig. 10(c) into a rectangular reciprocal lattice as shown. The new symmetry directions of the rectangular BZ are labeled in Fig. 10(c) and placed over the real lattice for reference in Fig. 10(b). As a consequence of the different shapes of the triangular lattice BZ and the SL BZ, those k vectors that lie outside of the rectangular BZ, but within the hexagon of the triangular BZ are translated into the rectangle by a multiple of $\mathbf{b}_1$ and $\mathbf{b}_2$. Thus, these points are

'folded' back into the rectangular BZ, which is smaller and of lower symmetry. In total, there are two equivalent X and Y points, and four equivalent M points in the first BZ because of the SL.
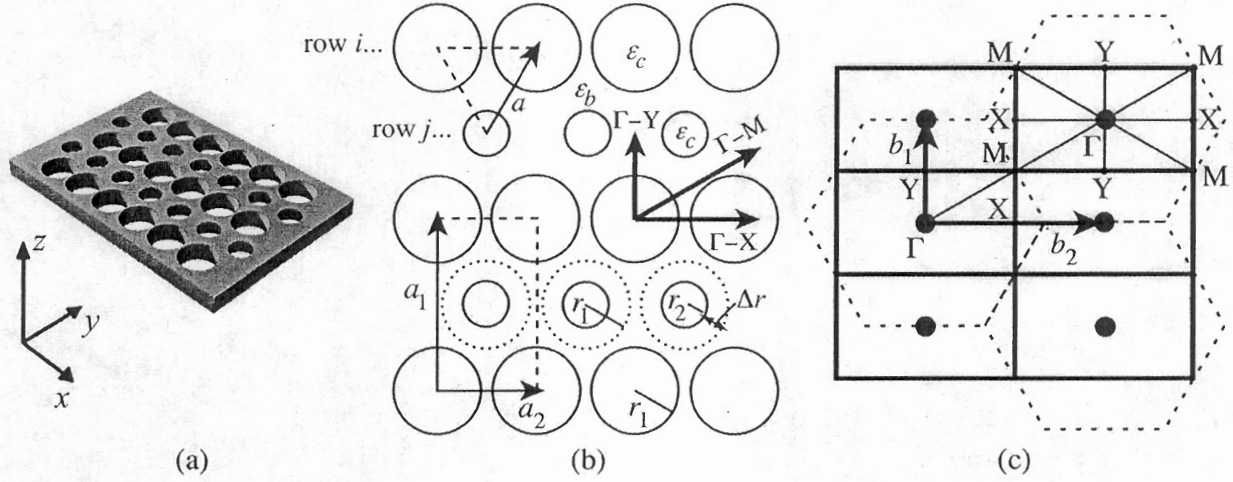

Figure **10.** Details of the SL structure: (a) An illustration of a SL slab waveguide. (b) A schematic showing the parameters of the structure. (c) Reciprocal lattice representation.

The strength of the SL modulation is controlled by $\Delta r = r_1 - r_2$ and characterized by the radius ratio, r_2/r_1, which incorporates the relative sizes of the two holes. For the structures investigated r_1 was held constant at $0.35a$ while r_2 was decreased. Thus, as r_2/r_1 decreases, the SL strength, or modulation, increases. In a simplified approximation, the addition of dielectric material as r_2 is decreased can be used to calculate an effective ε for r_2 holes. For a pure 2D structure, this involves averaging the dielectric constant of the area of material added over the entire area of a r_1 hole. Assuming the additional material has the same dielectric constant as the background material, the effective dielectric constant of a row j hole is given by:

$$\varepsilon_{eff} = \varepsilon_b \left(1 - \left(\frac{r_2}{r_1} \right)^2 \right) + \varepsilon_c \left(\frac{r_2}{r_1} \right)^2$$

where ε_c is the dielectric constant inside a row i hole. This equation shows that the magnitude of the dielectric modulation between rows is directly related to the difference between the hole sizes. For example, a change in radius of $\Delta r = 0.05a$, from $r_1 = 0.35a$ to $r_2 = 0.3a$, corresponds to a r_1 hole with $\varepsilon = 3.918$, equivalent to an index change $\Delta n = 0.979$ between $[i, j]$ rows for $\varepsilon = 12$. Thus, radius modulated SLs with strengths $r_2/r_1 = 0.857$ and 0.571 introduce an index modulation equivalent to $\Delta n = 0.979$ and 1.90, respectively, between adjacent rows, clearly showing that the magnitude of the SL modulation is unprecedented in comparison to the previously reported SL which is limited by the NL properties of the material infiltrated into the holes. For this reason, a radius modulated SL is unique in its impact on this lattice structure.

At the end of this program, SL structures were made and optical characterizations performed. Figure 11 briefly details the geometry and processing steps used to fabricated these structures and an SEM of a typical sample, and Figure 12 the measurement system and spectra obtained. Figure 13 shows the excellent agreement that was obtained between experiment and
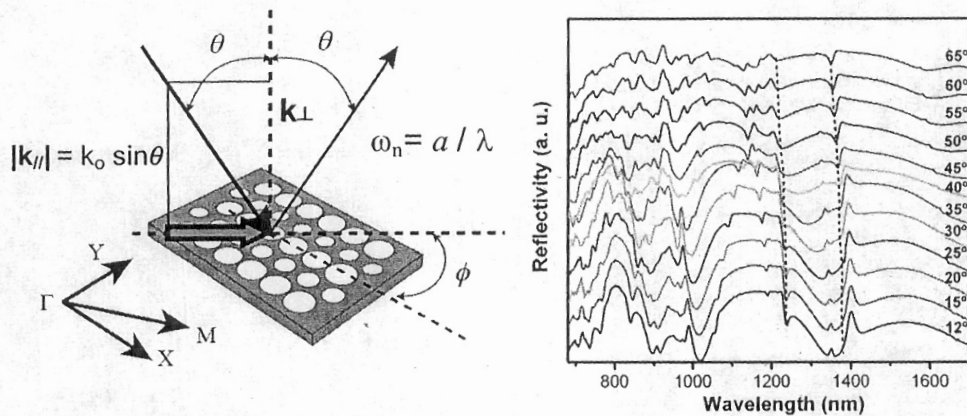
the theoretical predictions. This agreement adds a high level of credibility to the predicted optical response of the refraction and dispersion properties of these structures that can be computed from the dispersion counters, or equal frequency curves.

- E-beam lithography
  - 1 mm^2 area written using smaller unit patterns

- ICP dry etching with Chlorine/C$_4$F$_6$ recipe

- Parameters of Si Slab WG
  - $a = 358$ nm
  - $r_1 = 125$ nm
  - $r_2 = 73$ nm

- Define Dielectric Strength:
  - $k = r_2 / r_1 = 0.584$

~300 nm

1 μm

Si
SiO
Si

Γ-M

Γ-X

Γ-Y

200 nm
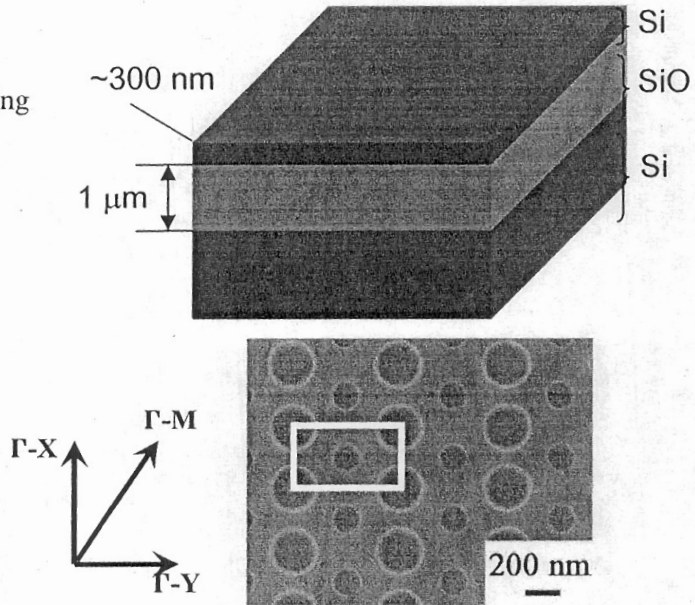
T. Yamashita, *PhD Thesis*, GT (2005).
C. W. Neff *et al. Opt. Exp.13, 3166* (2005)

Figure 11. Geometry and parameters of 2D PC silicon slab waveguides fabricated with a superlattice-based superlattice

θ θ

$k_\perp$

$|k_{//}| = k_o \sin\theta$ $\omega_n = a / \lambda$

Y

Γ

M

X

ϕ

65°
60°
55°
50°
45°
40°
35°
30°
25°
20°
15°
12°

Reflectivity (a. u.)

800   1000   1200   1400   1600
Wavelength (nm)

- Resonant-band coupling technique
  - $k_{//}$ component couples into WG: dip in reflectance spectra
  - Lattice direction selected by ϕ (0 to 360°)
  - $k_{//}$ component selected by θ
  - Normalized frequency inversely proportional to wavelength

V. N. Astratov *et al., Phys. Rev. B* (1999).

Figure 12. Schematic of measurement technique and example of spectral data obtained.
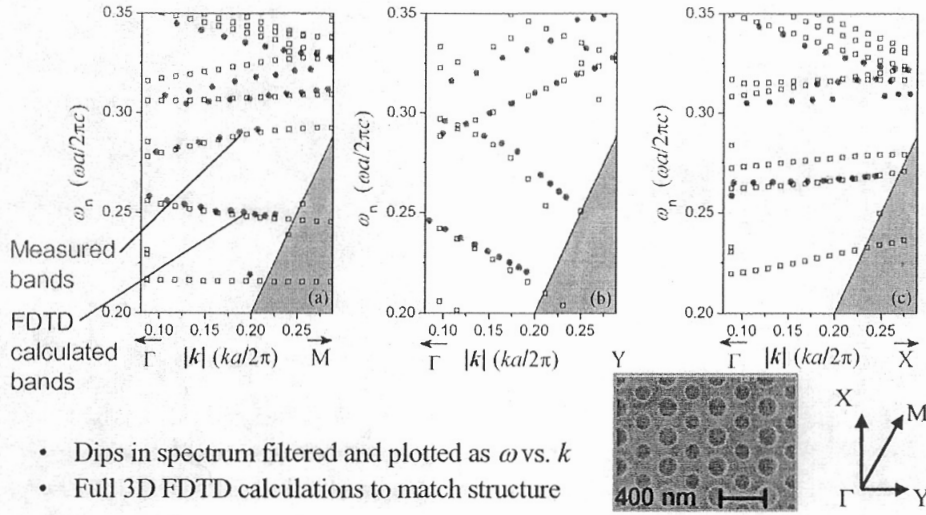
Figure 13. Measured & calculated photonic band structure of a 2D superlattice photonic crystal.

The full potential of these devices is discussed in published papers. Figures 14, 15 and 16, respectively, demonstrate the structures that were investigated and the large refractive and dispersion properties predicted for these devices. We are also working to make these structures in titania/PLZT thin films for visible and tunable applications, respectively. Our studies show that structures shown in Figure 14 can be designed to exhibit both positive and negative refraction and a very high degree of tunability. Structures in which it is possible to tune the angle of refraction over ~80° have been designed. These properties greatly enhance applications to beam steering and compact sensors and spectrometer devices that can be integrated onto a chip.
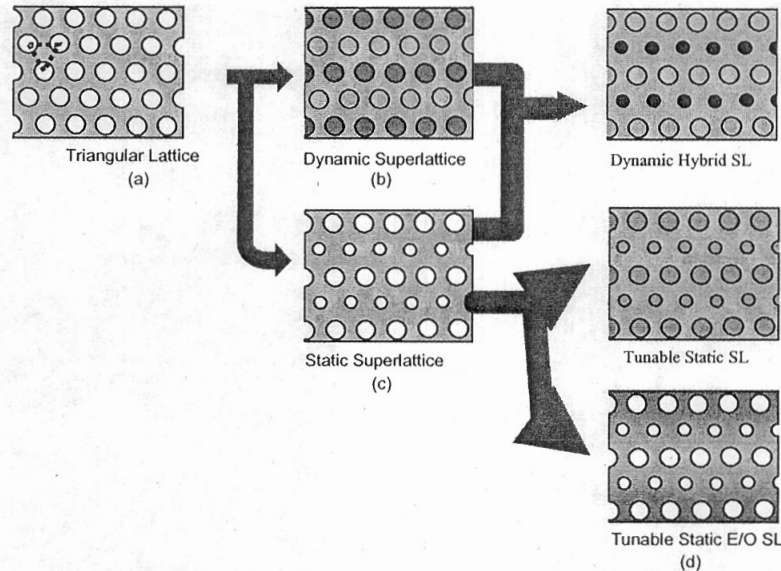

Figure 14. Schematic of various types of photonic crystal superlattices based upon (a) the triangular lattice: (b) Dynamic superlattice imposed by a differential bias along rows of holes filled with a nonlinear or electro-optical material; (c) Static superlattice in which alternate rows

13

have different diameters and are permanently written into a slab; and (d) Hybrid superlattices in which alternate rows have different diameters and are permanently written into a slab to form static superlattices and are also filled with an optically nonlinear or EO material that can be electrically or optically biased.
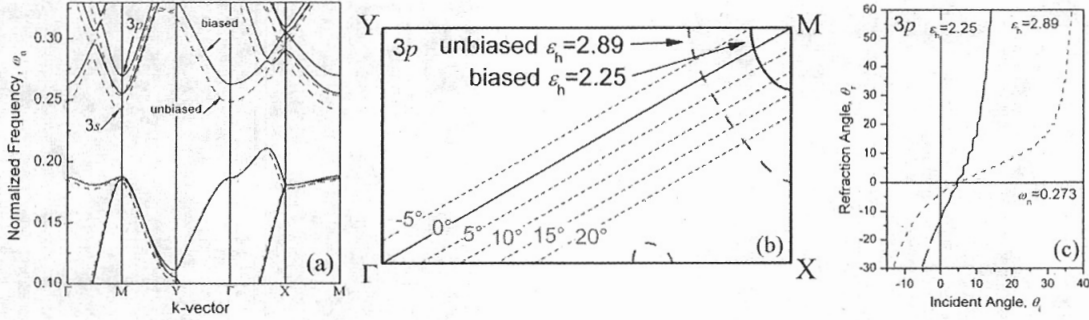

Figure 15. (a) Band structures, (b) dispersion contours and (c) refraction response of the 3p band of the large area addressed infiltrated superlattice structure (Fig. 15(b)) at a normalized frequency of ω_n=0.273.
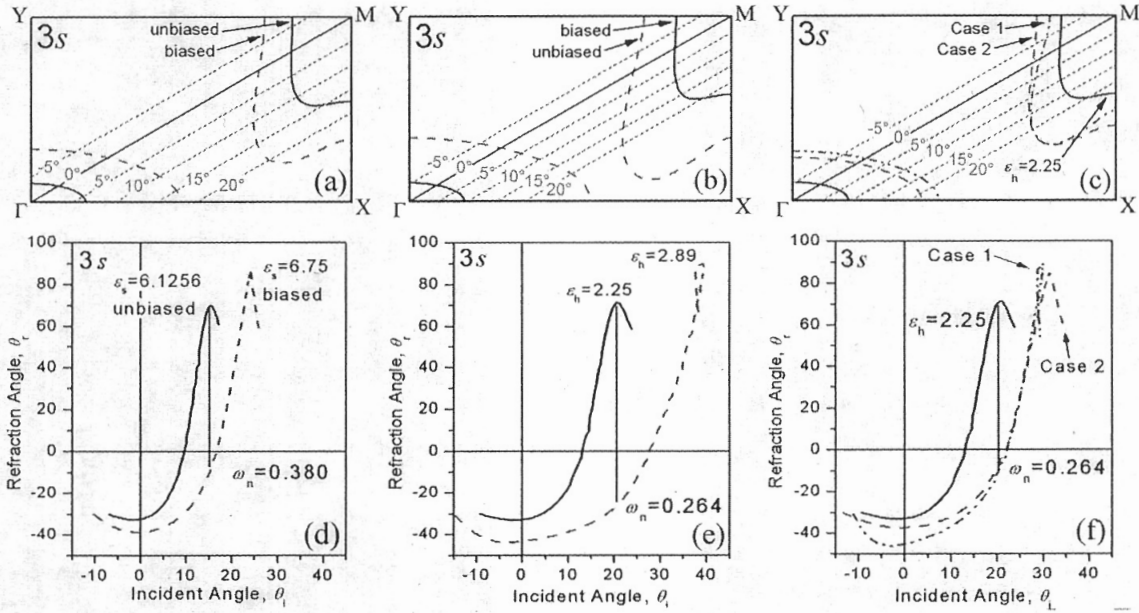

Figure 16. Irreducible BZ dispersion contours and the corresponding refraction response as calculated by the k-vector method for the EO superlattice (a) and (d), the large area addressed infiltrated superlattice (b) and (e), and the interdigital addressed superlattice (c) and (f). Case 1: the larger holes unbiased (ε_{h1} = 2.89), smaller holes biased (ε_{h2} = 2.25). Case 2: the opposite configuration (ε_{h1} = 2.25, ε_{h2} = 2.89).

14

3.2 The virtual waveguide photonic crystal structure

This concept uses a 2D PC slab designed to guide light within a crystal with a significant decrease in beam divergence, thereby collimating light and creating a "virtual waveguide". As discussed previously, the photonic band diagram and dispersion curves provide a complete description of the propagation of light within a crystal. Thus, once the ω vs. **k** relationship is solved, the direction of energy propagation is found by taking the normal direction to the constant frequency dispersion surface. The curvature of the dispersion surface determines the degree of beam spread inside of the photonic crystal. Therefore, a linear section in the dispersion curve gives rise to self-collimated beams traveling in a direction normal to the line. The photonic band structure and resulting dispersion plots for a square lattice device are shown in Figures 17 and 18 below and are used to calculate the propagation properties of a plane wave traveling through the structure (Figure 19).
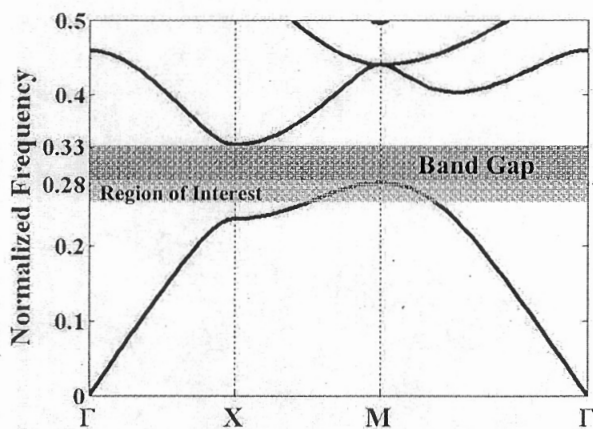

Figure 17. TE mode band diagram of the square lattice photonic crystal of silicon pillars in a silica matrix with radii of 0.2a in the reduced Brillouin zone.
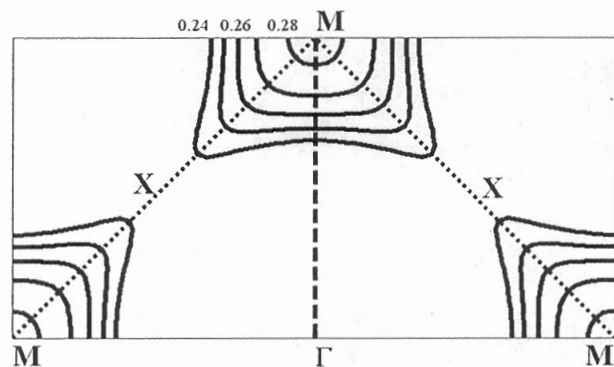
Figure 18. Dispersion curve showing a flattening of the curve along the Γ-M direction resulting in a self-collimated
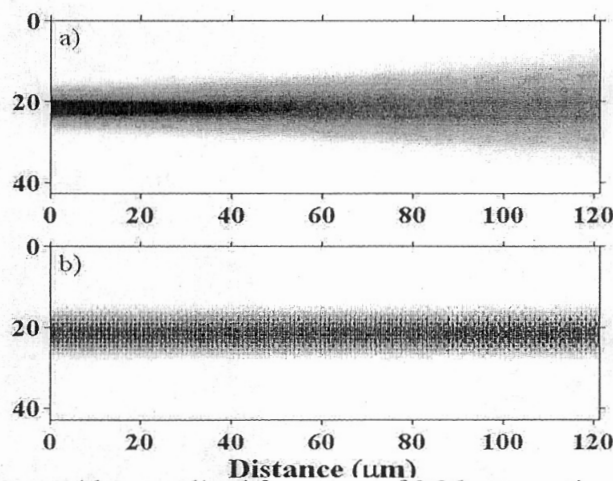

Figure 19. Gaussian beam with normalized frequency of 0.26 propagating in a) silica and b) photonic crystal virtual waveguide. Significant beam spreading is seen in silica while the photonic crystal keeps the beam intact.

Figure 19, depicts the plot of the time-averaged electric field intensity pattern of a Gaussian beam propagating in silica compared to the inside of a virtual waveguide for a normalized frequency of 0.26. After 120μm of propagation, no observable spreading occurs in the virtual waveguide compared to significant spreading in the silica slab. These structures were designed for a square lattice PC in a Si waveguide and several protocols were developed for making and testing them. As shown in Figures 20(d) and 20(e) the beam collimation effect has been experimentally confirmed at ~1500nm in structures fabricated in Si. No beam spread allows beam guiding for new optical circuit designs as shown in Figure 21.
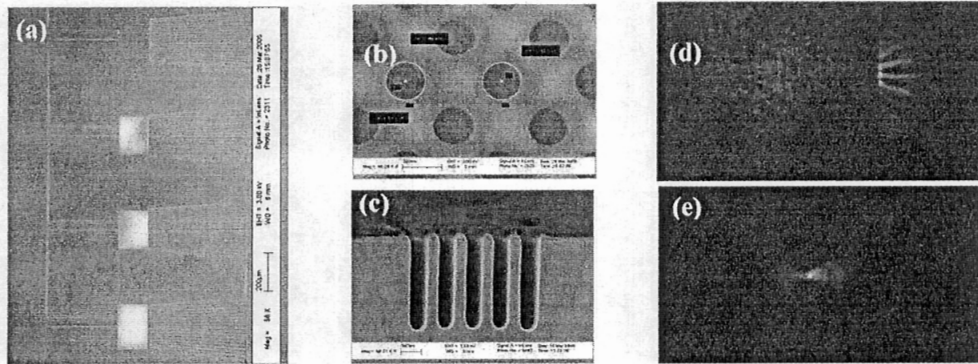

Figure 20 Fabrication of low-divergence waveguide structure in silicon. (a) Layout of optical circuit showing optical input coupling to a "virtual waveguide" PC device and out coupling waveguides angled to investigate beam collimation/divergence, (b) 200nm holes on 283 nm square lattice and (c) 200 nm wide trenches, (d) & (e) IR images showing light guiding achieved without (fanned output) and with (single line output) a self-collimating PC device, respectively.
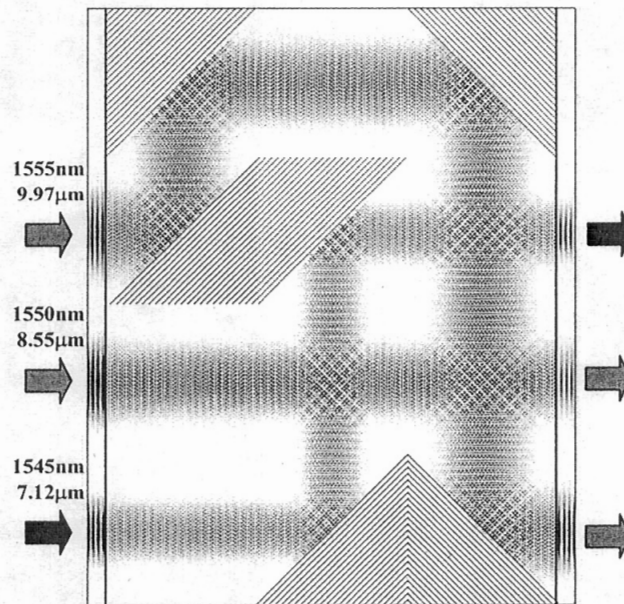

Figure 21. Schematic showing the potential of routing three parallel beams with different wavelengths and widths within a single signal layer using the photonic crystal virtual waveguide.

3.3 Fabry-Perot Resonator

The beam collimation effect can also be used to develop novel filter designs and resonator structures, for example, as a filter with 90% transmission, or as a bistable device. In a conventional Fabry-Perot etalon, for small beam widths (as required for on-chip optical beam processing) the field spreads with each transverse of the structure and consequently broadens due to the intrinsic beam divergence, as shown on the right in Figure 22, such that the total transmission can be drastically reduced, (<16%). However, by collimating the beam using a PC virtual waveguide the beam excursions are drastically reduce, as shown on the left in Figure 22 and the transmitted intensity is increased to 98%. Thus, the device acts as a compact spectral filter or potentially, with the incorporation of nonlinear materials into the Fabry-Perot structure, as bi-stable element.
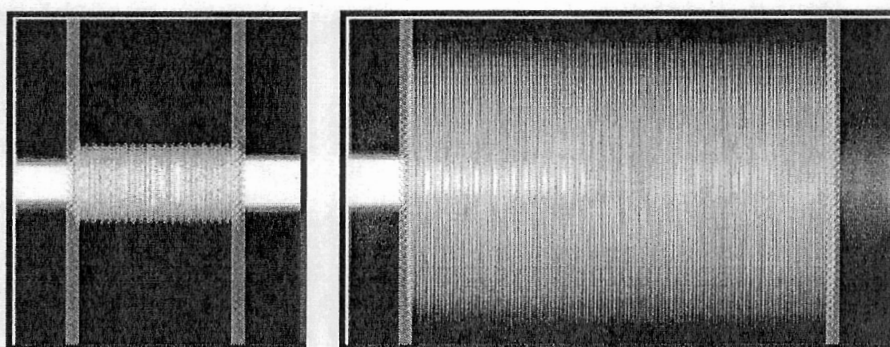
Photonic crystal   No photonic crystal

Figure 22. Behavior of an optical beam through a Fabry-Perot Etalon with and without the presence of a photonic crystal virtual waveguide in the etalon structure.

3.4 Negative Index Imaging Lens

These devices have the potential to produce a sub-wavelength focus and therefore are ideal for processing light in confined geometries as envisaged for this project and other on-chip signal processing devices. Thus, PCs with variations based on the square or triangular lattice have been configured to perform collimation and sub-wavelength focusing by adjusting the dispersion contour from a concave, to flat, to convex curvature along the direction of beam propagation. Specifically we have investigated negative index imaging at near-infrared wavelengths for a photonic crystal structure whose effective index was closely matched to air. The device geometry for this experiment is shown in Figure 23(a). A tapered waveguide was used to generate a point-like source objective field, and to investigate the focusing behavior an array of ridge waveguides was placed at the back plane of the PC lens. This array consisted of nine 500 nm wide photonic wires spaced by 1 μm. For transverse magnetic (TM) polarization a well-defined focus with a waist of $1.7\lambda_0$ was measured as shown in Figure 23(b). For the same wavelength the transverse electric (TE) polarization mode was spatially spread out and had a very low transmission. The measured wavelength dependence also confirmed the behavior of the PC as a negative index lens.
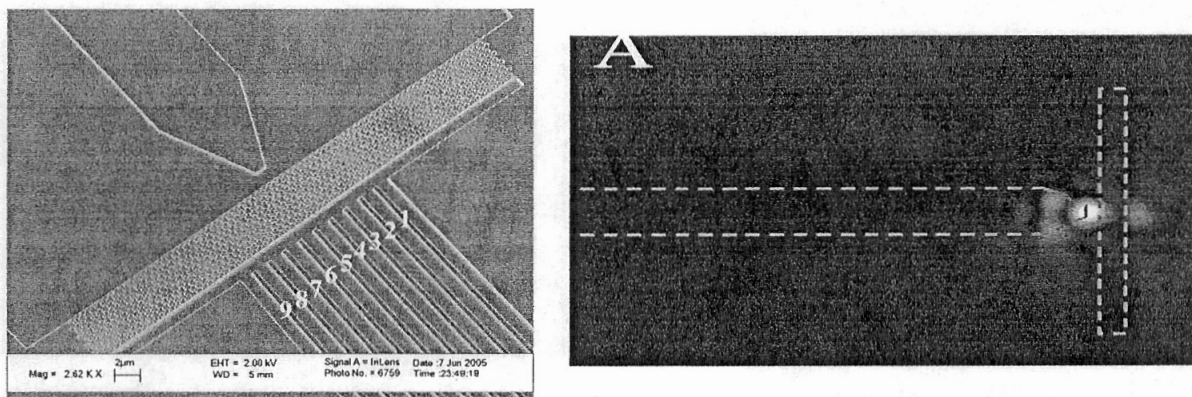
Figure 23. SEM of a negative index triangular lattice PC device and associated test structure. Experimental characterization of device at a wavelength of 1562 nm for TM mode showing focus produced by tapered waveguide (bright spot on right) and a $1.7\lambda_o$ focused spot produced by the PC (less bright spot on the left). Dotted lines indicate the positions of tapered waveguide and photonic crystal, respectively.

3.5 Polarized Beam Splitter

We have also designed and characterized a photonic crystal polarization beam splitter with an extinction ratio of greater than 15 dB. The design takes advantage of the fact that due to their large index contrast with air, silicon based PCs can exhibit large anomalous dispersion over large bandwidths. Thus a large spectral shift is observed in the dispersion plots of the lowest-order even (TE-like) and odd (TM-like) modes due to the SOI confinement. Therefore, if the TE-mode is chosen to lie close to the directional gap at the top of the band, the TM-like mode lies in a lower-frequency regime where the dispersion curves are almost isotropic. Using a diagonal interface between two triangular PCs with different hole sizes it is therefore possible to use this property to design a switch. This polarization switching mode has been observed for TM and TE modes as shown in Fig. 24 below.
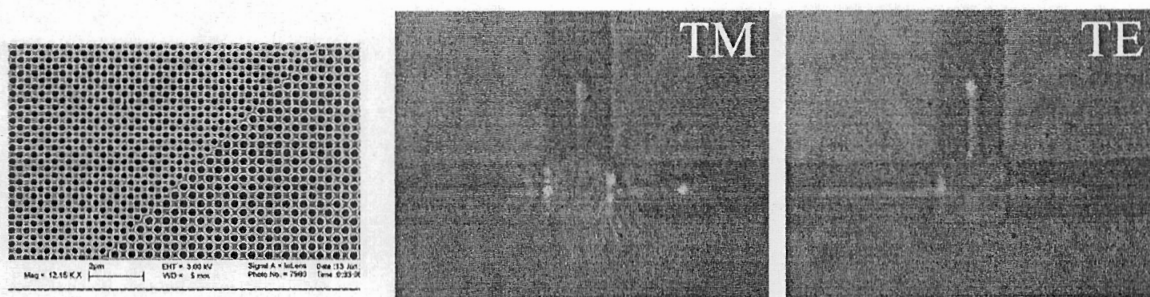

Figure 24. SEM showing the diagonal interface between two square lattice PCs: The LHS has a lattice constant of 353 nm and the RHS a lattice constant of 438 nm. Both structures have the same radius to lattice constant ratio of 0.35. PC device integrated into two ridge waveguides: LHS input and TOP and RHS output waveguides. Out-of-plane scattered light shows the pathways of each polarization and confirms high transmission through the structure when

18

illuminated with TM light and the 90° switching of TE polarized incident on the structure to pass through the top waveguide.

3.6 Modification of 2D Photonic Crystal Structures by ALD

In our final studies, we investigated the application of ALD to form multilayer 2D PC devices. As has been well documented, the properties of 2D PCs are critically dependent on the precise distribution of dielectric material, as patterned by electron-beam lithography, consisting of a periodic dielectric modulation with integrated line, point and periodic defects. Thus, the optical properties of 2D PC slab waveguides are determined by the precision of the lithography process, with limited post fabrication tunability. We have recently reported on the ability of atomic layer deposition to modify photonic bands within these structures and to produce significant new effects. Thus, this ALD coating technique has the potential to form new types of composite/multilayer waveguides by conformally coating the 2D PC structure.
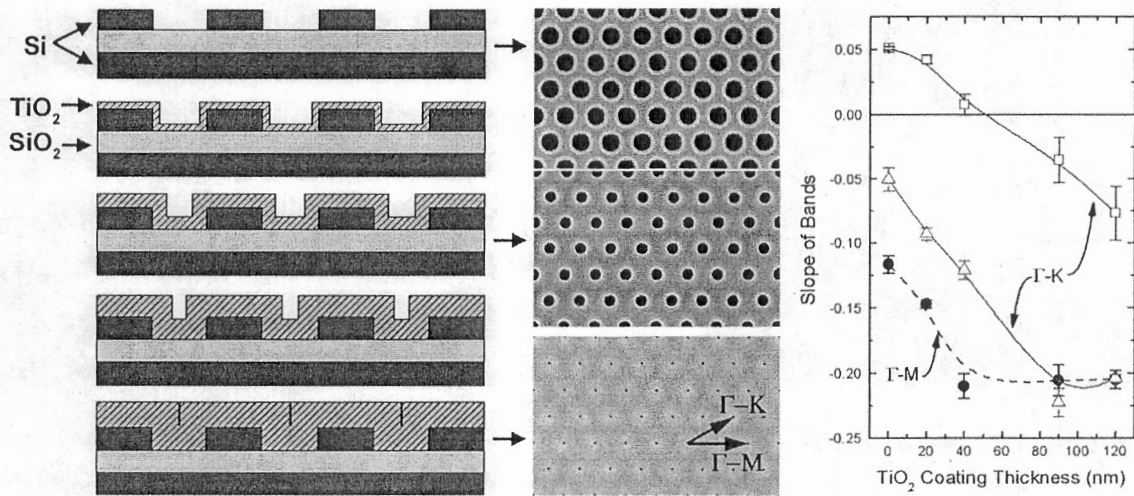

Figure 25. Schematic cross-section of the 2D triangular lattice illustrating the progressive coating of TiO_2 onto the lattice. The conformal deposition by ALD yields equal growth at the bottom and sides of the air holes as well as the top surface of the slab. For full TiO_2 infiltration, the air holes are completely filled, creating a TiO_2 cladding layer. The SEM images show the top surface of the uncoated sample and after coating with 40 nm and 120 nm of TiO_2. The right panel shows the measured slopes of several bands that are observed to decrease with increasing TiO_2 coating thickness.

Figure 25 shows the conformal coating of a 2D PC silicon slab waveguide with successive coatings of TiO_2, up to a total of 120 nm at which point the periodic hole structure was completely filled. As shown, very conformal coverage was obtained through all infiltration stages until the holes were completely filled. The photonic band structure was significantly affected and exhibited large changes: the dielectric bands decrease in energy as a result of the added dielectric material and change slope. In addition several bands along high symmetry directions were observed to change slope from a positive to negative gradient, as shown in Fig.

25. This study demonstrates the potential to tune structures for slow light applications, where greatly enhanced light-matter interactions can be exploited.

For the specific case of the Si waveguide structure investigated; a triangular lattice with unit cell dimensions of 360 nm and hole size of 240 nm, a tuning range of 12% to a precision of 0.005% was demonstrated in the photonic band structure and resulting optical properties with the deposition of TiO_2. By depositing films with lower refractive index, a finer degree of control and tuning can be achieved. Conversely, the tuning range can be increased by depositing higher index films, with the precision being determined by the deposition rate. Of great importance is the fact that adjustments can be made not only to the band frequency, but also to the dispersion, enabling precise tuning to achieve a zero group velocity for slow-light applications. Thus, this technique enables unprecedented adjustment to the dispersion properties of any 2D photonic crystal. Additionally, by the application of multi-component ALD, this technique facilitates the formation of layered and composite 2D PC waveguides thus opening new fabrication routes to control dispersion, propagation and dielectric contrast. Also the technique can be used to add increased functionality and to fabricate active device structures for integration with electronic devices.

4. Summary

We have demonstrated that ALD combined with conventional and new template technologies enables novel 3D structures as a result of its ability to deposit very conformal and smooth films at low temperature and with "digital control". Using opal based templates we have fabricated inverse opals with void space air pockets that are predicted to enhance the PBG. Also these studies have been extended to the structural modification of the template so as to form NCP opals that have been demonstrated to have large and highly tunable (static and dynamic) PBGs. Studies have also been reported of multi-layered, luminescent and high index inverse opals demonstrating modified photoluminescence. We also note that for NCP structures the thickness of the backfill layer or backfilling volume is very large (> 50 % of the total volume) and does not necessarily have to be uniformly filled with the same material, as demonstrated in our TiO_2/ZnS:Mn study. Thus, these structures greatly enhance the flexibility to grow a number of multilayers TiO_2/ZnS:Mn (GaP:N) and also other materials that will allow highly luminescent and tunable devices to be investigated.

In a pioneering study with Oxford University, holographically derived PCs have been inverted with ALD deposited TiO_2 and shown to reproduce the structure very precisely and with a smooth surface. Measurements of the reflectivity showed significantly enhanced optical and photonic band gaps and a perfect match between the features observed in reflectivity and the calculated band structure. From the success achieved with these relatively simple 3D and 2D PC structures, it will be interesting to see what can be achieved for more complex structures and the true interplay between templating and conformal coating techniques. The application of these techniques to other lattices is still in its infancy, but promises to be an active area of research with enormous potential.

New material developments have resulted in the conformal growth of high index (n = 3.34) optoelectronic GaP films and the inversion of silica opals to form inverse structures that display not only enhanced (111) pseudo photonic band gaps, but also a 3D full photonic band gap in the red region of the spectrum. This, and similar material developments coupled with new lattice templates holds the promise to achieve the goal of 3D laser and optoelectronic circuits.

Moreover, we have also reported the invention of a series of 2D PC structures and devices for on-chip signal processing. The superlattice photonic crystal provides a means for steering and dispersing light and when fabricated in an electro-optical material a wide degree of dynamical tuning of these properties. The virtual waveguide effect and its application to a photonic crystal Fabry-Perot Resonator provides a mechanism for on-chip spectral filtering and potentially as a non-linear element for making optical bi-stability devices. A more conventional switching mode can be achieved using the polarized beam splitter and recently we have observed negative index focusing in 2D PC structures. The latter effect is creating much excitement and has the potential for sub-wavelength high resolution imaging as well as the development of conformal lenses for sensors and novel beam steering control for lasers. Thus, this menu of devices directly addresses the object of this program for novel means to control light on a chip for the computation of advance algorithms and signal processing with applications to communication, identification and display technologies.

A wide range of novel structures have also been created with ALD ranging from TiO_2/ZnO aligned nano-rod arrays, TiO_2 nano-bowl arrays & masks, to biologically modified templates. All of these studies demonstrate that ALD provides new pathways, not only for photonic crystal band gap engineering, but also for the generation a variety of 2D and 3D structures.

Finally we note that recent applications of ALD to tune the photonic band structure and resulting optical properties of 2D PC structures has demonstrated significant (12%) modifications in the band structure, with a precision of 0.005%. Changes were observed in band slopes and from a negative to positive slope that will have great impact on slow light effects. Thus, we have demonstrated static photonic band tuning in a two-dimensional triangular lattice photonic crystal Si slab waveguide by nanoscale modification of the dielectric contrast using atomic layer deposition of TiO_2. The application of these concepts to the devices described above as well as other devices promises to provide great flexibility and functionality in these areas. Moreover the incorporation of electro-optic and non-linear materials provides a further platform for innovation and system applications.

5. Papers, Conference Presentations, Patents and Graduate Student and Post Doctoral Fellows Support.

5.1 Publications

1. **Invited**: Park, W., J. S. King, C. W. Neff, C. Liddell, C. J. Summers. "ZnS-Based Photonic Crystals." *Physica Status Solidi. (b)*. 229, 949-960 (2002).

2. **Invited**: C. J. Summers, J. King, and W. Park, "New Phosphor and Material Structures for Displays: Proceedings of Second International Meeting on Information Displays, Korea, Daegu, Korea (2002)

3. W. Park and C. J. Summers, "Extraordinary Refraction and Dispersion in 2D Photonic Crystal Slabs", *Optics Letters,* **27**, 1397 (2002)

4. X. Wang, P. Gao, Jing Li, C. J. Summers and Z. L. Wang, " Rectangular ZnO-ZnS Nanocables and ZnS Nanotubes, *Advanced Materials,* 23, 1732 (2002)

5. C. M. Liddell and C. J. Summers, "Monodispersed ZnS Dimers, Trimers, and Tetramers for Lower Symmetry Photonic Crystal Lattices," *Adv. Mater.* 15, 1715 (2003).

6. J. S. King, C. W. Neff, D. Heineman, E. Graugnard and C. J. Summers, "Optical and Crystallographic Properties of Inverse Opal Photonic Crystals Fabricated Using Atomic Layer Deposition." Proceedings of the MRS Fall Meeting, Boston, MA. December 2003.

7. C. M. Liddell, C. J. Summers, A. M. Gokhale. "Stereological Estimation of Morphology Distribution of ZnS Colloidal Clusters for Photonic Crystal Applications," *Mater. Charac.* 50, 69 (2003).

8. C. J. Summers, C. W. Neff, and W. Park, "Active Photonic Crystal Nano-Architectures," *J. Nonlinear Optical Phys. and Materials* 12(4), 587-97 (2003).

9. S. King, C.W. Neff, W. Park, D. Morton, E. Forsythe, S. Blomquist, and C. J. Summers, "High filling fraction inverted ZnS opals fabricated by atomic layer deposition" *Appl. Phys. Lett.* **83**, 2566 (2003).

10. X. Wang, Christopher J. Summers, and Zhong L. Wang, "Large-Scale Hexagonal-Patterned Growth of Aligned ZnO Nanorods for Nano-Optoelectronics and Nanosensor Arrays" *Nano Lett.*, 4 (2004) 423-426. (featured by ACS website in their Heart Cut section on April. 26, 2004)

11. J. S. King, C. W. Neff, S. Blomquist, E. Forsythe, D. Morton, and C. J. Summers, "ZnS-based photonic crystal phosphors fabricated using atomic layer deposition,", *Phys. Stat. Sol. (b),* 241 (3), 763-766 (2004).

12. X.D. Wang, E. Graugnard, J.S. King, Z.L. Wang, C.J. Summers, "Large-scale Fabrication of Ordered Nano-Bowl Arrays." *Nano Letters* 4, 2223-2226, (2004).

13. X. D. Wang, C. J. Summers, Z. L. Wang, "Mesoporous Single-Crystal ZnO

Nanowires Epitaxially Sheathed with Zn_2SiO_4", *Adv. Mater.*, 16 (2004) 1215-1218

14.   W. Park and C. J. Summers, Optical Properties of Superlattice Photonic Crystal Waveguides, *Applied Phys. Lett.* 84, 2013, (2004)

15.   C. M. Liddell and C. J. Summers "Non-Spherical Colloidal Building Blocks for Diamond-Analog Photonic Crystal Structure" *J. Colloid and Interface Science*, 274.1, 103-106, (2004)

16.   C. M. Liddell, Giang Vo and C. J. Summers. "Zinc Sulfide Colloidal Multimers for Photonic Crystal Applications via Preform Coagulation," *Langmuir* (2004)

17.   X. D. Wang, Y. Ding, C. J. Summers, and Z. L. Wang, "Large-Scale Synthesis of Six-Nanometer-Wide ZnO Nanobelts" *J. Phys. Chem. B*, 108 (2004) 8773-8777.

18.   X. D. Wang, C. J. Summers and Z. L. Wang, "Self-attraction among aligned Au/ZnO nanorods under electron beam", *Appl. Phys. Lett.*, 86 013111 (2005)

19.   T. Yamashita and C. J. Summers, "Evaluation of Self-collimated beams in photonic crystals for optical interconnect," *J. Selected Areas in Communication* 23, 1341 (2005).

20.   C. W. Neff and C. J. Summers, "A photonic crystal superlattice based on triangular lattice," *Optics Express* 13, no. 8, 3166-3173 (2005).

21.   X. D. Wang, C. Neff, E. Graugnard, Y. Ding, J.S. King, L.A. Pranger, R. Tannenbaum, Z.L. Wang, C.J. Summers, "Photonic crystals fabricated using patterned nanorod arrays," *Advanced Materials* 17, 2103 (2005).

22.   E. Graugnard, J. S. King, S. Jain, Y. Zhang-Williams, I. C. Khoo, C. J. Summers, "Electric field tuning of the Bragg peak in non-close-packed TiO_2 inverse shell opals," *Phys. Rev. B* 72, 233105 (2005).

23.   D. Gaillot, T. Yamashita, C.J. Summers, "Photonic bandgaps in highly conformal inverse opal based photonic crystals, "P*hys. Rev. B.* 72, 205109 (2005) Selected for the *Virtual Journal of Nanoscale Science & Technology*, 12 November 21 (2005).

24.   J. S. King, D. Heineman, E. Graugnard, and C.J. Summers, "Atomic layer deposition in porous materials: 3D photonic crystals," *Appl. Surf. Sci.* 244 511 (2005).

25.   J. S. King, E. Graugnard, and C.J. Summers, "TiO_2 inverse opals fabricated using low temperature atomic layer deposition," *Adv. Mater.* 17 1010 (2005).

26.   X. D. Wang, J. H. Song, P. Li, J. H. Ryou, R. D. Dupuis, C. J. Summers and Z. L. Wang, "Growth of uniformly aligned ZnO nanowire heterojunction arrays on GaN, AlN, and $Al_{0.5}Ga_{0.5}N$ substrates," *J. Amer. Chem. Soc.* 127 (21), 7920-7923 (2005).

27.   X. D. Wang, C. S. Lao, E. Graugnard, C.J. Summers, and Z. L. Wang, "Large-size liftable inverted-nanobowl sheets as reusable masks for nanolithography," *Nano Lett.* 5 (9), 1784-1788 (2005).

28. M. R. Weatherspoon, M. S. Haluska, Y. Cai, J. S. King, C. J. Summers, R. L. Snyder and K. H. Sandhage, "Phosphor Microparticles of Controlled Three-dimensional Shape from Phytoplankton," *J. Electochemical Society* 153, H34-37 (2006)

29. Jeffrey S. King, Elton Graugnard, and Christopher J. Summers, "Photoluminescence modification by high-order photonic bands in TiO_2/ZnS:Mn multilayer inverse opals," *Appl. Phys. Lett.* 88, 081109 (2006)

30. E. Schonbrun, T. Yamashita, W. Park and C. J. Summers, "Negative-index imaging by an index-matched photonic crystal slab." Physical Review B 73, 195117 (2006)

31. E. Graugnard, J. S. King, D. P. Gaillot and C. J. Summers, "Sacrificial-layer atomic layer deposition for fabrication of non-close-packed inverse opal photonic crystals," *Adv. Func. Mater.* 16, 1187 (2006).

32. I.C. Khoo, Y. Williams, A. Diaz, K. Chen, J. Bossard, D. Werner, E. Graugnard, J. S. King, S. Jain, and C. J. Summers, "Liquid-Crystals for optical filters, switches and tunable negative index material development," *Molecular Crystals and Liquid Crystals*, 453, 309 (2006).

33. J. S. King, E. Graugnard, O. M. Roche, D. N. Sharp, J. Scrimgeour, R. G. Denning, A. J. Turberfield, and C. J. Summers, "Infiltration and inversion of holographically-defined polymer photonic crystal templates by atomic layer deposition," *Adv. Mater.* 18, 1561 (2006).

34. J. S. King, D. Gaillot, E. Graugnard, and C. J. Summers, "Conformally back-filled, non-close-packed inverse opal photonic crystals," *Adv. Mater.* 18, 1063 (2006)

35. G. Ahmed, M. B. Dickerson, B. C. Church C. J. Summers, K. Sandhage, " Rapid room-temperature formation of crystalline calcium molybdate phosphor microparticles via peptide-induced precipitation" Advanced Materials 18, 1759 (2006)

36. C. J. Summers, E. Graugnard, D. P. Gaillot and J. S. King, "Luminescent and Tunable 3D Photonic Crystal Structures," *J. Nonlinear Optical Phys. and Materials* 15, 203 (2006)

37. E. Schonbrun, Q. Wu, T. Yamashita, W. Park and C. J. Summers, "Polarized beam-splitter based on a photonic crystal heterostructure," Optics Letters 31, 3104 (2006)

38. E. Graugnard, D. P. Gaillot, S. N. Dunham, C. W. Neff, T. Yamashita and C. J. Summers, "Photonic band tuning in two-dimensional photonic crystal slab waveguides by atomic layer deposition," Applied Physics Letters 89, 181108 (2006)

39. E. Graugnard, V. Chawla, D. Lorang and C. J. Summers, "High Filling Fraction gallium phosphide inverse opals by atomic layer deposition," *Applied Physics Letters* 89, 211102 (2006)

40. D. P. Gaillot and C. J. Summers, "Photonic band gaps in non-close-packed inverse opals", *J. Appl. Phys.* 100, 113118 (2006)

41. C. W. Neff, T. Yamashita and C. J. Summers, "Observation of Brillouin zone folding in photonic crystal waveguides possessing a superlattice pattern," Applied Physics Letters 90, 021102 (2007)

42. **Invited:** E. Graugnard, J. S. King, D. Gaillot and C. J. Summers, "Atomic Layer Deposition for Nano-Fabrication of Optoelectronic Devices," J. Electrochem. Soc (2007)

5.2 Conference Papers

1. C.J. Summers, J. S. King & W. Park "New Phosphor and Material Structures for Displays" Proceedings: Second International Meeting on Information Display, Daegu, Korea 2002.

2. ZnS-based Photonic Crystal Phosphors Fabricated Using Atomic Layer Deposition." J. S. King, C. W. Neff, S. Blomquist, E. Forsthe, D. Morton, and C. J. Summers, Physica Status Solidi C, accepted, March 2004 issue

3. "Optical and Crystallographic Properties of Inverse Opal Photonic Crystals Fabricated Using Atomic Layer Deposition." J. S. King, C. W. Neff, D. Heineman, E. Graugnard and C. J. Summers, Proceedings of the MRS Fall Meeting, Boston, MA. December 2003,

4. J.S. King, D. Gaillot, T. Yamashita, C.W. Neff, E. Graugnard, and C.J. Summers, "Complex, 3D Photonic Crystals Fabricated by Atomic Layer Deposition," Proceedings of the MRS Fall Meeting, Boston, MA, December (2004)

5. C.W. Neff and C.J. Summers, "Photonic Crystal Superlattices," Proceedings of the 17th Annual Meeting of the IEEE Lasers and Electro-Optics Society, Rio Grande, Puerto Rico, November 2004. extended abstract

6. C.W. Neff and C.J. Summers, "Photonic Crystal Superlattices in Electro-Optic Slab Waveguides," in Tuning the Optical Response of Photonic Bandgap Structures, ed. Philippe M. Fauchet, Paul V. Braun, Proceedings of SPIE 5511, 104-111, (2004)

7. C.J. Summers, C.W. Neff, B.K. Wagner, and W. Park, "Tunable Photonic Crystal Structures **(Invited Paper)**," in Tuning the Optical Response of Photonic Bandgap Structures, ed. Philippe M. Fauchet, Paul V. Braun, Proceedings of SPIE 5511, 81-92, (2004)

8. C.J. Summers, E. Graugnard, J.S. King, "3D luminescent photonic crystal structures," Proceedings of SPIE, Cockpit and Future Displays for Defense and Security, 5801 142 (2005).

9. E. Graugnard, D.P. Gaillot, J.S. King, C.J. Summers, "Photonic band gap response of structurally modified non-close-packed inverse opals by template directed multi-layer atomic layer deposition," Proceedings of SPIE, Photonic Crystal Materials and Devices III, (2006).

10. D.P. Gaillot, E. Graugnard, J.S. King, C.J. Summers, "Photonic bandgap response of structurally modified inverse non-close-packed opals by template directed multilayer

atomic layer deposition," Proceedings of SPIE, Photonic Crystal Materials and Devices III, (2006).

5.3 Invited Presentations

1. W. Park and C. J. Summers, "Photonics - A Primer", Physics Colloquium, School of Physics, Georgia Institute of Technology, Atlanta, GA, Oct. 11, 2000.

2. ZnS-Based Photonic Crystals, W. Park, J. S. King, C. W. Neff, C. Liddell and C. J. Summers. Tenth International Conference on II-VI Compounds, Bremen, Germany, September 2001.

3. C. J. Summers, "Photonic Crystals" DARPA Workshop on Optical Materials for Future Devices and Systems", Tampa, FL, 10-12 September 2001.

4. C. J. Summers, "New Concepts in Photonic Crystals", Department of Materials Science, Seoul National University, Seoul, Korea, Nov. 22, 2001.

5. C.J. Summers, J. S. King & W. Park "New Phosphor and Material Structures for Displays" Proceedings: Second International Meeting on Information Display, Daegu, Korea 2002.

6. C. J. Summers, "Active and Emissive Photonic Crystal Nano-Architectures" 6th Mediterranean Workshop and Topical Meeting "Novel Optical Material and Applications" Cetraro, Italy. June 8 – 13, 2003

7. C. J. Summers, W. Park and I. C. Khoo, "Novel Photonic Architectures: Liquid Crystal Infiltrated Photonic Crystals", SPIE, August 3-10th 2003, San Diego, CA.

8. C. J. Summers, "Emissive and Active Photonic Crystals" University of Rochester, 12th November 2003

9. C. J. Summers, J.S. King, D. Heineman, C. W. Neff, and E. Graugnard, "Atomic Layer Deposition in Porous Materials: 3D Photonic Crystals", 12th International Conference on Solid Films and Surfaces, June 21-25 2004, Congress Center, Hamamatsu, Japan.

10. C.J. Summers, C.W. Neff, B.K. Wagner, and W. Park, "Tunable Photonic Crystal Structures," in Tuning the Optical Response of Photonic Bandgap Structures, 48th Annual Meeting of SPIE, Denver, Colorado, 4-5 August 2004.

11. C. J. Summers, J.S. King, D. Heineman, C. W. Neff and E. Graugnard "Atomic Layer Deposition in Porous Materials: 3D Photonic Crystals:, University of Colorado, Boulder, Colorado, 6th August 2004.

12. C. J. Summers, New Photonic Crystal Structures: The Dynamic, Static and Hybrid Superlattices", LG-Philips – LCD, Kumi-city, Kyungbuk, Korea, August 25th 2004.

13. C.J. Summers "Novel Photonic Architectures: Liquid Crystal Infiltrated Photonic Crystals" SPIE 49th Annual Meeting "International Symposium on Optical Science

& Technology" Tunable Photonic Crystal, Denver Convention Center, USA, August 3 – 8, 2004.

14. "Photonic Crystal Superlattices in Electro-Optic Slab Waveguides", C. W. Neff & C. J. Summers, SPIE 49th Annual Meeting "International Symposium on Optical Science & Technology" Tunable Photonic Crystal, Denver Convention Center, USA, August 3 – 8, 2004.

15. E. Graugnard, J. S. King, D. Heineman, and C. J. Summers, "Atomic Layer Deposition for Photonic Crystal Devices, International Conference on Atomic Layer Deposition, 2004, August 16 – 18, 2004.

16. C. J. Summers, "Active and Emissive Photonic Crystals" Electrical & Computer Engineering Seminar, University of Charlotte, May 2, 2005.

17. C. J. Summers, E. Graugnard, D. Gaillot and J. S. King, "Luminescent and Tunable 3D Photonic Crystal Structures," 7th Mediterranean Workshop and Topical Meeting Novel Optical Materials and Applications, Cetraro, Italy, May 30th - June 3rd, 2005.

18. C. J. Summers, E. Graugnard, J. S. King, "ALD: A new tool for photonic crystal fabrication," Invited, Atomic Layer Deposition 2005, San Jose, CA, August 8-10, 2005.

19. D. Gaillot, E. Graugnard, J. S. King, and C. S. Summers, "Highly Tunable Photonic Band Gaps in Non-Close-Packed Inverse Shell Opals,", IEEE-LEOS Annual Meeting, 25 October 2005, San Diego, California.

20. C. J. Summers, C. W. Neff and T. Yamashita, "Photonic Crystals with Tunable Refraction and Dispersion," SPIE 50th Annual Meeting, 31 July - 5 August, 2005, San Diego, California.

21. C. J. Summers, C. W. Neff and T. Yamashita, "Novel 2D Photonic Crystals Structures," First International Symposium on Optoelectronics in Optics Valley of China, Wuhan, China, 2-4 November 2005.

22. C. J. Summers, C. W. Neff, T. Yamashita and C. P. Wong, "Photonic Crystal Sensors," 6th East Asia Conference on Chemical Sensors, Guilin, China, 6-9 November 2005.

23. C. J. Summers, D. Gaillot, E. Graugnard, C. W. Neff, and T. Yamashita, D. Citrin and D. Lippens, "Photonic Crystal Biochemical Sensors," International Meeting on Chemical Sensors, Brescia, Italy, July 16-19th 2006

24. C. J. Summers E. Graugnard and D. P. Gaillot, Y. Zhang-Williams and I. C. Khoo, "Tunable 3D Photonic Crystals by Liquid Crystal Infiltration," SPIE 51st Annual Meeting, 13-17 August, 2006, San Diego, California.

25. Christopher J. Summers & Elton Graugnard, "Atomic Layer Deposition for Nano-Fabrication of 3D Optoelectronic Devices" 210th Electrochemical Society Meeting, Cancun, Mexico, 29 October - 3 November 2006

5.4 Contributed Presentations

1. C. M. Liddell and C. J. Summers. "Non-Spherical ZnS Colloidal Building Blocks for Three-Dimensional Photonic Crystals." Conference on Nanoscience and Nanotechnology, Atlanta, GA, Oct. 30-Nov. 1, 2002

2. J.S. King, C. W. Neff, W. Park, D. Morton, E. Forsythe, S. Blumquist, and C .J. Summers, "Properties of Inverse Opal Photonic Crystals Grown By Atomic Layer Deposition," Presented at 2002 MRS Fall Meeting, Boston.

3. J.S. King, C.W. Neff, D. Heineman, S. Blomquist, E. Forsythe, D. Morton, E. Graugnard, and C. J. Summers, "Optical and Crystallographic Properties of Inverse Opal Photonic Crystals Grown by Atomic Layer Deposition," 2003 MRS Fall Meeting, Boston.

4. J. S. King, C. W. Neff, C. J. Summers, S. Blumquist, E. Forsythe and D. Morton, "ZnS-based Photonic Crystal Phosphors Fabricated Using Atomic Layer Deposition"11th International Conference on II-VI Compounds, 22-26 September, 2003, Niagara Fall, USA

5. C. M. Liddell and C. J. Summers, "Non-Spherical ZnS Colloidal Building Blocks for Diamond-Analog Photonic Crystal Structures", Materials Research Society Symposium, San Francisco, CA, Apr. 21-25, 2003

6. T. Yamashita, C. J. Summers, "Design and Simulation of Novel Optoelectronic Interconnect using Photonic Crystal Virtual Waveguide with Robust Fabrication and Misalignment Tolerances," submitted to 54th Annual Electronic Components and Technology Conference, Las Vegas, June 2004.

7. W. Park and C. J. Summers, "ZnS-Based Two-Dimensional Photonic Crystals", The First Georgia Tech Conference on Nanoscience and Nanotechnology, Atlanta, GA, Oct. 16-18, 2000.

8. C. Neff, J. King, W. Park, Z. L. Wang and C. J. Summers, "Template Directed Growth of Opal Photonic Structures of Silica and Polystyren Nanospheres", The First Georgia Tech Conference on Nanoscience and Nanotechnology, Atlanta, GA, Oct. 16-18, 2000.

9. W. Park and C. J. Summers, "Tunable Refraction in 2D Slab PC", Photonic and Elecromagnetic Crystal Structures PECS-IV, October 28-31, 2002, Los Angeles, CA

10. J.S. King, C. W. Neff, W. Park, D. Morton, E. Forsythe, S. Blomquist, and C.J. Summers, "Properties of Inverse Opal Photonic Crystals Grown By Atomic Layer Deposition," Presented at 2002 MRS Fall Meeting, Boston.

11. C. W. Neff, W. Park, and C. J. Summers, "Dynamic Photonic Crystal Superlattices," IEEE-LEOS Annual Meeting, October 2003, Tucson, AZ.

12. J. S. King, E. Graugnard, C. J. Summers, "Luminescent Composite 3D Photonic Crystals Fabricated by Atomic Layer Deposition." International Symposium on Photonic & Electromagnetic Crystal Structures V, 7-11, Kyoto, Japan, March 2004.

13.   Yamashita, T. and C. J. Summers, "Virtual Waveguiding of Gaussian Beams in 2D Photonic Crystals." (Poster) International Symposium on Photonic and Electromagnetic Crystal Structures V, 7- 11 March 2004, Kyoto, Japan.

14.   Yamashita, Tsuyoshi, Christopher Summers. "Design and Simulation of Novel Optoelectronic Interconnect Using Photonic Crystal Virtual Waveguide with Robust Fabrication and Misalignment Tolerances." Proceedings - Electronic Components and Technology Conference, May (2004).

15.   Davy Gaillot, Wounjhang Park, Jeff King, Elton D. Graugnard and Christopher Summers "Experimental and Theoretical Investigations of 3D Inverted opals" Dijon Photonics Summer School – 21-25th June 2004. Poster presentation

16.   C.W. Neff and C.J. Summers, "Photonic Crystal Superlattices in Electro-Optic Slab Waveguides,"in Tuning the Optical Response of Photonic Bandgap Structures, 48th Annual Meeting of SPIE, Denver, Colorado, 4-5 August 2004.

17.   E. Graugnard, J.S. King, D. Heineman, C.J. Summers," Atomic layer deposition for photonic crystal devices." AVS/BALD Atomic Layer Deposition Conference, Helsinki, Finland, August 16-18th (2004).

18.   C.W. Neff and C.J. Summers, "Photonic Crystal Superlattices," Proceedings of the 17th Annual Meeting of the IEEE Lasers and Electro-Optics Society, Rio Grande, Puerto Rico, 7- 11th November 2004.

19.   E. Graugnard, J.S. King, X.D. Wang, D. Heineman, Z.L. Wang, C.J. Summers, "Atomic layer deposition for precise, large-scale nanostructure fabrication." The 5th Georgia Tech Conference on Nanoscience and Nanotechnology, Atlanta, GA., November 2004.

20.   "ZnO Nanorods Imbedded TiO_2 2D Photonic Crystal through a Bottom-up Process", X. D. Wang, C. Neff, E. Graugnard, Y. Ding, J. S. King, Z. L. Wang and C. J. Summers, 2004 MRS Fall Meeting, November 29-December 3, 2004, Boston, MA

21.   J. S. King, D. Gaillot, T. Yamashita, C. Neff, E. Graugnard, and C. J. Summers, "Complex, 3D Photonic Crystals Fabricated by Atomic Layer Deposition," MRS Fall Meeting, Boston, MA, November 29-December 3, 2004.

22.   C. J. Summers, E. Graugnard and J. S. King, "3D luminescent Photonic Crystal Structures" Proceeding of SPIE, Session: Cockpit and Future Displays for Defense and Security, April 2005

23.   J. S. King, E. Graugnard, O. M. Roche, D. N. Sharp, C. J. Summers, R. G. Denning and A. J. Turberfield, (Oral) "Infiltration and Inversion of Holographically-Defined Polymer Photonic Crystal Templates using Atomic Layer Deposition," International Symposium on Photonic and Electromagnetic Crystal Structures VI, Crete, June 2005.

24.   C. W. Neff, T. Yamashita and C. J. Summers, "Refraction and dispersion in non-linear photonic crystal superlattices," IEEE-LEOS Annual Meeting, Sydney, Australia, October 2005.

25. D. Gaillot, E. Graugnard, J. S. King, and C. S. Summers, "Highly Tunable Photonic Band Gaps in Non-Close-Packed Inverse Shell Opals," IEEE-LEOS Annual Meeting, Sydney, Australia, 25 October 2005.

26. E. Graugnard, J.S. King, C.J. Summers, "Nanostructure fabrication through template directed multi-layer atomic layer deposition: non-close-packed inverse opals," (poster) Materials Research Society Symposium, Boston, MA November 29-December 3, 2005.

27. J.S. King, E. Graugnard, D.P. Gaillot, C.J. Summers, "Advanced Photonic Crystals by Holographic Lithography and Atomic Layer Deposition," (poster) Materials Research Society Symposium, Boston, MA., November 29-December 3, 2005.

28. E. Graugnard, D.P. Gaillot, J.S. King, C.J. Summers, "Tunable electro-optic photonic crystals fabricated through template directed multi-layer atomic layer deposition," SPIE, Photonics Europe, Strasbourg, France (2006).

29. D.P. Gaillot, E. Graugnard, J.S. King, C.J. Summers, "Photonic bandgap response of structurally modified inverse non-close-packed opals by template directed multilayer atomic layer deposition," SPIE, Photonics Europe, Strasbourg, France (2006).

30. E. Graugnard, J.S. King, S. Jain, Y. Zhang-Williams, I.C. Khoo, C.J. Summers, "Tuning the optical properties of colloidal thin films using dual-frequency liquid crystal," Materials Research Society Symposium, San Francisco, CA (2006).

5.5 Patents

1. "Photonic Crystal Structures", Patent No. 6,999,669, C. J. Summers & W. Park (2006)

5.6 Conference Chairs and Session Chairs

Chair, First International Conference on Science and Technology of Emissive Displays and Lighting, San Diego, Ca	2001
International Program Committee, Tenth International Conference on II-VI Compounds, Bremen, Germany	2001
Overseas Advisor, Seventh International Displays Workshops, Nagoya, Japan	2001
International Program Committee, Tenth International Conference on II-VI Compounds, Bremen, Germany	2001
Program Committee, International Meeting on Inorganic and Organic Electroluminescence, Ghent, Belgium	2002
Chair, International Conference on Science and Technology of Emissive Displays and Lighting, Ghent, Belgium	2002
Co-Chair, Global Phosphor Summit, Scottsdale, AZ, March19-21,	2003
International Program Committee, Eleventh International Conference on II-VI Compounds, Niagara Falls, NY, October	2003
Chair, Global Phosphor Summit, Miami, USA, March	2004
Organizing Committee, Twelfth International Conference on Solid Films and Surfaces, Hamamatsu, Japan	2004
Session Chair, Phosphors for Solid-State Lighting, SPIE Annual Meeting, Denver, 4/5 August,	2004
Co-Chair, Int. Conf. on Science & Technology of Emissive Displays	

and Lighting, Toronto, Canada, September	2004
Session Chair, Nonlinear-Optical Materials, LEOS, Puerto Rico. November	2004
Chair, Global Phosphor Summit, San Diego, California, USA, March	2005
Session Chair, Novel Optical Materials & Applications, Italy, June	2005
Program Committee, Twelfth International Conference on II-VI Compounds, Warsaw, Poland, September,	2005
Session Chair, International Meeting on Chemical Sensors, Bresica, Italy	2006
International Program Committee, Phosphors & Emissive Materials, Korea, 18-20th September	2006
International Display Research Conference, Kent State,	2006

5.7 Graduate Students

Chekesha Liddell (MSE), Ph.D. Thesis: Non-Spherical ZnS Colloids as Building Blocks for Three-Dimensional Photonic Crystals. (Graduated Summer 2003)

Jeff King (MSE), Ph. D. Thesis Title: Fabrication of Opal-based Photonic Crystals using Atomic Layer Deposition. (Graduated August 2004)

Tsuyoshi Yamashita (MSE), Ph.D. Thesis Title: Unraveling Photonic Bands: Characterization of Self-Collimation Effects in Two-Dimensional Photonic Crystals. (Graduated August 2005)

Curtis Neff (MSE), Ph. D. Thesis Title: Optical Properties of Superlattice Photonic Crystals, (Graduated December 2005)

Xudong Wang (MSE), Ph. D. Thesis Title: Patterned and Aligned ZnO 1D Nanostructures: Fabrication, Characterization and Applications (Graduated December 2005)

Zhitao Kang (MSE), Ph. D. Thesis Title: Preparation of new phosphor systems for X-ray detectors and Solid State Lighting (Graduated December 2006)

Davy Gaillot (MSE), Ph. D. Thesis Title: Optical Properties of Complex Periodic Media (2007)

Dawn Hieneman (MSE), M.S., "Atomic Layer Deposition of TiO_2 for Photonic Crystal Waveguides" 2001 – 4/2004

5.8 Post Doctoral Fellows

Dr Jeffrey King, "Non-Close Packed Photonic Crystal Opals", 8/2004 – 1/2006

Dr. Elton Graugnard, "Atomic Layer Epitaxy for Photonic Crystal Applications," 3/2003 – 8/2006

Final Report

Intelligent Luminescent, Display, Communications and Identification
- Liquid Crystal Electro- and Nonlinear Optics-

MURI - Army Research Office

Submitted By:

Principal Investigator: Prof. I. C. Khoo

Electrical Engineering Department
The Pennsylvania State University
University Park, PA 16802
Tel: 814-863-2299 Fax: 814-865-7065   email: ick1@psu.edu

I. Technical Summary

The objectives of this research program are to develop the basic optical materials, optical elements and photonic devices/components that possess properties and performance characteristics required to develop a new generation display and optical signal/image processing devices. These optical elements/components will have built-in sensing and computing functions, and 'inter-pixel' connections that could result in collective responses otherwise not possible from individual 'pixel', in analogy to the well developed neural network employed in digital processing/computing. One physical realization of such collective phenomena is exhibited in self-organizing materials such as colloidal nano-spheres and other nano-particulate that make up photonic crystals. The optical properties of 2- and 3-D photonic crystals [regular array of these nano-particles in 2- or 3-D lattices] are dramatically different from individual nano-particles very much as the optical properties of a crystal [having undergone a phase transition from uncorrelated molecules to well organized crystal lattice] is totally different [and far more useful] than individual molecules.

In these regards, liquid crystals are another important manifestation of self-organized systems which exhibit many optical properties that are entirely different from individual constituent molecules. As a result of the unique phase in which they exhibit both crystalline and fluid properties, liquid crystals possess many unique optical properties that make them particularly interesting and important for both fundamental and applied research. These include a very broadband [near UV – far infrared] birefringence and a large transmission window. The birefringence Δn of liquid crystals has recently reached a value of near unity, but typically it is ~ 0.2, which ranks as the largest among all known optical materials.

2
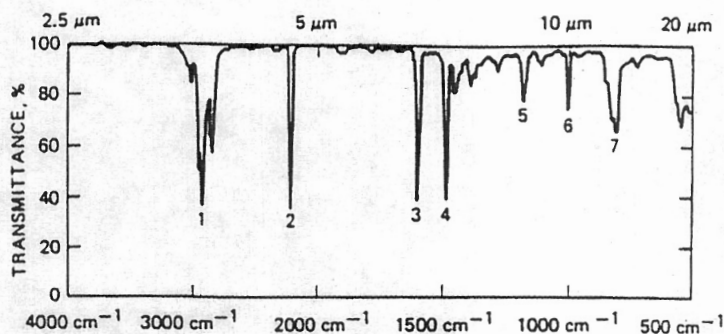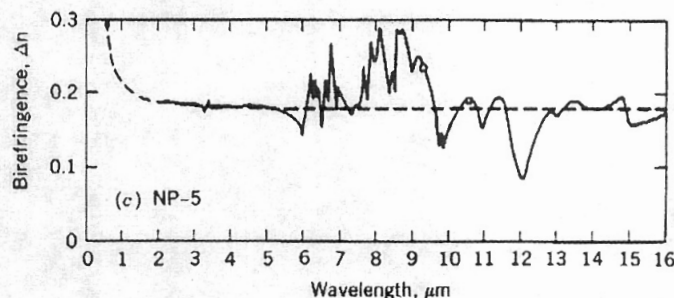
Due mainly to these unique and unusual physical properties, nematic liquid crystals have become the premier materials employed in display and optical information processing devices.

In traditional 'non-intelligent' type of display, the image or signal output is basically a direct reproduction of the input. The input to and output from each individual pixel are not connected. In early part of the program, we demonstrate that by linking nearest neighbors [pixels] to each pixel, and perform a weighted sum for each pixel, one can obtain smart image processing operation such as edge enhancement. An optoelectronic realization of such nearest neighbor connected pixel approach in the form of 'smart' display has been developed previously, and pixilated liquid crystal spatial modulators have been employed to perform various correlation functions.[See for example *K. M Johnson, d. J. Mcknight and I. Underwood, IEEE JQE 29, 699-714 (1993)*]. The drawback of such approach is the VLSI [Very Large Scale Integration] technologies required to fabricate the interconnected pixels and the complexity of the electronics-photonics interconnections and operations.

Our group has approached the problem from a nonlinear optics point of view, and has demonstrated the feasibility of constructing such 'intelligent' display by ***purely or mostly optical*** means [see for example publications #3, #16]. Specifically, we show that the inter-pixel connection can be 'naturally' achieved through the diffraction properties of light wave, and the coupling of light in a nonlinear optical medium [e.g. liquid crystals] to enable image processing functions such as image inversion, edge enhancement, addition and subtraction in an all-optical manner. We have also revisited [both theoretically and experimentally] self-starting optical phase conjugation and how such processes may be incorporated in a holographic associative memory system.

Paralleling these efforts, we have also investigated how such highly nonlinear optical materials could lead to new and enhanced functions when incorporated in photonic crystal matrices. In collaboration with the Georgia Tech group, we have demonstrated very wide electrically tunable Bragg reflection. More recently, we also showed that liquid crystal cladded nano-structures could give very wide tunable optical filters and beam steering functions [see for example publication #28].

The basic mechanisms that enable these operations are the electro-optical and nonlinear optical properties of the liquid crystals. Accordingly, throughout the program, a concerted effort is also devoted to developing extremely nonlinear optical liquid crystals so that the resultant deices can be triggered with very low optical power or threshold electrical voltages [see for example publications # 1, #14]. To date nematic liquid crystals have been conclusively demonstrated to be the most nonlinear optical materials known, with a nonlinear index coefficient n2 that can be as high as 1000 cm^2/W. Such supra-nonlinear optical films allow various nonlinear optical operations with extremely low power threshold requirements.

We have also recently studied dual frequency liquid crystals whose crystalline orientation can be switched to-fro two directions simply by changing the frequency of the applied ac fields at high speed. We have also investigated various nano-dopants capable of photo-conductivity and photo-charge generation and space charge fields to enhance the photorefractive response of nematic liquid crystals. For example, using CdSe nano-rods, we have demonstrated a 20 folds enhancement of the nonlinear index coefficient [see for example publications #10, #21, #29].

II. Summary Achievements

II.A Publications

1. I. C. Khoo, M. Y. Shih and A. Shishido, "Supra Optical Nonlinearities of Photosensitive Nematic Liquid Crystals," Mole. Cryst. Liquid. Cryst. 364, 141-149, (2001).

2. Atsushi Shishido, Ivan B. Diviliansky, I. C. Khoo and Theresa S. Mayer' Suzushi Nishimura, Gina L. Egan, Thomas E. Mallouk, "Direct Fabrication of Two-Dimensional Titania Arrays using Interference Photolithography," Appl. Phys. Letts. 79, 3332-3334 (2001).

3. M. Y. Shih, A. Shishido and I. C. Khoo, " All-optical image processing by means of photosensitive nonlinear liquid crystal film: edge enhancement and image addition/subtraction," Opt. Letts. 26, pp 1140-1142 (2001).

4. Atsushi Shishido, Ivan B. Divliansky, Suzushi Nishimura, Yana Zhang, Thomas E. Mallouk, Theresa S. Mayer, I. C. Khoo, "Nonlinear liquid crystals in periodic structures," Proceedings of Liquid Crystals V –SPIE International Symposium on Optical science and Technology, Vol. 4463 (2001).

5. I. C. Khoo, M. Kaczmarek, M. Y. Shih, A. Shishido, J. Ding, Y. Zhang and M. V. Wood "Communication-wavelength (1.55 µm) laser induced refractive index change in nematic liquid crystalline films," Proceedings of Liquid Crystals V –SPIE International Symposium on Optical science and Technology, Vol. 4463 (2001).

6. Ivan B. Diviliansky, Atsushi Shishido, I. C. Khoo, Theresa S. Mayer, David Pena, Suzushi Nishimura, and Thomas E. Mallouk, "Fabrication of two-dimensional photonic crystals using interference lithography and electrodeposition of CdSe," Appl. Phys. Letts. 79, 3392-3394 (2001).

7. I. C. Khoo, M. Kaczmarek, M. Y. Shih, M. V. Wood, A. Diaz, J. Ding and Y. Zhang, "Nonlinear optical effects in nematic liquid crystal films in the 1.55 µm spectral region," Mol. Cryst. Liq. Cryst. 374, pp. 315-324 (2002).

8. M. Peccianti, G. Assanto, A. De Luca, C. Umeton, M. A. Karpierz, and I. C. Khoo: Light Self-Confinement in Planar Cells with Nematic Liquid Crystals J. Communications Technology and Electronics , 47(7), 790 (2002).

9. G. Assanto, M. Peccianti, C. Umeton, A. De Luca and I. C. Khoo, "Coherent and incoherent spatial solitons in bulk nematic liquid crystals," Mol. Cryst. Liq. Cryst. 375, pp 617-629 (2002).

10. Malgosia Kaczmarek, Min-Yi Shih, Roger S. Cidney and I. C. Khoo, "Electrically tunable, optically induced dynamic and permanent gratings in dye-doped liquid crystals", IEEE J. Quantum Electronics 38, pp 451-457 (2002).

11. I. C. Khoo and J. Ding, "All-optical cw laser polarization conversion at 1.55 micron by two beam coupling in nematic liquid crystal film," Proceedings of Liquid Crystals VI –SPIE International Symposium on Optical science and Technology, Vol. 4799, pp. 31-36 (2002).

12. I. C. Khoo, Yana Zhang, A. Diaz, J. Ding, I. B. Divliansky, Kito Holliday, T. S. Mayer, V. Crespi, D. Scrymgeour, V. Gopalan, "Widely tunable nonlinear liquid crystal-based photonic crystals," Proceedings of Liquid Crystals VI –SPIE

International Symposium on Optical science and Technology, Vol. 4799, pp. 48-53 (2002).

13. I. C. Khoo and J. Ding, "All-optical cw laser polarization conversion at 1.55 micron by two beam coupling in nematic liquid crystal film," Appl. Phys. Letts. 81, pp. 2496-2498 (2002).

14. I. C. Khoo, J. Ding, Y. Zhang, K. Chen and A. Diaz, "Supra-Nonlinear Photorefractive Response of Single-wall Carbon Nanotube- and C60-Doped Nematic Liquid Crystas81," Appl. Phys. Letts. 82, pp. 3587-3589 (2003).

15. I.C. Khoo and A. Diaz, "Nonlinear dynamics in laser polarization conversion by stimulated scattering in nematic liquid crystal films," Phys. Rev. E68 pp 042701-1 to - 4 [2003]

16. I. C. Khoo, K. Chen and A. Diaz, "All-Optical Neural-net like Image Processing with Photosensitive Nonlinear Nematic Film," Optics Letts. 28, pp 2372-2374 [2003].

17. Y. Ye, T. S. Mayer, I. Khoo, I. B. Divliansky, N. M. Abrams and T. E. Mallouk, "Self-assembly of three-dimensional photonic crystals with air-core line defects," J. Mater. Chem. 12, 3637 (2002).

18. I. C. Khoo, Yana Zhang, A. Diaz, J. Ding and K. Chen, "Supra-photorefractivity of C60- and Carbon Nanotube- doped Nematic Liquid Crystals," In Liquid Crystals VII, Proceeding of SPIE International Symposium on Optical science and Technology, San Diego, California August 4-7 (2003)

19. O. Ruzak, N. Collings, W. A. Crossland, T. D. Wilkinson, A. B. Davey and I. C. Khoo, "Dynamic Holographic Gratings in Methyl Red-Doped Nematic Liquid Crystals," J. Non. Opt. Phys. & Mat. Vol 12, pp441-446 (2003).

20. Y. Ye, J. Ding, D. Jeong, I. Khoo and Q. Zhang, "Finite-size effect on one-dimensional coupled-resonator optical waveguides" Phys. Rev. E 69, 056604 (2004).

21. Malgosia Kaczmarek, Andrey Dyaduysha, Sergei Slussarenko and I.C. Khoo, "The role of surface charge field in two-beam coupling in liquid crystal cells with photoconducting polymer layers," J. Appl. Phys. 96, pp. 2616-2623 [2004].

22. I. C. Khoo, J. Ding and A. Diaz, "Dynamics of laser self-induced polarization conversion in nematic liquid crystals," Liquid Crystals VIII - Proceedings of SPIE Vol. 5518. Denver, CO [2004]

23. I. Khoo, Y. Z. Williams, K. X. Chen, "Nonlinear polymer dispersed liquids and liquid crystals for holographic and photonic crystal applications," Liquid Crystals VIII - Proceedings of SPIE Vol. 5518, Denver, CO. [2004]

24. Iam Choon Khoo, Jianwu Ding, and Andres Diaz, "Dynamics of Cross-polarization Stimulated Orientation Scattering in Nematic Liquid Crystal Film," J. Opt. Soc. Am. B 22, pp. 844-851 [2005]

25. 185. Jae-Hong Park and Iam Choon, "Liquid crystal beam steering device with a photopolymer prism," Appl. Phys. Letts 87, 091110- 091112 [2005].

26. I. C. Khoo, Y. Z. Williams, B. Lewis B and T. Mallouk, " Photorefractive CdSe and gold nanowire-doped liquid crystals and polymer-dispersed-liquid-crystal photonic crystals," Mol. Cryst. Liq. Cryst. 446, pp. 233-244 (2005).

27. Yana Williams, Kan Chen, Jae Hong Park, Iam Choon Khoo, Brad Lewis, Thomas E. Mallouk, "Electro-optical and nonlinear optical properties of semiconductor nanorod doped liquid crystals," Liquid Crystal IX, SPIE Proceeding Vol. 5936 [2005]

5

28. E. Graugnard, J. S. King, S. Jain, C. J. Summers, Y. Zhang-Williams and I. C. Khoo, "Electric field tuning of the Bragg peak in large-pore TiO2 inverse shell opals," Phys. Rev. B72, 233105 (2005)

29. I. C. Khoo, Yana Williams, Andres Diaz, Kan Chen, J. Bossard, D. Werner, E. Graugnard and C. J. Summers, "Liquid-Crystals for optical filters, switches and tunable negative index material development," Molecular Crystal Liquid Crystal 453, 309 (2006).

II. B Conference Presentations [* : Invited talk]

*1. I. C. Khoo, "Nonlinear nematic liquid crystals and phototunable 2-and 3-D photonic crystal for visible – 1.55 micron spectral region," Invited Paper – International Conference on Frontiers of Polymers and Advanced Materials, Recife, Brazil, March 4-9, 2001.

*2. I. C. Khoo, "Novel nonlinear optics of liquid crystals," Invited Paper – 5th International Topical Meeting on Novel Optical Materials and Applications, Cetraro, Italy, May 21-26, 2001

3. I. C. Khoo et al, "Communication-wavelength (1.55 μm) laser induced refractive index change in nematic liquid crystalline films ", presented at the SPIE International Symposium on Optical Science and Technology, San Diego, 7/30, 2001.

*4. I. C. Khoo et al , "Nonlinear liquid crystals in periodic structures," Invited paper. SPIE International Symposium on Optical Science and Technology – Liquid Crystal V, 7/2001 San Diego.

*5. I. C. Khoo, "Recent studies of optical limiting, image processing and novel nonlinear optics with nematic liquid crystals," Invited paper, 9th International topical Meeting on Optics of Liquid Crystals, Sorrento, Italy, 10/2001.

*6. I. C. Khoo, "Photosensitive nematic liquid crystals for intelligent photonics," Invited paper. International Symposium on Organic electronic and Photonic Materials and Devices, Osaka, Japan 11/2001.

*7. I. C. Khoo, "Nonlinear Photonics of Liquid Crystals," Materials Ireland Center, Physics Department, Trinity College, Dublin, Ireland, December 11, 2001.

*8. I. C. Khoo, "Liquid Crystal nonlinear optics," Physics Department, Chalmers University of Science and Technology, Goteborg, Sweden. April 4th, 2002.

*9. I. C. Khoo, "New Frontiers in Nonlinear Optical Materials Research", Physics Department, University of Calabria, Cosenza, Italy. May 14, 2002.

*10. I. C. Khoo, "Nonlinear Photonics of Liquid Crystals,"Electrical Engineering Department, Cambridge University, Cambridge, England. May 20, 2002.

*11. I. C. Khoo, Yana Zhang, A. Diaz, J. Ding, I. B. Divliansky, Kito Holliday, T. S. Mayer, V. Crespi, D. Scrymgeour, V. Gopalan, "Widely tunable nonlinear liquid crystal-based photonic crystals," Invited Paper - Liquid Crystals VI –SPIE International Symposium on Optical science and Technology, Seattle, Washington July (2002).

*12. I. C. Khoo, "Nonlinear photonics of liquid crystals," Invited paper. International Conference on Modern Optics and Applications, Bandung, Indonesia July 3-5 (2002).

13. I. C. Khoo and J. Ding, "All-optical cw laser polarization conversion at 1.55 micron by two beam coupling in nematic liquid crystal film," Liquid Crystals VI –SPIE International Symposium on Optical science and Technology, Seattle, Washington. July 8-12 (2002).

14. I. C. Khoo, J. Ding, K. chen and A. Diaz,"High efficiency all-optical polarization conversion of cw 1.55 μm lasers with liquid crystals by non-resonant optical wave mixing," IEEE-Lasers and electro-Optics Society Annual Meeting, Glasgow, Scotland. November 10-14 (2002).

15. I. C. Khoo, Y. Zhang, A. Diaz, J. Ding, I. divliansky, K. Holliday, T. S. Mayer, V. Crespi, D. Scrymgeour and V. Gopolan, "Tunable nonlinear liquid-crystal photonic crystals," IEEE-Lasers and electro-Optics Society Annual Meeting, Glasgow, Scotland. November 10-14 (2002).

*16. I. C. Khoo, "Photorefractivity in Liquid Crystals," Invited Keynote Plenary Seminar at 2003 British Liquid Crystals Society Annual Meeting, Fitzwilliam college, Cambridge University, April 7-10, 2003.

17. O.Ruzak[†], N.Collings[†], W.A. Crossland[†], T.D. Wilkinson[†], I.C. Khoo[‡] "Orientational Photorefractivity for novel OASLMs *[† Photonics and Sensors Group, Department of Engineering, Cambridge University, Cambridge, UK ‡ Department of Electrical Engineering, Pennsylvania State University, University Park, PA, USA]* Presented at 2003 British Liquid Crystals Society Annual Meeting, Fitzwilliam college, Cambridge University, April 7-10, 2003.

18. A. Diaz, I. C. Khoo, J. Ding Y. Zhang, and K. Chen, "Supra-Nonlinear Photorefractive Response of C60 and Single-wall Carbon Nanotube-Doped Nematic Liquid Crystal," Conference on Lasers and Electro-Optics, Baltimore, June 2-5, 2003.

*19. I. C. Khoo, "Supra Nonlinear Optics of Liquid Crystals," in Int. Topical Meeting on Novel Optical Materials and applications NOMA,", Cetraro, Italy June 8-13, 2003

20. A. Diaz and I. C. Khoo, "Nonlinear Dynamics in Polarization Conversion by Stimulated Scattering in Nematic Liquid Crystals," in Int. Topical Meeting on Novel Optical Materials and applications NOMA,", Cetraro, Italy June 8-13, 2003.

21. I. C. Khoo, Yana Zhang, A. Diaz, J. Ding and K. Chen, "Supra-photorefractivity of C60- and Carbon Nanotube- doped Nematic Liquid Crystals," In Liquid Crystals VII, SPIE International Symposium on Optical science and Technology, San Diego, California August 4-7 (2003)

*22. I.C. Khoo[*], A. Diaz, J. Ding, "Multiphoton and excited-state absorptions of an organic liquid for optical transmission control application," Invited Paper, in 'Nonlinear Transmission', SPIE International Symposium on Optical science and Technology, San Diego, California August 4-7 92003).

*23. I. C. Khoo, "Nonlinear Optics of the Mesophases of Liquid Crystals for Optical Power Limiting applications," 3rd International Symposium on Optical Power Limiting, Sedona, Arizona, September 28-Oct. 2 (2003).

24. I. C. Khoo, K. Chen, A. Diaz, J. Ding and Yana Zhang, "All-Optical Neural-net like Image Processing with Local and Nonlocal Nonlinear Optical Thin Films" Lasers and Electro-Optics Society Annual Meeting, Tucson, AZ Oct. 27-31 (2003)

*25. I. C. Khoo, "Nonlinear Optics of the Mesophases of Liquid Crystals" International Conference on Organic Nonlinear Optics, Serak, Korea, November 3-9 (2003).

26. S. Yin, Z. Liu, I. C. Khoo, K. W. Chung, Y Yang, "Tunable photonic crystal fibers and their applications," American Ceramic Society Meeting on Optical Waveguides: Unconventional Approaches and Applications, October 2003, Corning, NY.

*27. I. C. Khoo, "Ultra-large Dynamic Range Nonlinear Absorption Materials" International Conference on Photoresponsive Organics and Polymers, Busan, Korea, Feb. 16-20 (2004).

*28. I. C. Khoo, "Nonlinear Optics of the Mesophases of Liquid Crystals," CREOL, April, 2004

*29. I. C. Khoo, "Nonlinear Optics of the Mesophases of Liquid Crystals," Peking University,[June 11], Tsinghua University [June 14] 2004

30. I. C. Khoo, J. Ding and A. Diaz, "Dynamics of laser self-induced polarization conversion in nematic liquid crystals Liquid Crystals VIII - SPIE Annual *International Symposium on Optical Sciences and Technology*, Denver, CO. August 1-5, 2004.

31. I. Khoo, Y. Z. Williams, K. X. Chen, "Nonlinear polymer dispersed liquids and liquid crystals for holographic and photonic crystal applications", in Liquid Crystals VIII - SPIE Annual *International Symposium on Optical Sciences and Technology*, Denver, CO. August 1-5, 2004.

32. Jae-Hong Park, Iam Choon Khoo, Sin-Doo Lee, "Binary phase gratings in liquid crystal-polymer composites using anisotropic phase separation method", Frontiers in Optics 2004 (The 88th OSA annual meeting), Rochester, NY, October 2004.

33. Jianwu Ding, Iam Choon Khoo, "Orientational photorefractive effect in photo-sensitive-dye doped nematic liquid crystals", Frontiers in Optics 2004 (The 88th OSA annual meeting), Rochester, NY, October 2004.

34. Kan Chen, Iam-Choon Khoo, "Interface Induced Effect in Liquid Crystal Photorefractive Nonlinearity", Frontiers in Optics 2004 (The 88th OSA annual meeting), Rochester, NY, October 2004.

*35. I. C. Khoo, "Liquid crystals-Photonic crystals" Invited paper. Annual Meeting of the IEEE-Lasers and Electro Optics Society, Nov. 8, 2004, Puerto Rico

36. I. C. Khoo, "All-Optical Self-Polarization Switching via two-wave mixing in nematic Liquid Crystals – from visible to infrared", Annual Meeting of the IEEE-Lasers and Electro Optics Society, Nov. 11, 2004, Puerto Rico.

*37. I. C. Khoo, "Holographic fabrication of polymer dispersed liquid crystal photonic crystals," Invited paper, Materials Research Society Fall Meeting, Boston, Dec. 2, 2004

*38. I. C. Khoo, "Liquid Crystals Ultra Broadband All-Optical Devices", 8th Int. Conference on Frontiers of Polymers and Advanced Materials, Cancun, Mexico April 23-28, 2005.

*39. I. C. Khoo, "Fundamentals and Applications of Ultra-Broadband Liquid-Crystal All-Optical and Electro-Optical Properties and Processes," Int. Conference on Photonics, Biophotonics and Nanophotonics, Nanjing, China May 14-19, 2005.

*40. I. C. Khoo, "Electro- and Nonlinear –optical Properties of Liquid Crystals,", 7th Int. Topical Meeting on Novel Optical Materials and Applications," Cetraro, Italy. May 29 – June 4, 2005.

41. Andres Diaz, J. Ding, Kan Chen and I. C. Khoo, "Nonlinear dynamics of stimulated cross-polarization scattering in a nematic liquid-crystal film," in 7th Int. Topical Meeting on Novel Optical Materials and Applications," Cetraro, Italy. 6/2005.

42. Yana Williams, Kan Chen, Jay Hong Park, I. C. Khoo, B. Lewis and T. Mallouk, "Photorefractive effect in semiconductor nanorod doped liquid crystal," 7th Int. Topical Meeting on Novel Optical Materials and Applications," Cetraro, Italy. 6/2005.

43. Y. Zhang-williams, K. Chen, J. H. Park, J. Ding, A. Diaz and I. C. Khoo, "Nonlinear and Tunable photonic crystals with nano-particulate doped polymer dispersed liquid crystals," In *Liquid Crystal Conference IX* - SPIE Symposium on Optics and Photonics, San Diego, California 8/2005. Proceeding Vol. 5936

44. Kan Chen, Y. Zhang-Williams, J. H. Park, A. Diaz and I. C. Khoo, "Light induced photorefractive effect threshold lowering in pure nematic liquid crystal cells," In *Liquid Crystal Conference IX* - SPIE Symposium on Optics and Photonics, San Diego, California 8/2005. Proceeding Vol. 5936.

*45. E. Graugnard, J. S. King, D. Gaillot, C. J. Summers, Y. Zhang-williams and I. C. Khoo, "Liquid crystal infiltration of template patterned 3-D photonic crystals," Invited Paper in *Conference on Tuning the Optical Response of Photonic Bandgap Structures II* – SPIE Symposiumon Optics and Photonics, San Diego, California, 8/2005.

46. I. C. Khoo, Jay Hong Park, Yana Z. Williams, Kan Chen and Andres Diaz, "Liquid Crystals for switching, frequency filters and tunable negative index material development", in *Optics of Liquid Crystals* conference," Clearwater, Florida, 10/2005.

47. Jae Hong Park and I. C. Khoo, I. C. Khoo, "Liquid crystal beam steering device with a photopolymer prism ," in *Optics of Liquid Crystals* conference," Clearwater, Florida 10/2005.

*48. I. C. Khoo and A. Diaz, "Self-action cw-pulsed lasers and glares attenuators," Invited paper, IEEE-Lasers and Electro-Optics Society Annual Meeting, Sydney, Australia [10/2005].

II.C Invention Disclosure

- I. C. Khoo, "*All-optical polarization rotation, switching, and optical limiting device for broadband [0.4 micron -1.5 micron] application*". PSU Invention Disclosure #2002-2692. Filed on August 8, 2002. [Army]

- I. C. Khoo, "Fiber Array with Two-Photon+Reverse-Saturable Absorbing core for optical limiting and eye/sensor protection against agile frequency short-pulsed lasers". PSU Invention Disclosure #2002-2707. Filed on Oct. 8, 2002 [Army and Navy]

II.D Ph. D and Master Graduates
1. Min-Yi Shih [Ph. D. EE, 2001]

Thesis Title: Investigation and applications of nonlinear optics by dopant enhanced nematic liquid crystal films

2. Michael V. Wood [Ph. D. EE, 2001]
   Thesis: An investigation of nonlinear cored fiber structures for optical limiting applications.

3. Benjamin Campbell [MS. 2003]
   Thesis: A Further Study of the Laser Balation Characteristics of Mercury Cadmium Telluride for the Purpose of Forming P-N Junctions and Other Micro Applications.

4. Andres Diaz [Ph. D. 2003]
   Thesis: Theory and Applications of Molecular and Collective Nonlinear Optical Behavior of Nematic Liquid Crystals.

5. Jiangwu Ding [Ph. D. 2005]
   Thesis: Wave-mixing and Photorefractivity in Liquid Crystals

II.E Technology transfer
   1. Army Research Office SBIR Phase II- [Beam Corporation, Winter Park, Fl]
   Nano-dispersed liquid crystals for image processing and optical limiting devices

2. Navy Air Warefare Center, Patuxent River, Maryland – Development of Helmet-mount eye/sensor protection against short-pulsed agile frequency laser [SRI International, CA].

3. Wright Patterson Air force Base SBIR Phase II [BEAM Corporation, Winter Park, Florida] – Next generation liquid crystal spatial light modulator and holographic image processing films, and also low threshold cw-light source optical limiting devices.

Final Report

Unviersity of Florida MURI Activities on
Intelligent Luminescence for Communication, Display and Identification

Prepared by:
Paul Holloway
Department of Materials Science and Engineering
University of Florida
Gainesville, FL 32611-6400
352-846-3330
pholl@mse.ufl.edu

Participating Faculty at the University of Florida
Paul Holloway, Susan Sinnott, David Norton, Mark Davidson

Summary

Research in intelligent luminescence at the University of Florida was conducted in four areas. The first area was development of novel luminescent sources, and progress was reported in polymer light emitting diodes (PLEDs), alternating current thin film electroluminescent (ACTFEL) devices emitting in the visible and near infrared, in luminescent nanoparticles (quantum dots-Qdots) and Qdot direct current electroluminescent (DCEL) devices. The second area was semiempirical calculations of the effects upon luminescence of structural changes produced by derivative groups on polymeric oligomers. Specifically, emission from monomers and copolymers of polythiophene vinylene and poly para-phenylene vinylene (TV-PPV), TV-PPV with cyano substitution, TV-PPV with $-O-CH_2-CH_3$ substitution, and unsubstituted poly(3,4 – ethylenedioxythiophene - vinylene – para-phenylene vinylene) or PEDOT-V-PPV were calculated, as was the Stokes shift in the unsubstituted single monomer of TV-PPV. In the third area, ZnO was synthesized as thin films or nanoparticles and its use was demonstrated in transparent field effect transistors, as a p-type thin film semiconductor, as ZnMgO nanorods, and as nanoparticle sensitizers in $SiO_2:Eu^{2+}:ZnO$ and $SiO_2:Ce^{3+}:ZnO$ phosphors. In the fourth area, optoelectronic circuits were designed and shown to produce the three basic functions of the Cortoconic model of the brain. These circuits were bread boarded and incorporated into a 3x4 array on a mother board and are ready to demonstrate an intelligent display.

Objectives of Research

The objectives of this research project was to develop new materials that exhibit photoluminescence and electroluminescence at visible and near infrared wavelengths, develop computational methods to predict the wavelength and intensity of photoluminescent organic and inorganic materials, develop transparent ZnO with low electrical resistivity, and develop an optoelectronic bread board circuit of a small array of pixels to emulate simple functions described by the Corticonic model of the human brain.

Results from Research

I. Electroluminescent Materials and Devices (Paul Holloway and Mark Davidson)

Materials and devices that were electroluminescent in the visible and near infrared (NIR) were demonstrated. Specifically, NIR emission from lanthanide ligands in polythiophenes was demonstrated, and the rates and mechanisms of loss of emission intensity from conjugated polymer light emitting devices (PLEDs) were studied.

I.1 NIR Emission from PLEDs

Near-infrared- emitting polymer light-emitting diodes (PLEDs) have been fabricated using blends of conjugated polymers and lanthanide tetraphenylporphyrin complexes. Host polymers include MEH-PPV and a bis-alkoxy-substituted poly(p-phenylene) (PPP-OR11), and the lanthanide complexes include Yb(TPP)acac and Er(TPP)acac (where TPP = 5,10,15,20-tetraphenylporphyrin and acac = acetylacetonate). Electroluminescence (EL) is observed at 970 nm from devices fabricated using MEH-PPV or PPP-OR11 blended with Yb(TPP)acac, and EL is observed at 1560 nm from a device fabricated using a blend of MEH-PPV and Er(TPP)acac. Visible EL from the host polymer was strongly suppressed in all of the devices. In the device fabricated using the PPP-OR11 polymer, blue emission from the host is completely quenched. Very efficient quenching of the visible EL from the host in the PPP-OR11 device is believed to occur due to efficient Förster energy transfer, which is facilitated by the excellent spectral overlap between the PPP-OR11 fluorescence and the Soret absorption band of the TPP ligand.

I.2 Degradation of PLED Emission Intensity

Bubble formation on calcium/aluminum contacts to bilayer poly(n-vinyl carbazole) (PVK)/poly(3,4-ethylenedioxythiophene)-poly(4-styrenesulfonate) (PEDOT-PSS) polymer light-emitting devices (PLEDs) was studied using optical and electron microscopies and Auger electron spectroscopy (AES). The formation of bubbles was shown to correlate with pinholes in the metal contact thin film and with excess absorbed water, primarily in the PEDOT-PSS layer, in the presence of the calcium layer. AES data show oxidation at the Ca/Al interface during this process. Gas evolution and relaxation of compressive stress when voltage is applied to the PLED devices were postulated to cause formation of the bubbles.

Further, the mechanisms leading to decay of blue light emission from conjugated polymer light emitting devices (PLEDs) constructed with a bis-alkoxy-substituted poly(p-phenylene) derivative (PPP-OR11) emissive layer were studied. The PLED consisted of an ITO transparent conducting oxide, coated with a layer of poly(3,4-ethylenedioxythiophene) doped with poly(styrene sulfonate) (PEDOT-PSS), the PPP-OR11 layer, and a top electrode of 10 nm Ca covered by 200 nm of Al. Significant degradation was observed after only 15 min. of operation in laboratory air due to development of non-emissive areas which appeared as black spots, similar to devices made with tris-(8-hydroxy-quinolinate) aluminum (Alq$_3$), poly(phenylene vinylene) (PPV) and poly(vinyl carbazole) (PVK). Scanning electron micrographs showed that the metal cathode layers (Ca/Al) often was delaminated from the emissive polymer layer and

formed bubbles during this degradation. It was concluded that the 'black spot' mechanism of degradation was the same for Alq$_3$, PVK and PPP layers, and resulted from the surface topography of the PEDOT-PSS layer leading to reactions of water with the metallic electrodes.

I.3 NIR Emission from Doped ACTFELDs

Novel infrared (IR) electroluminescent (EL) thin film phosphors were radio frequency magnetron sputter deposited by co-sputtering of an undoped ZnS target together with ZnS: 1.5 mole% ErF$_3$ or ZnS: 1.5 mole% NdF$_3$ targets. The ZnS:ErF$_3$ and ZnS:NdF$_3$ thin film phosphors were annealed in a N$_2$ ambient at temperatures ranging from 350-475°C for an hour to increase radiance. The maximum EL radiance observed was 28μW/cm^2 at 1550nm for ZnS:ErF$_3$, and 26μW/cm^2 at 910nm and 15μW/cm^2 at 1060nm for ZnS:NdF$_3$ (at 40V above the threshold voltage) after a 425°C, 1 hour anneal in nitrogen. For anneals above 425°C visible emission increased, while NIR emission from both ZnS:ErF$_3$ and ZnS:NdF$_3$ was either constant or decreased. For ZnS:ErF$_3$, the 1550 nm near infrared (NIR) peak decreased, but the 990 nm peak remained constant in intensity. The crystallinity of ZnS was improved by annealing, and these results are consistent with the postulate that residual defects limit the acceleration of 'hot' electrons for anneals at T $\leq$ 425°C. Under these conditions, hot electrons only have sufficient energy to excite Er^{+3} into the lower lying ^{4}I$_{13/2}$ excited state which leads to 1550nm NIR emission. With increasing annealing temperatures, hot electrons can excite from the ^{4}I$_{15/2}$ ground state into higher energy excited states (e.g. the ^{4}F$_{7/2}$ state for 990nm emission). The near IR emissions from ZnS:NdF$_3$ at 910 and 1060nm originate from the same excited state and both peaks exhibited maximum NIR intensities after annealing at 425°C. While the emission spectra from Er were independent of annealing temperature, peak shifts were observed for Nd. These shifts were discussed in terms of the nephelauxetic effect and hybridization of the 5d-4f orbitals.

Using a full factorial design-of-experiment procedure, near infrared emission at a wavelength of 1.55 μm from zinc sulfide (ZnS) doped with erbium trifluoride (ErF$_3$) has been studied in alternating current thin film electroluminescent devices (ACTFELDs). The thin film phosphors were deposited by radio frequency (RF) planar magnetron sputtering of a 1.5 mol% ErF$_3$-doped ZnS target and an undoped ZnS target. The intensity of near infrared emission is related to the processing parameters used in film deposition and post-deposition annealing. Thin films, approximately 650 nm thick, were deposited at 100 W from both targets. Deposition temperature, duty cycle, sputtering gas pressure and post-deposition annealing temperature were varied. As deposition temperature was increased from 120 °C to 150 °C, the near infrared electroluminescence increased by ~180% at an operating voltage 20 volts above the threshold voltage (B$_{20}$). This is attributed to better activation of erbium luminescent centers on zinc lattice sites results in a greater number of radiative events, increasing luminescence. Increasing the duty cycle applied to the ZnS:ErF$_3$ doped target from 25% to 75%, increased the electroluminescence at B$_{20}$ by ~650%. This is attributed to a greater number of ErF$_3$ dopants incorporated into the phosphor. As the sputtering gas pressure increases from 1 mTorr to 24 mTorr, the electroluminescence at B$_{20}$ increases by ~80%. At lower pressure, the phosphor undergoes negative ion resputtering removing zinc and sulfur from the film. This creates a film with a higher proportion of ErF$_3$ dopant incorporated. After film

deposition, half of the phosphor films underwent annealing at 425 °C for 1 hour in ultra high purity nitrogen. Annealing the films increased electroluminescence at B_{20} by ~60%. The increase in brightness correlated with a reduction in fluorine concentration in the film. Additionally the number of sulfur vacancies is likely reduced. This probably alters the local crystal field around the erbium dopant, allowing for more adequate pathways for the near-infrared transitions, thus increasing the overall near infrared luminance. The highest brightness was observed for a deposition temperature of 150 °C, a duty cycle of 75%, argon sputtering gas pressure of 24 mTorr and post-deposition annealing at 425 °C. These conditions resulted in a brightness of the 1550 nm emission peak of 146 $\mu W/cm^2$ at 20 V above threshold.

Near-infrared (NIR) electroluminescent (EL) from ACTFELDs based on gallium nitride (GaN) doped with rare earth (RE) elements was also studied. The RE-doped GaN NIREL devices were fabricated with a thin-film multilayered structure in the metal-insulator-semiconductor-metal (MISM) configuration, which consists of a glass substrate, an indium-tin-oxide (ITO) transparent conducting electrode, an alumina-titania (Al_2O_3-TiO_2) dielectric layer, a RE-doped GaN NIR light-emitting layer, and an aluminum top electrode. The RE-GaN layer was deposited using planar magnetron sputtering. Strong NIR EL emission at wavelengths of 800, 1082, and 1550 nm was observed at room temperature from the trivalent thulium (Tm^{3+})-, neodymium (Nd^{3+})-, and erbium (Er^{3+})-doped GaN NIR EL devices, respectively. The fabricated RE-doped GaN NIR EL devices exhibited sharp turn-on voltages at 140-150 V and external power efficiencies of ~10^{-6}–10^{-5}, measured at 40 volts above the threshold voltage.

I.4 Visible EL from ZnS:Mn and CdS:Mn/ZnS Core/Shell Quantum Dots

Syntheses, characterization, and applications of two different Mn-doped semiconductor nanocrystals, ZnS:Mn and CdS:Mn/ZnS core/shell, were investigated. ZnS:Mn nanocrystals with sizes between 3 and 4 nm were synthesized via a competitive reaction chemistry. A direct current (DC) electroluminescent (EL) device having a hybrid organic/inorganic multilayer structure of an indium tin oxide (ITO) transparent conducting electrode, a (poly(3,4-ethylenedioxythiophene) /poly(styrenesulfonate) (PEDOT-PSS) and a poly(N-vinylcarbazole) (PVK) bilayer hole transport film, a ZnS:Mn nanocrystal layer, and Al dot contacts was demonstrated to emit blue (~445 and ~495 nm) from PVK and yellow (~600 nm) light from Mn activator in ZnS. The EL emission spectrum was dependent upon both the voltage and Mn concentration, showing a decreasing $I_{ZnS:Mn}/I_{PVK}$ emission ratio of 10 at 20 V to 4 at 28 V, and an increasing ratio of 1.3 at 0.40 mol % to 4.3 at 2.14 mol % Mn.

Mn-doped CdS core nanocrystals were produced ranging from 1.5 to 2.3 nm in diameter with a ZnS shell via a reverse micelle process. In contrast to CdS:Mn nanocrystals passivated by n-dodecanethiol, ZnS-passivated CdS:Mn (CdS:Mn/ZnS core/shell) nanocrystals were efficient and photostable. CdS:Mn/ZnS core/shell nanocrystals exhibited a quantum yield of ~18 %, and the PL intensity increased by 40 % after 400 nm UV irradiation in air. X-ray photoelectron spectroscopy (XPS) data showed that UV irradiation of CdS:Mn/ZnS nanocrystals induced photooxidation of the ZnS shell surface to $ZnSO_4$. This photooxidation product is presumably responsible for the increased PL

emission by serving as a better passivating surface layer. Luminescent lifetime data from the core/shell nanocrystals could be fit with two exponential functions, with a time constant of ~170 nsec for the defect-related centers and of ~1 msec for the Mn centers. The CdS:Mn/ZnS nanocrystals with a core crystal diameter of 2.3 nm and a 0.4 nm thick ZnS shell were used as an electroluminescent material. EL devices were tested having a hybrid organic/inorganic multilayer structure of ITO//PEDOT-PSS//conjugated polymer//CdS:Mn/ZnS nanocrystal//Al. Orange and green EL emissions were observed from devices with PVK or poly(p-phenylene vinylene) (PPV) devices, respectively. These observations are shown to be consistent with the energy level diagrams and interfacial barriers of the EL devices.

II. Computational Analysis of Luminescence (Susan Sinnott)

The emission spectra were calculated based on the optimized excited state geometry. In particular, the ZINDO, an Intermediate Neglect of Differential Overlap (INDO) semi-empirical electronic structure method, and time dependant-density functional theory methods within the *GAUSSIAN 03* software suite were used.

The structural changes produced by derivative groups on polymeric oligomers were predicted to have a significant effect on the optical properties of the oligomers. When molecules were forced to be planar, all substitutions lead to a red shift of the lead absorption peak. This forced configuration helped the monomer maintain π-overlap and steric repulsions were relieved by changes in the bond angle, as opposed to changes in the dihedral angle seen in the freely relaxed structure. Planar configurations could be obtained at times in crystalline polymers in the solid state and steric interactions with other chains maintained these configurations. In solution, vacuum, or non-crystalline materials, the torqued chain appeared more readily. Contortions of the chains caused a blue shift but also reduced the quantum efficiency of luminescence.

Emissions were calculated for a variety of monomer units that maintained a planar configuration in both the monomer and elongated oligomer form. The absorption/emission spectra for a variety of single monomer structures were determined, including copolymers of polythiophene vinylene and poly para-phenylene vinylene (TV-PPV), TV-PPV with cyano substitution, TV-PPV with $-O-CH_2-CH_3$ substitution, and unsubstituted poly(3,4 – ethylenedioxythiophene - vinylene – para-phenylene vinylene) or PEDOT-V-PPV. The Stokes shift in the unsubstituted single monomer of TV-PPV was calculated as 56 nm. Additions of electron donating groups to both conjugated chain and to the thiophene ring away from the conjugated chain result in a comparable increase in the Stokes's shift to 64 nm. Additions of electron withdrawing cyano groups to the conjugated chain lead to a greater increase in the Stokes's shift to 77 nm. Aside from the effect on the electron density, additions also affected the geometry of the excited state. In the case of the cyano addition, a large distortion from the planar geometry was observed, which contributed to the increase in the Stoke's shift.

III.   ZnO Conductors (David Norton, Paul Holloway)

III.1 Transparent ZnO Activity

In this project, we addressed the challenges in transparent thin film transistors (TTFT) in which transparent semiconducting oxides are used as the FET active channel materials, with transparent conducting oxides used as the source, drain, and gate metals. The primary interest are TTFT devices that operate in enhancement mode exhibiting a normally off (gate voltage $V_g = 0$) channel state. The focus is on unipolar FET structures in which the channel is a transparent semiconducting oxide with interconnects that are heavily doped transparent conducting oxide, all deposited on a glass substrate.

Thin-film field effect transistors can be bipolar (e.g. n^+-type semiconducting source and drain with p-type channel) or unipolar (n^+ metallic source/drain with n-type channel) in structure and function. A significant advantage of unipolar (single carrier type) FET devices is that they alleviate the difficulties encountered in p-n junction formation. With low carrier densities in the channel, one can operate in the enhancement mode, in which the channel conductance is low in the absence of an applied gate voltage. Most conventional a-Si:H TFT devices use an undoped amorphous Si:H layer as the channel and operate in the enhancement mode. In contrast, if a gate bias voltage is needed in order to deplete the channel of carriers, this is referred to as depletion mode. For low power displays, the primary interest is in TTFT devices that operate in enhancement mode exhibiting a normally off (gate voltage $V_g = 0$) channel state. To date, TTFT research for display electronics has focused on unipolar FET structures in which the channel is a transparent semiconducting oxide, the source and drain are heavily doped transparent conducting oxide, all deposited on a glass substrate. This device geometry is quite analogous, both in fabrication and desired performance, to previous activities directed at compound semiconductor (e.g. CdSe) thin film transistors.

A distinction should be made between a transparent semiconducting oxide (TSO) and transparent conducting oxide (TCO) based on the differing carrier densities for channel and interconnect performance. For the channel, significant modulation of the channel conductance is needed to achieve FET switching. For this, only moderate carrier densities (semiconducting behavior) are needed. For interconnects, TCOs with high conductivity are needed. Each of these materials is required to have significant transparency in the visible spectrum. Two problems emerge from TCO or TSO materials with marginal bandgaps for visible light transparency. First, the eventual polycrystalline nature of the functional device introduces defects that extend the optical absorption into the bandgap. This reduces the efficiency of the devices, particular at the blue end of the spectrum where luminescence is weakest. Second, the optical absorption by the channel region can lead to band-to-band excitations of carriers and subsequent shifting of transistor characteristics. For these reasons, TSO channel materials with bandgaps well above the visible absorption limit are of most interest. For future development of drive and/or computational electronics, it may prove advantageous to also have bipolar device structures. However, the focus of efforts to date has been on unipolar FET structures.

Different channel materials can be considered for polycrystalline FET development. Although most device applications of interest focus on inexpensive glass as the substrate of choice, experiments have also included epitaxial (on single crystals) channel materials in order to delineate the effects of crystallinity and grain boundaries on device performance. A key issue is to identify transparent materials that are suitable for use as channel materials in thin-film FET structures. Relevant factors include carrier density, carrier mobility, crystallinity, surface morphology, optical absorption, and photoconductivity over the visible spectrum. The latter is relevant to the stability of the TTFTs when coupled to PLED emitters. The primary focus for TSOs has been on materials with higher electron mobility and easily controlled carrier densities.

Zinc oxide has many characteristics that make it attractive for transparent electronics. ZnO is an n-type, direct bandgap semiconductor with $E_g = 3.35$ eV. The room temperature Hall mobility in ZnO single crystals is on the order of 200 cm^2 V^{-1}sec^{-1}. ZnO normally has a hexagonal (wurtzite) crystal structure with a = 3.25 Å and c = 5.12 Å. Each Zn atom is tetrahedrally coordinated to four O atoms, where the Zn d-electrons hybridize with the O p-electrons. Layers occupied by zinc atoms alternate with layers occupied by oxygen atoms. Electron doping via defects originates from Zn interstitials in the ZnO lattice. The intrinsic defect levels that lead to n-type doping lie approximately 0.05 eV below the conduction band. High electron carrier density can also be realized via group III substitutional doping. The growth of ZnO thin films has been demonstrated using a number of deposition techniques, including sputtering, pulsed-laser deposition (PLD) and molecular beam epitaxy.

In the present discussion, the fabrication and properties of top-gate-type thin film transistors using n-type ZnO as the active channel layer are described. $(Ce,Tb)MgAl_{11}O_{19}$ (CTMA) was chosen as the gate dielectric. A top-gate-type TFT geometry was realized using standard photolithography processing. The initial substrate material is commercial tin-doped indium oxide (ITO) coated glass. First, the ITO source and drain regions are defined using photolithography, with wet etching of the ITO performed with dilute HCl. After removing the source/drain photoresist patterns, ZnO is then deposited as the active channel layer on the ITO patterned glass substrate. An amorphous $(Ce,Tb)MgA_{11}O_{19}$ gate dielectric layer is then deposited on top of the ZnO. The gate aluminum electrode is formed by sputtering at room temperature. The gate electrode region is then defined with contact-mode photolithography alignment followed by selective wet etching aluminum, gate dielectric and channel layers with dilute phosphoric acid down to the ITO and the substrate. For these devices, the channel width and length are 90μm and 50μm, respectively.

One important aspect of oxide-based TTFT development is in controlling the transport properties of the channel material. For the devices discussed, pulsed laser deposition (PLD) was used to deposit the ZnO thin film channel. With pulsed laser deposition, stoichiometric transfer of target material to the substrate is generally accomplished, irrespective of the vapor pressure of individual constituent atoms in the material. A KrF excimer laser (λ=248 nm) was used as the ablation source. A laser repetition rate of 1 Hz was applied, with a laser pulse energy density of 300mJcm^{-2}. The deposition conditions

for ZnO thin films on glass substrates (Corning 7059 glass) focused on deposition at 400°C in an oxygen pressure ranging from 2mTorr to 300mTorr. Phosphorus-doped ZnO and (Zn,Mg)O thin films were also investigated as the channel materials, where the phosphorus served as a deep acceptor for controlling the carrier density. Post-annealing processes at 600°C and 100 Torr oxygen pressure for 1 hr were carried out to further lower the carrier concentrations of the thin films. The crystallinity of the ZnO samples was evaluated by X-ray diffraction. Resistivity, carrier concentration and Hall mobility of the films under different growth conditions were measured by four-point Van der Pauw Hall measurement. The surface morphology image of the ZnO films was obtained by an atomic force microscope (AFM). The cross section view of the ZnO/CTMA/ITO/glass structure was also observed using Scanning Electron Microscopy (SEM) in order to investigate the interface.

The electrical properties (carrier concentration, Hall mobility and resistivity) of the undoped polycrystalline ZnO thin films as a function of oxygen pressure during growth were measured. Note that all of the films are deposited on bare glass and post-annealed at 600°C in 100 Torr oxygen. For films deposited at $P(O_2) = 20$ mTorr, a Hall mobility of 26 cm^2 V^{-1}s^{-1} was realized. With increasing oxygen pressure, the n-type carrier concentration steadily decreases. This behavior reflects a suppression oxygen vacancies and/or Zn interstitials as growth pressure increases. These defects contribute shallow states near the conduction band in ZnO, thus inducing free electrons. While it is desirable to maximize the mobility in the active channel layer of the TFT structure, it is perhaps more important to minimize carrier density as it is the movement of charge density into and out of the channel region that yields FET functionality.

Crystallinity is an important factor is determining the transport properties of the channel material. One interesting aspect of ZnO is its strong tendency to maintain uniaxial texture in polycrystalline films deposited on almost any substrate. A XRD pattern of an undoped ZnO film grown on a glass substrate at P_{O2}=20mTorr showed that the (002) and (004) ZnO diffraction peaks are predominant indicting c-axis orientation in this polycrystalline film. However, this uniaxial texture does not eliminate grain boundaries. Grain size is on the order of 100-150 nm. In a field-gated structure, one must carefully consider the effect of grain boundary conductance and charge density when attempting to model the field-effect characteristics.

In order to field gate this structure, it is necessary to form either a Schottky barrier or gate oxide. For ZnO, Schottky barriers are low and are apparently unsuitable for field gated rectifying structures. For oxide gates, the gate dielectric must be chosen to have a band offset with the channel material so as to avoid carrier injection into the conduction band and/or valence band of the gate insulator. For wide bandgap semiconductors, such as ZnO, this necessitates the use of the larger bandgap oxides and precludes the use of many insulators being considered for field gated structures on other semiconductors. In this work, an aluminate was selected, namely $(Ce,Tb)MgAl_{11}O_{19}$ (CTMA), as the gate dielectric for the TFT. First a ZnO thin film of about 200nm was formed on the commercial Tin-doped Indium oxide coated glass substrates under the formerly described conditions. Then CTMA layer of the same thickness was deposited onto the ZnO. Finally,

200μm diameter aluminum electrodes were sputtered on the top. The leakage current-voltage characteristics of the two-terminal structure were used to evaluate the properties of the gate dielectric. Low leakage current about 10^{-7} A cm^{-2} can be obtained for this structure.

The electrical characteristics of the TFT device with undoped ZnO as the channel layer were measured. For this device structure, the ZnO film thickness was 20nm. This TFT device operates as an n-channel, normally-on device, as evident from the fact that a negative voltage is required to deplete the carriers in the channel layer. Note that the device drain currents I_{DS} are large, of order of mA, in its "ON" state is due to the high carrier concentration in the channel layer.

For efficient TTFT operation, an enhancement-mode device is preferable over depletion-mode, thus avoiding the need to apply voltage in order to turn the device off. Much less power dissipation is possible when normally-off, enhancement-mode devices are employed. For this motivation, alternative channel materials have been investigated in order to further decrease carrier density. Phosphorus-doped ZnO and (Zn,Mg)O have been deposited as the active channel layer for the TFT. A significant decrease in carrier density was obtained in P-doped ZnO subjected to a post-deposition oxygen annealing processes. For P-doped ZnO based TFT, the device has the same depletion-mode operation as the undoped ZnO one. A saturation of I_{DS} (pinch-off) is observed for small values of V_{DS}. This pinch-off behavior indicates that the channel layer is sufficiently depleted in this TFT. Carrier density as low as 3.9×10^{16} cm^{-3} was obtained for this channel materials, which is two orders lower than that in the undoped ZnO thin film. We also determined the field-effect (FE) mobility to be about 5.32 cm^2 V^{-1}s^{-1}, by being calculated from the linear part of the drain current-voltage curve.

III.2   p-Type ZnO Activities

One of the critical issues in developing ZnO optoelectronic devices is to realize low resistivity, high carrier density p-type ZnO material. While n-type ZnO is easily realized via Al, Ga or In doping, p-type doping ZnO has proven difficult to achieve. Several theoretical and experimental investigations have addressed this asymmetry in n-type versus p-type doping in ZnO. Low formation energies for intrinsic donor defects such as oxygen vacancies (V_O) and zinc interstitials (Zn_i) contribute to n-type doping compensation. Recent research in p-type dopants has focused on group V ions substituted on the O site. While there have been significant activities focused on nitrogen doping, few reported efforts have addressed phosphorus doping. Nevertheless, *p-n* junction-like behavior has been reported between an n-type ZnO substrate and a surface layer that was heavily doped with phosphorus. Work by K. Kim *et al.* on P-doped ZnO films showed that post-activation processing could yield phosphorus doped p-type ZnO grown by sputter deposition. Of significant importance for LED structures is p-type conductivity in (Zn,Mg)O films needed for carrier confinement. Previous results on phosphorus-doped (Zn,Mg)O device structures, in particular C-V and I-V characteristics, indicate that phosphorus yields an acceptor state and p-type behavior. However, these materials did not yield an unambiguous positive Hall voltage, presumably due to the low mobility and high carrier compensation.

In this project, an unambiguous positive Hall coefficient in phosphorus-doped (Zn,Mg)O epitaxial films grown on the undoped ZnO buffer layers is reported. The effect of oxygen partial pressure on the carrier type is described. In particular, at low oxygen growth pressures, phosphorus-doped (Zn,Mg)O films are n-type, but are p-type when grown at higher oxygen growth pressure. The residual donor concentration was systematically reduced with increasing oxygen partial pressure.

The phosphorus-doped $(Zn_{0.9}Mg_{0.1})O$ epitaxial films were grown via pulsed laser deposition (PLD) on c-plane sapphire substrates. The target was fabricated using high-purity ZnO (99.9995%) and MgO (99.998%), mixing with P_2O_5 (99.998%) as the doping agent. The phosphorus doping level in the target was 2 at%. The motivation for examining phosphorus doping in Mg-doped ZnO is two-fold. First, p-type (Zn,Mg)O will be necessary for LED heterostructures in which carrier confinement for efficient electron-hole recombination is needed. Second, the addition of Mg shifts the conduction band edge to higher energy, perhaps increasing the activation energy of the defect donor states. The laser ablation conditions for film growth have been described in the previous work. The ZnO growth chamber base pressure was 4×10^{-6} Torr. An undoped ZnO buffer layer (~50nm) was initially deposited at 400C and 20mTorr oxygen partial pressure before the growth of P-doped $(Zn_{0.9}Mg_{0.1})O$ films. Introducing a nucleation layer grown at lower temperature on sapphire prior to growing the active layer improves reproducibility and crystallinity. The undoped ZnO buffer layer was post-annealed at 650C in flowing O_2 for 1h in order to decrease the electron conductivity. Semi-insulating buffer layers are preferable in order to perform Hall measurements without influence from buffer layer conduction. With this post-anneal, the electron concentration of the undoped ZnO buffer films was reduced from 10^{16} cm^{-3} to 10^{14} cm^{-3}. The phosphorus-doped $(Zn_{0.9}Mg_{0.1})O$ films were then deposited on the annealed undoped ZnO buffer layer at a substrate temperature of 500C under oxygen partial pressure ranging from 20 mTorr to 200 mTorr. The total film thickness ranged from 500 to 700 nm. Four-point Van der Pauw Hall measurements were performed at room temperature to examine the transport properties of the P-doped $(Zn_{0.9}Mg_{0.1})O$ films. The film crystallinity and surface morphology were investigated using X-ray diffraction (XRD) and atomic force microscopy (AFM).

For many samples, a persistent n-type photoconductivity was observed that complicated the transport characterization. To eliminate the photoconductivity relaxation effect on the transport properties, the samples were maintained in the dark for 12 h prior to performing Hall measurements. Using this procedure, the carrier density and conduction type of P-doped $(Zn_{0.9}Mg_{0.1})O$ films was determined. Each sample was measured a minimum of twenty times to obtain the average results reported. Films deposited at oxygen partial pressures lower than 100 mTorr show n-type. With increasing oxygen pressure, the hole concentration increases whereas the electron concentration continuously decreases. Unambiguous conduction type was not observed for the samples grown at 100 and 120 mTorr apparently due to near-equivalent concentrations of holes and electrons in the films. When the oxygen partial pressure was increased to 150 mTorr during the deposition process, the Hall-effect data show consistent p-type carrier type. Interestingly, if the oxygen partial pressure was increased up to 200 mTorr, the films reverted to an

indeterminate carrier type. The indeterminate carrier type films yield large standard deviations compared with those with unipolar conduction type films. The p-type films show an average hole mobility of 8.2 cm^2/Vs at room temperature.

The Hall effect results show that p-type doping in P-doped $(Zn_{0.9}Mg_{0.1})O$ films is strongly dependent on the oxidation conditions. It is important to note that the effect of oxygen partial pressure on ZnO p-type conduction has been investigated previously by both experiment and theory. Xiong $et\ al.$ reported evidence for p-type conduction in undoped ZnO films grown at high oxygen partial pressure by reactive sputtering. The increased oxygen chemical potential by electronic excitation raises the formation enthalpy of the intrinsic donor V_O. Theoretical doping rules proposed by A. Zunger suggests that limitations to p-type doping can be overcome by manipulating the growth conditions, e.g. the use of the host anion-rich growth conditions to inhibit the formation of so-called "hole killer" defects. Calculations from chemical potentials suggest that the enthalpy of forming anion vacancies decreases under cation-rich (zinc-rich) conditions. In the present study, the growth condition necessary to obtain p-type P-doped $(Zn_{0.9}Mg_{0.1})O$ films is rather narrow (150 mTorr oxygen partial pressure). For the samples grown in the oxygen pressures of 100, 120, and 200 mTorr, the Hall-effect results do not show unambiguous p-type conductivity. The observation of indeterminate carrier type for a growth pressure of 200 mTorr may be explained by the "host anion poor" rule for the anion-substituting p-type dopants which conjectures that anion poor conditions are more favorable for a high solubility of acceptors on anion sites. As a result, the host anion condition has to be optimized in order to reach an equilibrium state under which p-type doping of ZnO can be realized.

X-ray diffraction was used to examine the crystallinity of the P-doped $(Zn_{0.9}Mg_{0.1})O$ films. No impurity phases were observed. This suggests that the solid solubility of phosphorus and magnesium has not been exceeded in the films. Note that there is no discernable change in the c-axis lattice parameter with increasing oxygen partial pressure. However, a slight decrease in diffraction intensity is observed as the oxygen pressure increases above 100 mTorr. This degradation in crystallinity may reflect a decreasing dopant solubility with increasing oxygen partial pressure, which is also consistent with the "host anion poor" rule mentioned above.

III.3 ZnO nanorods

In addition to ZnO thin films, we have also considered the possibility of embedding nanoscale devices into displays via the formation of ZnO-related nanowires. The fabrication of integrated systems using nanowire material requires the site-specific growth or placement of nanowires on relevant device platforms. Addressing these challenges could prove enabling in realizing integrated device functionality involving semiconducting nanowires for a number of applications, including nanoscale electric field-effect transistors, single electron transistors, optical emitters and detectors.

In this work, we report on the self-assembled growth of cored (Zn,Mg)O nanowires. The process is site-specific, as single crystal ZnO nanorod growth is realized via nucleation on Ag films or islands that are deposited on a SiO_2-terminated Si substrate surface.

Growth occurs at relatively low substrate temperatures, on the order of 300-500°C, making it amenable to integration on numerous device platforms. With this approach, nanorod placement can be predefined via location of metal catalyst islands or particles. The growth experiments were performed using a conventional MBE system. An ozone/oxygen mixture was used as the oxidizing source. The cation flux was provided by Knudsen effusion cells using high purity Zn metal and Mg as the source materials. Site-selective nucleation and growth of cored nanorods was achieved by coating Si substrates with Ag islands. For a nominal Ag film thickness of 20 Å, discontinuous Ag islands are realized. On these small metal catalyst islands, (Zn,Mg)O nanorods were observed to grow. The site specificity for nanowire growth using this technique is evident as (Zn,Mg)O nanorods form only on the Ag-coated regions.

Under continuous Zn, Mg, and O flux, nanorod material nucleates on the catalysts particles. However, close inspection of the nanorod structure indicates that the Zn and Mg concentrations are not uniformly distributed in the rods. Instead, there is a radial segregation into Zn-rich and Mg-rich regions, apparently reflecting differences in the solubility limits of bulk ZnO-MgO or Zn-Mg-Ag-O versus epitaxial solid solutions. Under low temperature MBE growth conditions, a solubility-driven segregation occurs during the catalyst-driven core formation, with the core composition determined by bulk solid solubility. Subsequently, an epitaxial sheath grows with Mg content and crystal structure determined by epitaxial stabilization. The net result is the growth of (Zn,Mg)O nanorods that are not uniform in composition across the diameter, but distinctly cored. Fundamentally, these 1-D ZnO nanostructures provide an attractive system for probing low-dimensional effects such as quantization, interface scattering, and ballistic transport. The relatively low growth temperatures suggest that cored (Zn,Mg)O nanorods could be integrated on device platforms for numerous applications, including chemical sensors, nano-optics, scanning probes and nanoelectronics. More generally, the spontaneous bimodal growth mode demonstrated for (Zn,Mg)O may prove applicable in the synthesis of heteroepitaxial cored nanowire materials where thermodynamics and epitaxy impose different cation or anion solubility limits.

III.4 ZnO Nanoparticles as Sensitizers for Phosphors

ZnO nanoparticles embedded into SiO_2 by an *ex-situ* method were shown to result in stable green photoluminescent emission with a peak at 510 nm compared to the normal peak at 495 nm from micron-sized ZnO powders. Green emission from ZnO nanoparticles was completely suppressed when they were embedded in SiO_2 doped with Eu^{3+}. Instead, the f-f emissions from Eu^{3+} were enhanced by 5 ~ 10 times by energy transfer from the embedded ZnO nanoparticles to Eu^{3+}. The Eu^{3+} luminescence increased as the Eu^{3+} concentration was increased from 1 vs. 5 mole %, (for 10 mole% ZnO). In addition, the intensity increased as the embedded ZnO nanoparticles concentration was increased up to 10 mole% (for 5 mole% Eu^{3+}). The effects of phonon mediated energy transfer, quenching by activator interactions between Eu^{3+} ions, and energy back-transfer from Eu^{3+} ions to ZnO nanoparticles were discussed.

ZnO nanoparticles were also synthesized and successfully incorporated in Ce^{3+}-doped SiO_2 matrix by a sol gel method. Photoluminescence intensities were compared for ZnO

nanoparticles, Ce^{3+}-doped SiO_2 ($SiO_2:Ce^{3+}$) and ZnO encapsulated $SiO_2:Ce^{3+}$ (ZnO-$SiO_2:Ce^{3+}$) fabricated from sol gels. Green emission from ZnO associated with anionic oxygen vacancies and blue broadband emission due to $5d^1 \to 4f^1$ transitions in Ce^{3+} ions were observed. The photoluminescence intensity of Ce^{3+} was enhanced considerably by energy transfer from ZnO nanoparticles.

IV.   Bread-Board Optoelectronics Pixelated Array of Cortoconic Model of Brain Functions (Mark Davidson, Paul Holloway)

IV.1   Introduction

One of the goals of this project was to implement the Corticonics algorithms in the hardware of a display. This algorithm involves three fundamental mathematical functions in series. Data are first subjected to a log function, then multiplied by a number referred to as "c", then the antilog is taken. These functions are to take place in each pixel with feedback from adjacent pixels. While highly accurate log-antilog functions can be complex to implement in hardware, we have noted that simple circuits are capable of these operations based on the log relationship between the base voltage and collector current of a simple bipolar transistor. Using a few simple components, we have developed circuits which perform these functions. In addition, the use of optically active components such as phototransistors, photoresistors and LEDs allows these circuits to function with all optical inputs and outputs, providing a first step towards implementation in an active intelligent luminescent display. As a first step towards implementing these circuits on the back plane of a display, we have built an optical breadboard intelligent display test bed with a 3x4 array of 2" pixels. This provides a test bed for looking at the effectiveness of various imperfect but simple circuits in the Corticonics model.

IV.2   Circuit designs
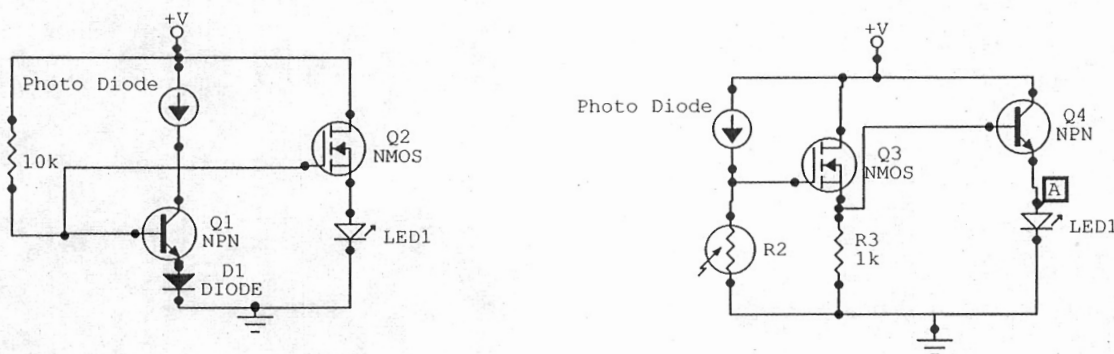
Figure 1 Basic Log (left) and antilog (right) circuits. Note that R2 in the antilog circuit is a photoresistor enabling the multiplication of the photodiode current by an optical signal prior to the antilog operation.

Both the log and antilog circuits have been implemented using simple circuitry as shown in figure 1. The goal of these circuits is to provide the non-linear functions required by the Corticonics model using only a couple of transistors per function. These are also to be optically coupled to allow easy integration into a display using, for example, the

transparent transistors being developed in John Wager's group at OSU or by David Norton at the University of Florida.

The log circuit (left in figure 1) uses an input of a photocurrent generated by either a photodiode or phototransistor. The component converts a light input (as from adjacent pixels) into a current proportional to the light intensity. Q1 is used as the log element. The photocurrent is applied to the collector of the transistor. The base voltage of a bipolar transistor is a good approximation of the log of the collector current. That base voltage can be used directly as the log signal, or it can be converted into a current by applying that voltage to the gate of MOSFET Q2. In practice, it has been found that a high gain NPN transistor functions better than a MOSFET in the Q2 spot due to inherent non-linearity in the typical MOSFET transfer curve. The current through Q2 is converted to a light signal by LED1 which could be an OLED or other device in the anticipated display. Note that it would be possible to use an infrared or ultraviolet device for these intermediate signals which could be shared between pixels steered by photonic crystals, if necessary.

The multiplication by "C" and antilog functions are provided by the antilog circuit (figure 1 right). This circuit converts an optical input signal into a photocurrent from a photodiode (or phototransistor). This current is then passed through R2 to convert it to a voltage equal to the product of the resistance of R2 and the photocurrent. That voltage is buffered by source follower Q3 and applied to the base of Q4. Since the collector current is proportional to the antilog (exponential) of the base voltage, the current passing through the output LED is proportional to the antilog of the input light. One advantage of this configuration is that the multiplication parameter "C" can be varied by an external optical signal if resistor R2 is a photoresistor. Alternately, a voltage controlled resistance can be used (MOSFET) in place of R2, providing for electrical input of the multiplication parameter.

These circuits were bread boarded and tested. The results are shown in figure 2. In order to get an accurate log, the gain of the output transistor in the circuit must be maximized.
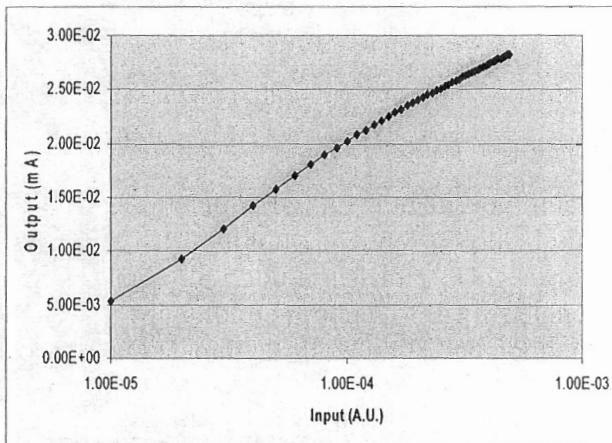
| **Figure 2** Modeled output of a device using a high gain bipolar transistor for maximum linearity | **Figure 3** Measured output of optical log circuit using bipolar Darlington transistor output. |
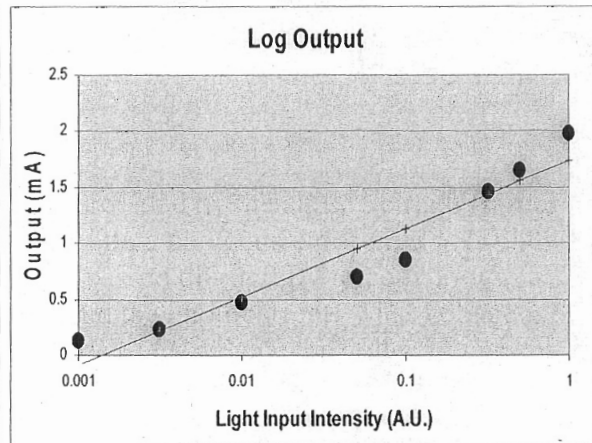
The accuracy of the log conversion is dependant on minimizing the base current drain from the base of the Q1 log transistor, since any stray current causes additional voltage drop across the bias resistor. The high gain transistor used in the modeling of the experimental data shown in figure 3 was not available in a through-hole package when the bread board was tested so a Darlington configured transistor was used for the output. Since the gain was not as high as the modeled part, the measured output deviates somewhat from a log function. The correct part has now been obtained and testing is in progress in the intelligent display test bed (see below).

We have a first design to generate the "C" function which is the last function needed for the full implementation of the Corticonic functions. This function is described as a partial upside-down parabola (figure 4). Once again, the design principle is to use off-the-shelf transistors, minimize the part count, and tolerate some distortion to get the general nonlinear shape for testing. The current design uses an enhancement and depletion mode MOSFET, one of which is configured to turn on and the other to turn off as the input continues to increase. One such implementation is shown in figure 5 and its simulated output is shown in figure 6. As the input voltage rises, depletion mode MOSFET Q2 begins to turn on, providing current to the LED. As the voltage continues to rise, Q1 turns on, reducing the current from the LED, and thus turning it off. The turn-on and especially the turn-off are too sharp to provide an extremely accurate representation of the "C" function. This is due to the design of these off-the-shelf transistors which have sharp characteristics. We believe that we use non-ideal transistors for an actual intelligent display application. For the bread board testing, we will be looking for other off-the-shelf transistors with softer turn on characteristics.
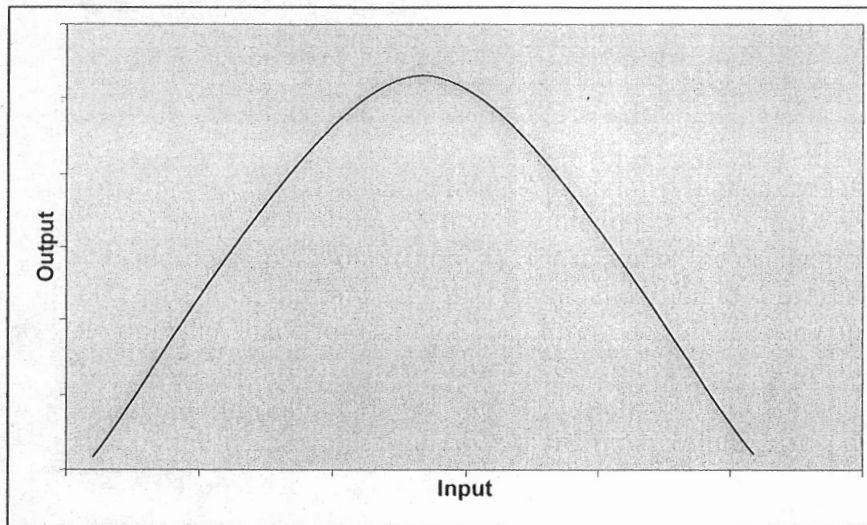
Figure 4 Desired "C" function for the Corticonics model.
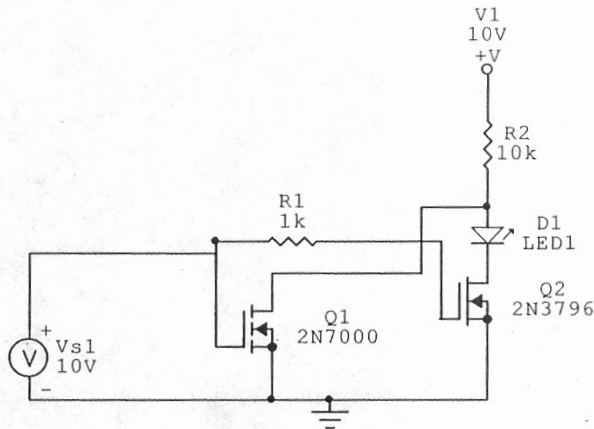
Figure 5 Circuit designed to produce an approximation of the desired "C" waveform from figure 4.
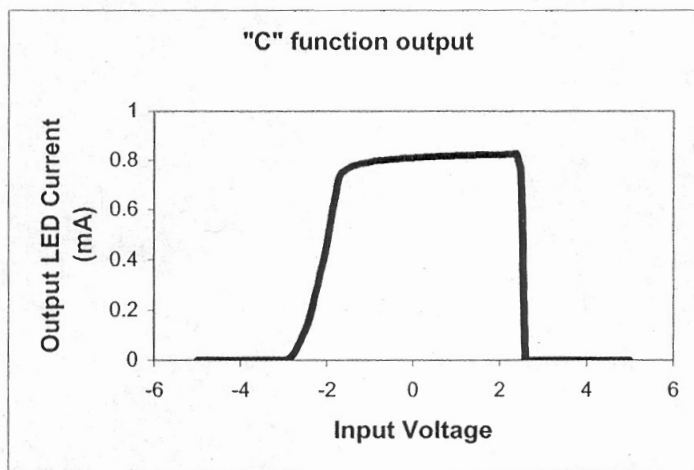
Figure 6 Simulated output of circuit shown in figure 5

IV.3   Intelligent corticonic display breadboard

We built a breadboard display which is designed to act as a test bed for these Corticonic circuits. The design goals were to provide a large scale, reconfigurable platform to test various circuitry. The "pixels" were to have the ability to be optically coupled for all functions, and to accepts inputs from a computer. Pixel outputs should be able to be monitored in real time by the computer. Pixels should also have the ability to be "directional" in their feed back. To this end, space for 4 separate log-antilog circuits is provided. To keep the sizes reasonable, we kept the pixels to 2"x2". Pixels are mounted on individual circuit boards to allow easy changing of circuit types without reconfiguring computer control, monitoring and power supplies. This system was constructed and is ready for testing.

The circuit was designed for maximum flexibility. Figure 7 shows a single quarter pixel circuit design. This design incorporates the log (right portion) and antilog functions. It is designed to be very flexible and permits substitution of various components, as well as

the "jumpering out" of undesired components.
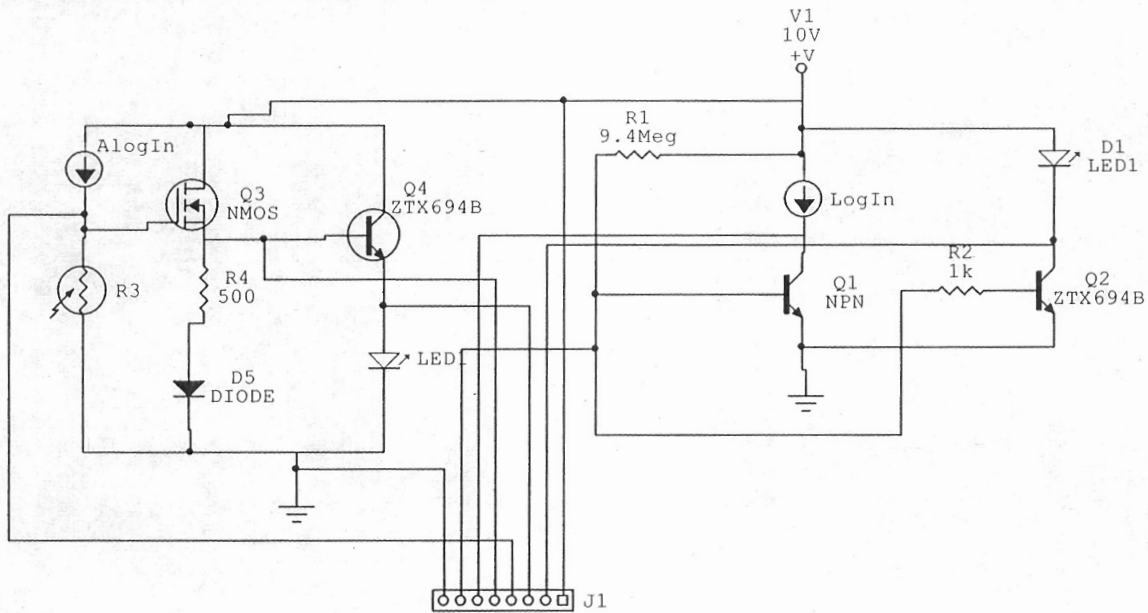
Figure 7 Schematic of one fourth of a pixel of the Corticonics test bed

Four of these circuits are put together to form a pixel board shown in figure 8. Each of the four sections is connected to the mother board independently for power, control and monitoring. The mother board schematic is shown in figure 9. The mother board is designed to hold an array of up to 3x4 pixels. Each pixel board can be arranged so that light from the board can impinge either partly or fully on the adjacent detectors, providing non-linear feedback if desired. Alternately, the pixels can be excited by external light or electrical sources to investigate the responses of isolated pixels. Designs for the pixel board and motherboard are shown in figures 10 and 11, with one completed board with pixel boards installed shown in figure 12.
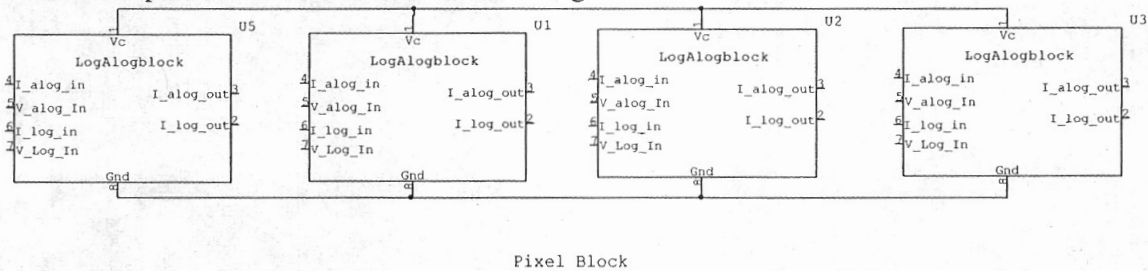
Pixel Block

Figure 8 Schematic of the pixel board. Four of the circuits in figure 1, labeled as LogAlogblock, are connected to power and ground and the appropriate J1 connector.
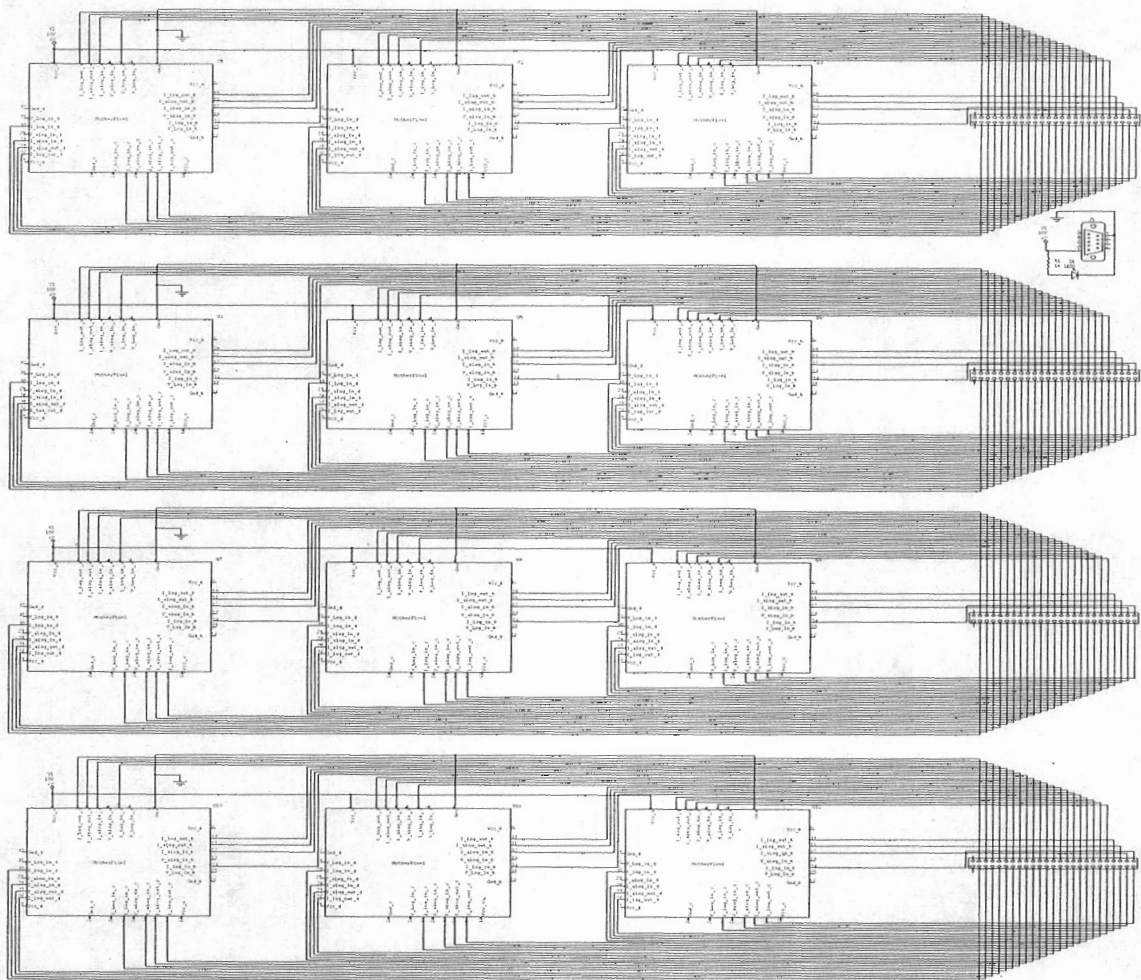
Figure 9 Schematic of the motherboard of the Coritconics test bed. Control/monitoring signals from each row is sent to a 50 pin connector. Power and power indicator are included.
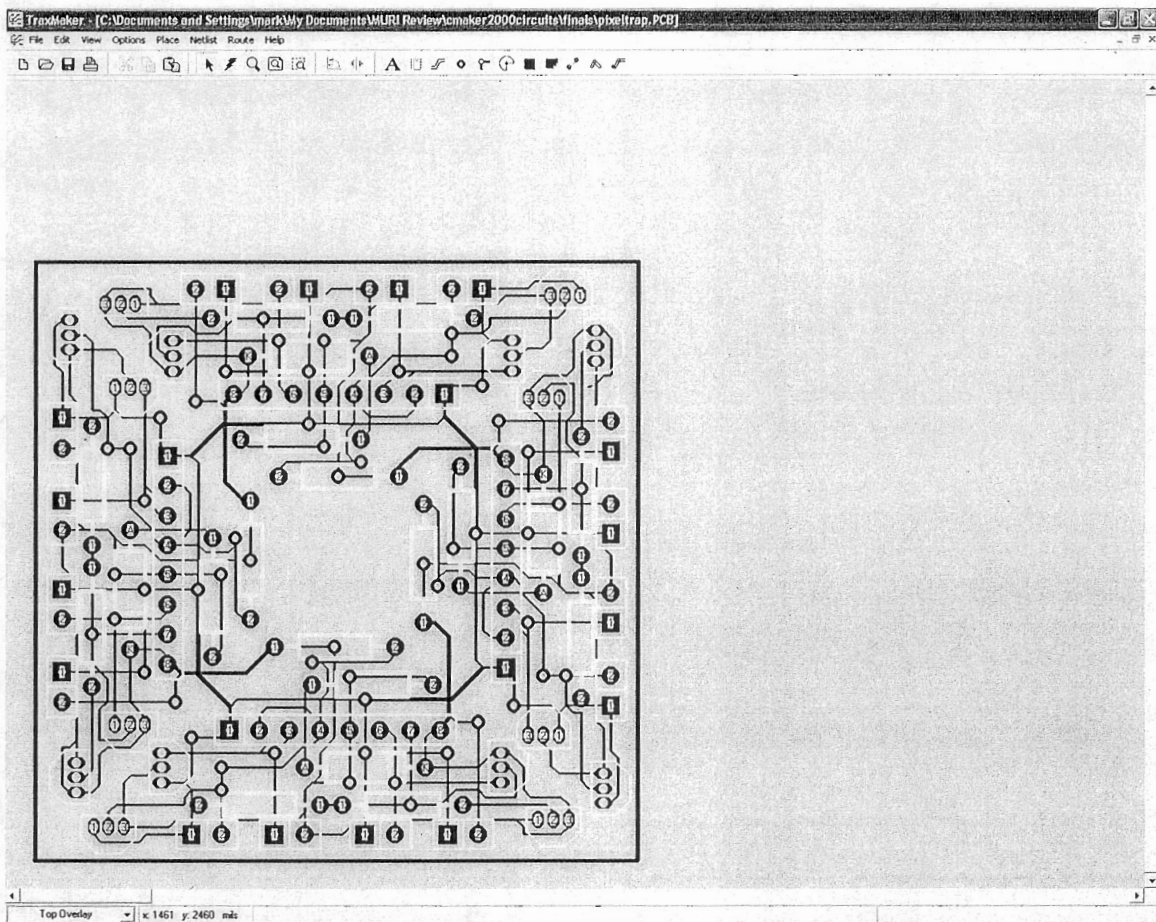
Figure 10 Layout of two sided circuit board for each pixel. Note the four fold symmetry showing the four sections available for directionality, if desired.
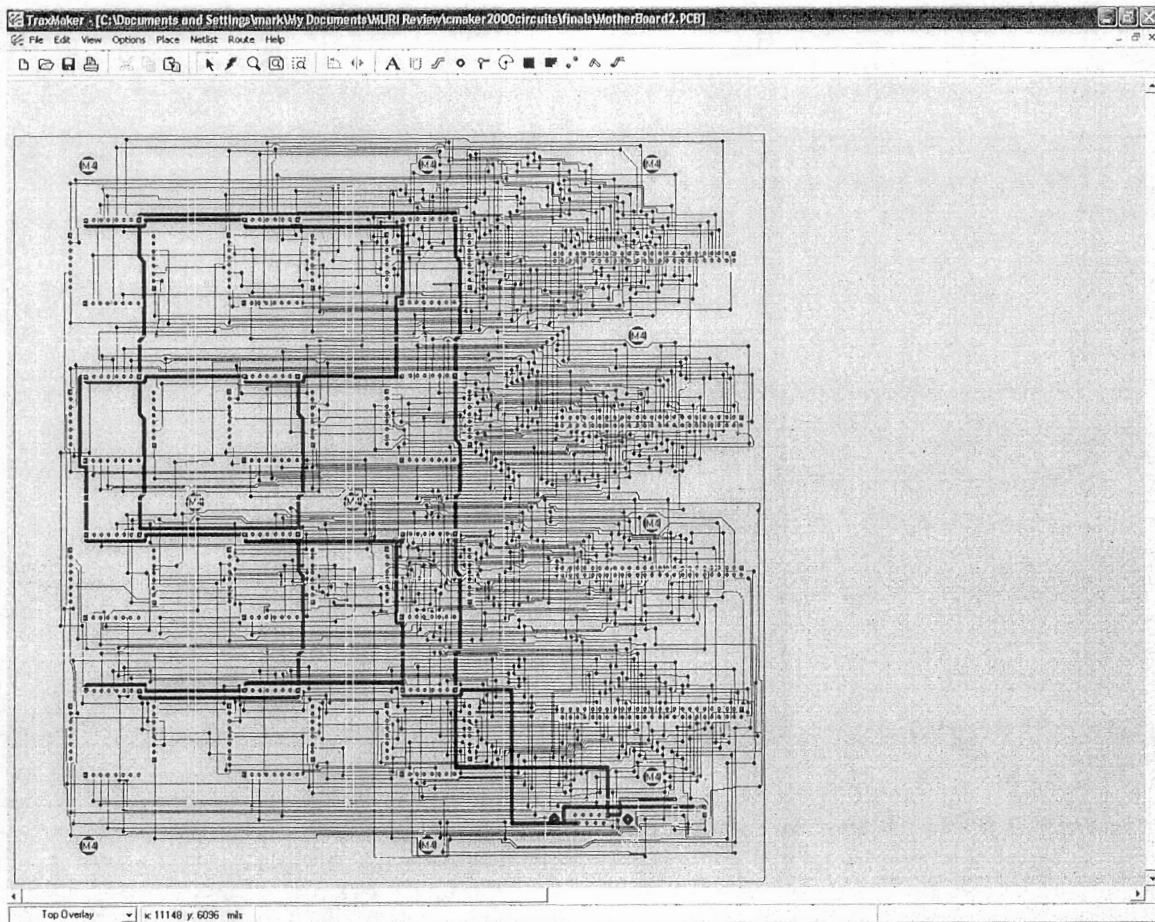
Figure 11 Circuit board design for the intelligent luminescence test bed mother board.
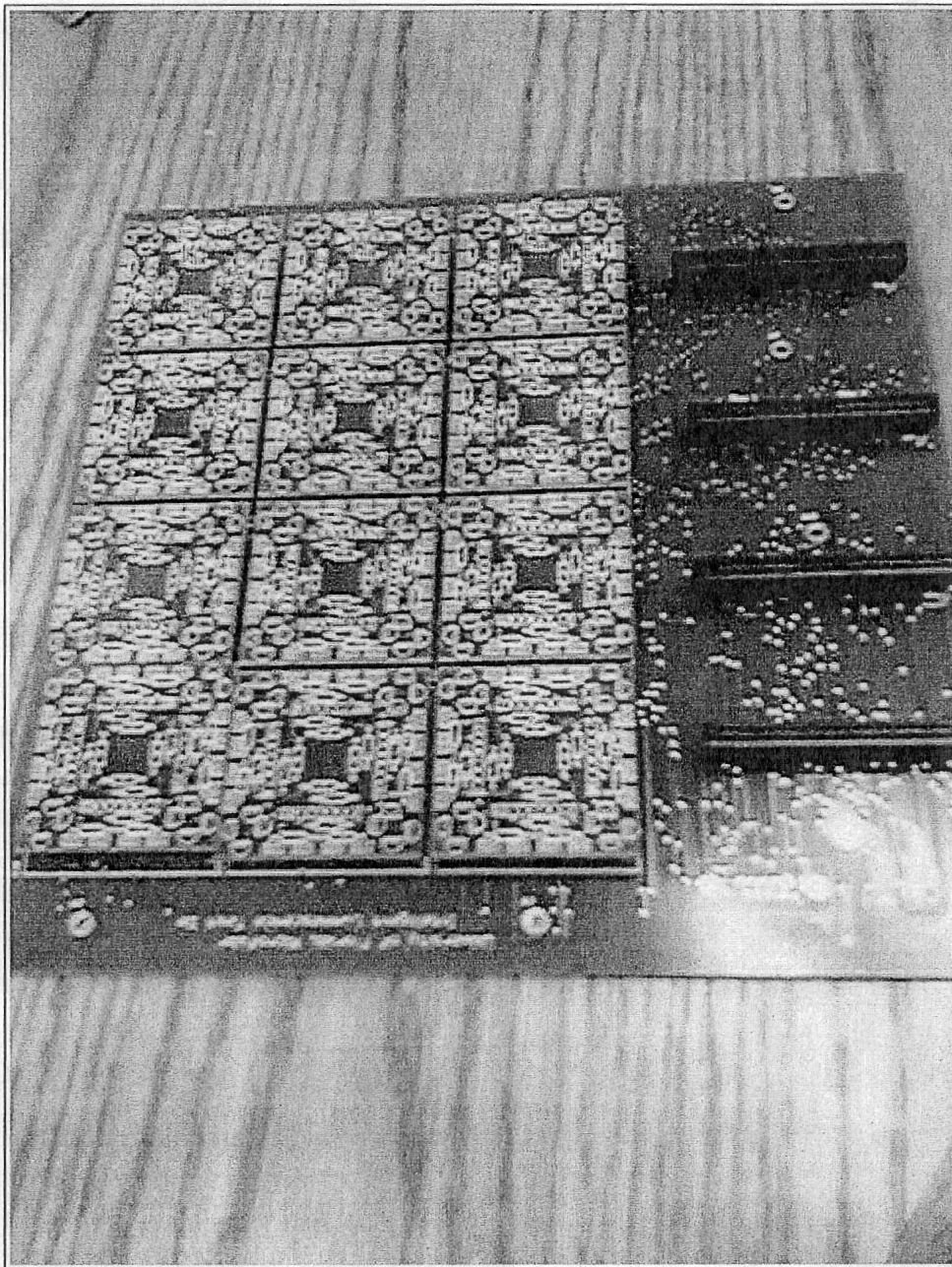
Figure 12 Intelligent luminescence 3x4 array test bed motherboard with pixel boards in place.

IV.4   Conclusions

We have designed and tested simple circuits that generate with reasonable accuracy the functions that enable the implementation of the Corticonics model of intelligent luminescence. We have individually tested the functional blocks. A full 3 x 4 pixel intelligent display test bed has been constructed and is ready to test the various methods for achieving intelligent luminescence.

V.   Personnel and Publications

V.1   Students Supported

1. De Vito, David   Ph.D.   Graduated 05/06
2. Williams, Lizandra   Ph.D.   Graduated 12/04
3.   Irving, Douglas   Ph.D.   Graduated 08/04
4. Yang, Heesun   Ph.D.   Graduated 12/03
5. Glass, William   Ph.D.   Graduated 12/03
6. Kim, Joohan   Ph.D.   Graduated 12/03
7. Kale, Ajay   Ph.D.   Graduated 12/03
8. Heo, Young-Woo   Ph.D.   Graduated 12/03
9. Kwon, Yong Wook   Ph.D.   Graduated 12/04
10. Li, Yuanjie   Ph.D.   Graduated 5/06
11. Chung, Philip   Ph.D.   Expected 12/06
12. Devine, Bryce   Ph.D.   Expected 05/08
13. Law, Evan   Ph.D.   Expected 12/08

V.2. Post Doctoral Associates Supported

1. Dr. Heesun Yang
2. Dr. Lei Qian

V.3. Paper Published

"Near-Infrared electroluminescence from MEH-PPV / Ln(TPP)acac blends", Benjamin S. Harrison, Timothy J. Foley, Joonbo Shim, Mohamed Bouguettaya, James M. Boncella, Paul H. Holloway, S. Ramakrishnan, John R. Reynolds and Kirk S. Schanze, *Appl. Phys. Lett*, **79** (23), 3770 (2001).

"Photoluminescent and Electroluminescent Properties of Mn Doped ZnS Nanocrystals", Heesun Yang, Paul H. Holloway and Banahalli B. Ratna, J. Appl. Phys, **93** 586-592 (2003).

"Growth and Characterization of Near-Infrared Emitting Thin Film Electroluminescent Phosphors", Ajay Kale, William Glass, Mark Davidson and Paul H. Holloway, Proc. of EL 2002, Ghent, Belgium, Sept. 23-26, 2002, pp 57-60.

"Infrared Emission from Electroluminescent Polymer LEDs", Joonbo Shim, Benjamin S. Harrison, Timothy J. Foley, Mohamed Bouguettaya, Nisha Ananthakrishnan, G. Padmanaban, James M. Boncella, S. Ramakrishnan, John R. Reynolds, Kirk S. Schanze and Paul H. Holloway, Proc. of EL 2002, Ghent, Belgium, Sept. 23-26, 2002, pp 279-282.

"Phosphor Technology", Mark R. Davidson and Paul H. Holloway, *McGraw-Hill Yearbook of Science and Technology 2004* (McGraw-Hill, NY, 2004) pp. 251-253.

"Electroluminescence from Hybrid Conjugated Polymer-CdS:Mn/ZnS Core/Shell Nanocrystal Devices", Heesun Yang and Paul H. Holloway, J. Phys. Chem. B, **107**, 9705-9710 (2003).

"Enhanced Photoluminescence from CdS:Mn/ZnS Core/Shell Quantum Dots", Heesun Yang and Paul H. Holloway, Appl. Phys. Lett., **82**, 1965-1967 (2003).

"Efficient and Photostable ZnS-Passivated CdS:Mn Luminescent Nanocrystals ", Heesun Yang and Paul H. Holloway, Adv. Funct. Mater., **14**,152-156 (2004).

"Sputter deposited GaN doped erbium thin films: photoluminescence and 1550nm infrared electroluminescence", Joo Han Kim, Nigel Shepherd, Mark Davidson and Paul H. Holloway, Appl Phys. Lett., **83**, 641-643 (2003).

"Infrared Emission from Zinc Sulfide: Rare Earth Doped Thin Films", A. Kale, N. Shepherd, W. Glass, D. DeVito, M. Davidson and P.H. Holloway, J. Appl. Phys. **94**, 3147-3152 (2003).

"Enhancement-mode thin-film field-effect transistor using phosphorus-doped (Zn,Mg)O channel", Y. Kwon, Y. Li, Y.W.Heo, M. Jones.; P.H. Holloway, D.P. Norton, Z.V. Park, S. Li, Appl. Phys. Lett., **84**, 2685-2687 (2004).

"Progress in Semiconducting Oxide-Based Thin Film Transistors for Organic Light Emitting Diode Displays", Y. J. Li, Y. W. Kwon, M. Jones, Y. W. Heo, J. Zhou, S.-C. Luo, P. H. Holloway, E. Douglas, and D.P. Norton, Semiconductor Science and Technology, **20**, 720-725 (2005).

"Transparent Transistors Based on Semiconducting Oxides," Y.W. Kwon, Y. Li, Y.W. Heo, M. Jones, Vijay, B.S. Jeong, J. Zhou, S. Li, P. Holloway, and D.P. Norton, MRS Proceedings Volume 786, *Fundamentals of Novel Oxide/Semiconductor Interfaces*, Editors: C.R. Abernathy, E. Gusev, D. Schlom, S. Stemmer, (MRS, 2004) E6.30

"Electric Field Modulation Of ZnO Film Conductance In ZnO-Based FET Structures", Y. Kwon, Y. Li, Y.W. Heo, M. Jones, P. H. Holloway, D.P. Norton, and S. Li, in State-of-the-Art Program on Compound Semiconductors XXXIX -and- Nitride and Wide Bandgap Semiconductors for Sensors, Photonics, and Electronics IV, editors A. G. Baca and R. F. Kopf, PV2003-11 Proceedings of the 204th Meeting of the Electrochemical Society, Orlando, FL, p. 68 (2004).

"Transport properties of phosphorus-doped ZnO thin films," Y. W. Heo, S. J. Park, K. Ip, S. J. Pearton, and D. P. Norton, "Appl. Phys. Lett. 83, 1128 (2003).

"Shallow Donor Formation in P-Doped ZnO Thin Films," Y. Heo, K. Ip, S.J. Park, S.J. Pearton and D.P. Norton, Appl. Phys. A78,53 (2004).

"Contacts to p-type ZnMgO," S. Kim, B. Kang, F. Ren, Y. Heo, K. Ip, D.P. Norton and S.J. Pearton, Appl. Phys. Lett. 84, 1904 (2004).

"p-type behavior in phosphorus-doped (Zn,Mg)O device structures," Y. W. Heo, Y.W. Kwon, Y. Li, S. J. Pearton, and D. P. Norton, Appl. Phys. Lett., 84, 3474 (2004).

"Synthesis and properties of epitaxial electronic oxide thin-film materials," D. P. Norton Materials Science and Engineering: R: Reports 43, 139 (2004).

"Structure and optical properties of cored wurtzite (Zn,Mg)O heteroepitaxial nanowires," Heo, Y.W., Abernathy, C., Pruessner, K., Sigmund, W., Norton, D.P., Overberg, M., Ren, F., Chisholm, M.F., Journal of Applied Physics, Volume 96, 2004, pp. 3424-3428.

"Depletion-mode ZnO nanowire field-effect transistor," Heo, Y.W.*, Tien, L. C., Kwon, Y., Norton, D. P., Pearton, S. J., Kang, B. S., Ren, F., Applied Physics Letters, Volume 85, 2004, pp. 2274-2276

"Electrical transport properties of single ZnO nanorods," Heo, Y.W. , Tien, L.C., Norton, D.P., Kang, B.S., Ren, F., Gila, B.P., Pearton, S.J., Applied Physics Letters, Volume 85, 2004, pp. 2002-2004.

"Electroluminescence from Tm-doped GaN Deposited by RF Planar Magnetron Sputtering", Joo Han Kim, Mark R. Davidson, and Paul H. Holloway, Appl Phys Lett, 83, 4746-4748 (2003).

"Localized Quantum State Luminescence from Wide Bandgap ZnS and GaN Thin Films", Nigel Shepherd, Ajay Kale, William Glass, Joo Han Kim, David DeVito, Mark Davidson and Paul H. Holloway, State-of-the-Art Program on Compound Semiconductors XXXIX and Nitride and Wide Bandgap Semiconductors for Sensors, Photonics, and Electronics IV -- Ed. by A. G. Baca and R. F. Kopf (The Electrochemical Society, Pitscataway, NJ, 2003) p. 244-269.

"Near-Infrared Display Materials", Paul H. Holloway, Mark Davidson, Nigel Shepherd, Ajay Kale, William Glass, Benjamin S. Harrison, Timothy J. Foley, John R. Reynolds, Kirk S. Schanze, James M. Boncella, Susan Sinnott and David Norton, Proc. Of Conference 5080 on Cockpit Displays X, Ed. by Darrel G. Hopper, Orlando, FL, April 21-25, 2003 (SPIE, Bellingham, WA, 2003), p. 340-345.

"CdS:Mn Nanocrystals Passivated by ZnS: Synthesis and Luminescent Properties", Heesun Yang, Paul H. Holloway, Garry Cunningham and Kirk S.Schanze, J. Chem. Phys. 121, 10233-10240 (2004).

"Near-Infrared Electroluminescence at Room Temperature from Neodymium-Doped Gallium Nitride Thin Films", J. H. Kim, M. R. Davidson, and P. H. Holloway, Appl. Phys. Lett., 85, 1689-91 (2004).

"Formation of bubbles on electrical contacts to polymer light-emitting diode devices", Shyh-Chyang Luo, Hsiu-Hsin Chung, Eugene T. Pashuck, Elliot P. Douglas, and Paul Holloway, Thin Solid Films, **478**, 326-331(2005).

"Enhanced Luminescence from $SiO_2:Eu^{3+}$ by Energy Transfer from ZnO Nanoparticles", Jungsik Bang, Heesun Yang and Paul H. Holloway, J. Chem. Phys., **123**, 084709-1:5 (2005).

"Enhanced photoluminescence of Ce^{3+} induced by energy transfer from ZnO nanoparticles encapsulated in SiO_2", O.M. Ntwaeaborwa and P.H. Holloway, Nanotechnology, **16**, 865-868 (2005).

"Near-Infrared Electroluminescent Light-Emitting Planar Optical Sources Based on Gallium Nitride Doped with Rare Earths", J. H. Kim and P. H. Holloway, Advanced Materials, **17**, 91-96 (2005).

"Electroluminescence Based on Efficient, Photostable ZnS-Passivated CdS:Mn Core/Shell Nanocrystals", Heesun Yang and Paul H. Holloway, Proc. of EL 2004, Ed. by A. Kitai, Toronto, 20-23, 2004.

"Chapter 2: Zinc Sulfide", Nigel Shepherd and Paul H. Holloway, in *The Handbook of Electroluminescent Materials*, Edited by D. R. Vij, (Institute of Physics Ltd, London, 2004) pp. 25-123

"Anisotropic Growth of Luminescent Eu^{3+} or Er^{3+} Doped Gd_2O_3 Nanocrystals", Heesun Yang, Hyeokjin Lee and Paul H. Holloway, Nanotechnology **16**, 2794-2798 (2005).

"Photoluminescence of cerium-europium co-doped SiO_2 phosphor prepared by a sol-gel process", O.M. Ntwaeaborwa, H.C. Swart, R.E. Kroon, P.H. Holloway, R.E. Botha, Surface and Interface Analysis, **38**, 458-461 (2006).

"Computational Study of Steric Effects on the Optical Properties of Oligomers", D.L. Irving, B.D. Devine, and S.B. Sinnott, *Journal of Luminescence* (in press).

MURI Intelligent Luminescence for Communication, Display, and Identification
FINAL REPORT
J. F. Wager, D. A. Keszler, and J. Tate
Oregon State University
Corvallis, OR 97331-5501
25 May 2006

HIGHLIGHTS:

- Highly transparent ZnO-based thin-film transistors (TTFTs) are fabricated for the first time. The realization of highly transparent TTFTs coupled with recognition of the application potential of such devices bodes well for the nascent field of transparent electronics.
- A ZnO TTFT with a channel layer formed via spin-coating deposition is demonstrated for the first time. Spin-coating deposition offers a simple and low-cost processing alternative to vacuum deposition.
- A new class of electronic materials is identified. They may be described as amorphous multicomponent heavy metal cation (a-MHMC oxides). These materials are shown to be suitable for transparent thin-film transistor (TTFT) and other applications.
- A TTFT with a tin oxide channel is demonstrated for the first time.
- A TTFT with a zinc tin oxide channel is demonstrated for the first time.
- A TTFT with a zinc indium oxide channel is demonstrated for the first time.
- A TTFT with an indium gallium oxide channel is demonstrated for the first time.
- Transparent integrated circuits (inverters and ring oscillators) are demonstrated for the first time.
- A device physics based review article on TFT modeling is in press which overviews several new device models and demonstrates their utility via simulation examples.
- $BaCu_2S_2$ has been identified as a novel p-type conductor having materials properties appropriate for tandem thin-film solar-cell applications, and it is also transparent in the IR.
- MCuQF (M = Ca, Sr, Ba; Q = S, Se, Te) has been identified as a new family of p-type transparent conductors. Band gaps in these materials have been selectively tuned from 2.7 to 3.1 eV, and electrical conductivities for pressed pellets have exceeded 100 S/cm and almost 1000 S/cm in films. Thin films of BaCuTeF can be grown with very smooth surface morphology and strong c-axis texture. Following appropriate preparative conditions and doping, saturated red and green optical emission has been observed at room temperature, while saturated blue emission is observed at low temperatures. These findings provide opportunities for fabrication of new types of efficient, all solid-state light sources.

1

ACHIEVEMENTS:

I. **ZnO-Based Transparent Thin-Film Transistors and Transparent Electronics**: A novel, transparent, thin-film transistor (TTFT) has been invented which is ~75% transparent across the visible portion of the electromagnetic spectrum; exhibits prototypical n-channel, enhancement-mode (normally off) transistor electrical characteristics; and possesses an on-to-off current ratio of ~10^6. Additionally, inverter operation has been demonstrated (an inverter is the most basic digital electronics building-block). Many commercial applications are likely to emerge for this device. One important, immediately-evident application involves the use of a transparent transistor as a pixel-select transistor in an active-matrix liquid crystal display (AMLCD). Currently, only ~1-5% of the incident backlight illumination is transmitted through an AMLCD display. If opaque, silicon-based pixel-select transistors are replaced by transparent transistors, a significant improvement in AMLCD performance is anticipated. AMLCD flat-panel displays currently constitute an ~$15B/year market. Another possible application involves the use of TTFTs as transparent back-plane electronic drivers on transparent substrates, facilitating the realization of transparent displays. To date, this transparent-electronics work has resulted in six invention disclosures / patent applications, licensing of this technology to the Hewlett-Packard Corporation and collaboration towards commercialization, an invitation to write a 'Perspectives' article in the journal **Science**, participation on National Public Radio's 'Talk of the Nation Science Friday', and a significant amount of media attention including posting on a CNN website and an interview with MIT's **Technology Review**.
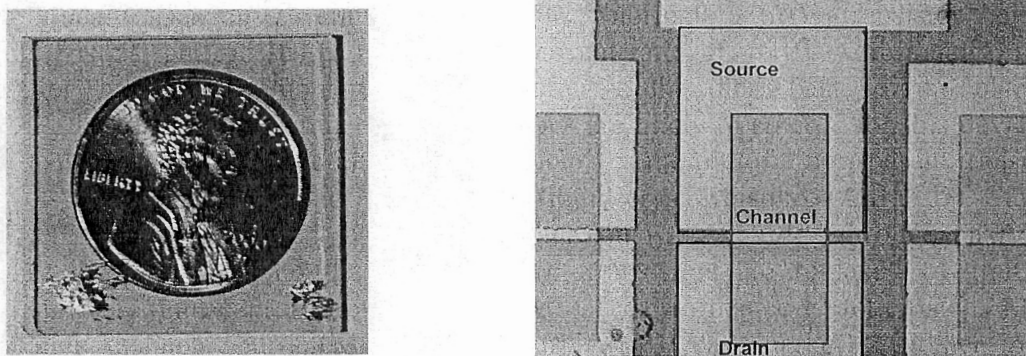
Figure 1. ZnO-based transparent transistors. Patterned transparent transistor test structures are evident, upon close inspection, in the upper portion of the glass substrate, which sits on a penny (**left**). Solder contacts are present near the bottom corners of the glass. An enhanced-contrast, magnified image is shown of a bottom-gate transparent transistor test structure (**right**). The glass substrate is blanket-coated with a lower layer of indium-tin oxide (ITO), which serves as a gate, and an upper layer of aluminum-titanium oxide (ATO), which serves as the gate dielectric. Dark green regions are only coated with these ITO and ATO layers. ITO source and drain contacts (tan) and a ZnO channel layer (light green) are labeled. [J. F. Wager, Science **300**, 1245-1246 (2003)]

II. **Spin-Coated ZnO Transparent Thin-Film Transistors**: Spin-coating deposition offers a simple and low-cost processing alternative to vacuum deposition. High quality ZnO thin films have been prepared by spin-coating using a novel ZnO precursor (zinc nitrate), resulting in dense, oriented films. A ZnO TTFT with a channel layer formed via spin-coating deposition is demonstrated. The TTFT is highly transparent and exhibits n-channel, enhancement-mode behavior with a channel mobility as large as 0.20 cm^2 V^{-1} s^{-1} and a drain current on-to-off ratio of nearly 10^7. Spin-coated ZnO TTFTs manufactured to date exhibit more light sensitivity than devices prepared by ion-beam sputtering; this is tentatively attributed to a larger degree of surface roughness of the spin-coated ZnO thin films. Continued development of the spin-coating and annealing procedures should lead to a reduction in light sensitivity and higher mobilities.
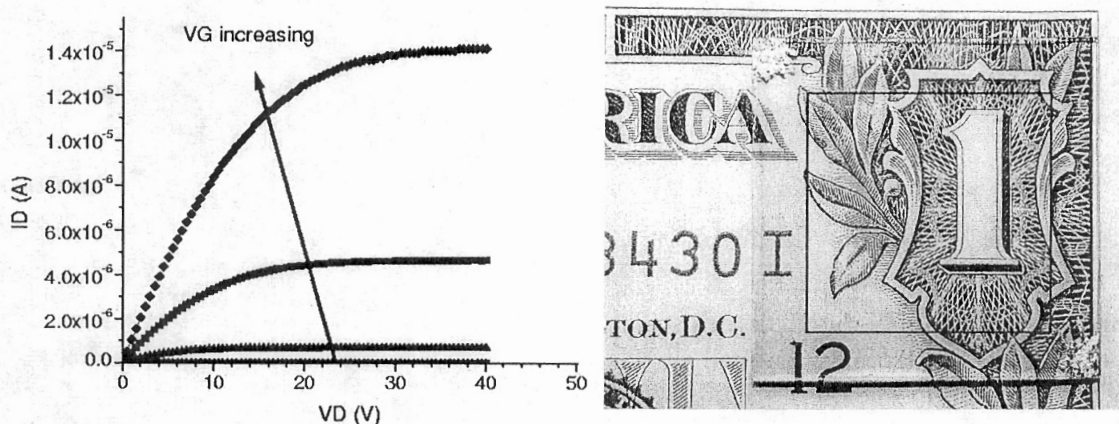
Figure 2. Spin-coated ZnO transparent thin-film transistors. Drain current-drain voltage curves of a spin-coated ZnO TTFT with gate voltages of 0, 10, 20, 30, and 40 V and drain voltages of 0 to 40 V, and a width-to-length ratio of 8 (**left**). Photograph of a 1" × 1" glass substrate patterned with spin-coated ZnO TTFTs, which sits on a corner of a dollar bill. Indium solder contacts are evident on the glass in the upper-left and lower-right corners (**right**). Fifty-six patterned ZnO TTFTs and twenty-four contact resistance test structures are present inside the box indicated on the figure. The size and transparency of these structures renders them invisible. [B. J. Norris et al., J. Phys. D. **36**, L105-L107 (2003)]

III. __SnO$_2$-Based Transparent Thin-Film Transistors__: A SnO$_2$ transparent thin-film transistor (TTFT) is demonstrated. The SnO$_2$ channel layer is deposited by RF magnetron sputtering and then rapid thermal annealed in O$_2$ at 600 °C. The TTFT is highly transparent, and enhancement-mode behavior is achieved by employing a very thin channel layer (10-20 nm). Maximum field-effect mobilities of 0.8 and 2.0 cm^{2}V^{-1}s^{-1} are obtained for enhancement- and depletion-mode devices, respectively. The transparent nature and the large drain current on-to-off ratio of $\sim$10^5 associated with the enhancement-mode behavior of these devices may prove useful for novel gas-sensor applications.
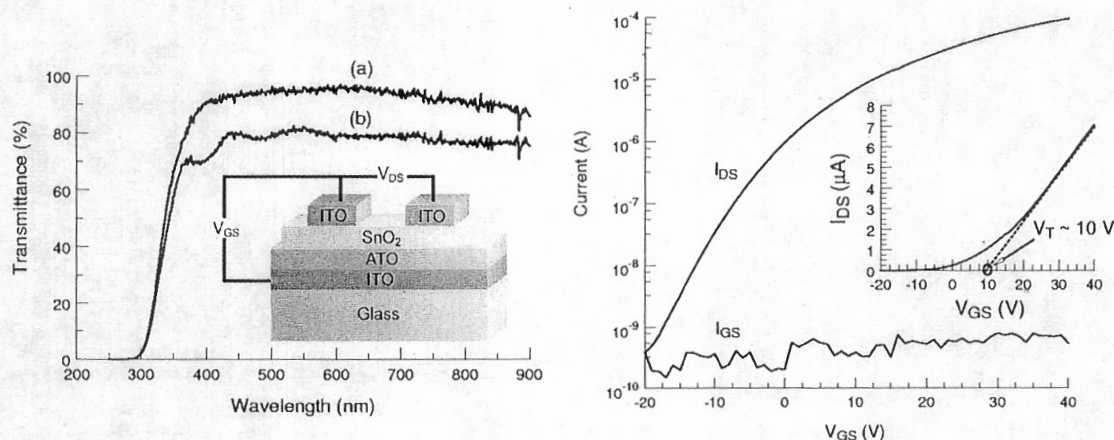
__Figure 3. A SnO$_2$-based transparent transistor.__ Optical transmittance as viewed through the ITO source/drain and the channel of a SnO$_2$ TTFT (__left__). Curve (a) is corrected for reflectance, i.e., T / (1 - R), whereas curve (b) is the raw transmission through the entire stack, including the substrate. Inset illustrates the bottom-gate TTFT structure and biasing scheme employed. Log(I$_D$)-V$_{GS}$ and Log(I$_{GS}$)-V$_{GS}$ characteristics at V$_{DS}$ = 35 V for a SnO$_2$ TTFT with a channel width-to-length ratio of 5 (__right__). Inset shows an extrapolation of the linear portion of an I$_{DS}$-V$_{GS}$ curve, resulting in an estimated threshold voltage of V$_T$ $\approx$ 10 V. The SnO$_2$ channel layer is $\sim$10 nm thick, deposited by RF magnetron sputtering, and rapid thermal annealed in O$_2$ at 600 °C. [R. E. Presley et al., J. Phys. D. 37, 2810-2813 (2004)]

IV. **A New Class of Electronic Materials**: A new family of electronic materials is identified. This material class is describable as amorphous multicomponent oxides composed of heavy-metal cations (HMCs) with $(n-1)d^{10}ns^0$ $(n \geq 4)$ electronic configurations. Their application potential is illustrated by their performance as channel materials for transparent thin-film transistor (TTFT) applications, as discussed later in this report. Fifteen elements have been identified as candidate HMCs (Hosono 1996), i.e., Cu, Zn, Ga, Ge, As, Ag, Cd, In, Sn, Sb, Au, Hg, Tl, Pb, and Bi, so that there are 105 possible ternary oxide combinations (i.e., defining a ternary oxide as involving two cations and one anion). Moreover, the composition of a ternary oxide, in terms of the relative fraction of each single cation oxide constituent, is variable. Additionally, there is no reason to restrict attention exclusively to ternary oxide combinations; it is possible that optimal HMC materials will involve multiple combinations of single cation constituent oxides. The physical and chemical properties of these materials combined with their inherent manufacturability and almost limitless number of combinations bode well for future applications such as printed, low-cost, large-area, and/or transparent electronics. A January 20, 2005 Science Update story related to zinc tin oxide, one example of this new class of materials, is attached.

08-Transpar Transist
Story.mp3

RESEARCH NEWS

10   materialstoday   February 2005

Clear advantage for high-mobility material

ELECTRONIC MATERIALS
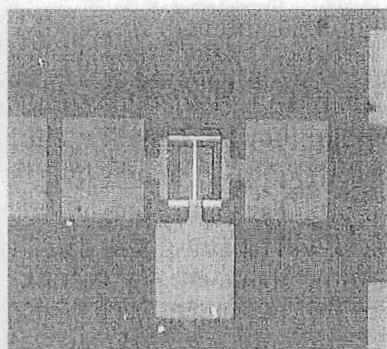
Enhanced contrast image of a patterned ZTO TTFT with a channel length of 25 μm. (Courtesy of John F. Wager.)

Transparent thin film transistors (TTFTs) could find many applications in light-emitting displays, smart windows, solar cells, security or military systems, and even toys. Researchers at Oregon State University and Hewlett-Packard have demonstrated that TTFTs with a new amorphous oxide as the channel layer, zinc tin oxide (ZTO), have high mobility and can be processed at low temperature [Chiang et al., Appl. Phys. Lett. (2005) 86, 013503].

"The performance, low deposition temperature, manufacturability, chemical stability, and physical robustness of these ZTO TTFTs means that they will compete very well in both flexible and nonflexible applications currently envisaged for carbon-based organic and polymer transistors," says John F. Wager of Oregon State University. "Already the performance of our devices in terms of electron mobility approaches the theoretical mobility limit of organic-based transistors."

The transparent TTFTs have a transmittance of ~84% at visible light wavelengths. Devices typically have a turn-on gate voltage of -5 V to 5 V, a drain current on-to-off ratio >10^7, and a field-effect mobility of 20-50 cm^2/Vs. "Until now, no one ever believed we could get this type of electronic performance out of transparent oxide transistors processed at low temperatures," Wager says.

Jonathan Wood

V. **Zinc Tin Oxide-Based Transparent Thin-Film Transistors**: Transparent thin-film transistors (TTFTs) with an amorphous zinc tin oxide channel layer formed via RF magnetron sputter deposition are demonstrated. Typical incremental mobilities (channel mobilities) of 5-15 and 20-50 $cm^2V^{-1}s^{-1}$ are obtained for devices post-deposition annealed at 300 and 600 °C, respectively. TTFTs processed at 300 and 600 °C yield devices with turn-on voltage of 0-15 V and -5-5 V, respectively. Under both processing conditions, a drain current on-to-off ratio greater than 10^7 is obtained. Zinc tin oxide is one example of a new class of high performance TTFT channel materials involving amorphous oxides composed of heavy-metal cations with $(n-1)d^{10}ns^0$ ($n \geq 4$) electronic configurations.
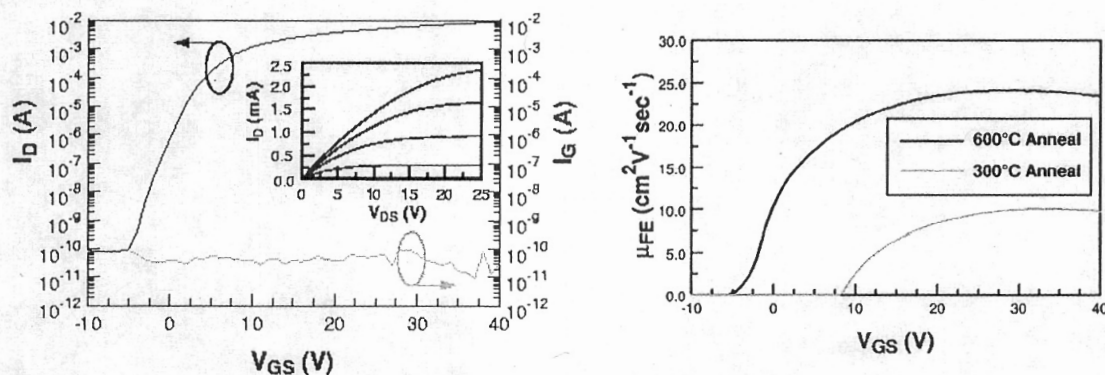
Figure 4. A zinc tin oxide-based transparent thin-film transistor. $Log(I_D)$-V_{GS} and $Log(I_{GS})$-V_{GS} characteristic ($V_{DS} = 40$ V). Inset shows I_D - V_{DS} characteristics (V_{GS} is varied from 0 to 15 V in 3 V steps and I_D increases with increasing V_{GS}) **(left)**. Representative μ_{inc}- V_{GS} characteristics for zinc tin oxide TTFTs fabricated on a Si substrate and annealed at 300 and 600 °C **(right)**. The higher annealing temperature yields a higher mobility and a lower turn-on voltage. [H. Q. Chiang et al., Appl. Phys. Lett. 86, 013503 (2005)]

VI. Zinc Indium Oxide-Based Transparent Thin-Film Transistors

VI. Zinc Indium Oxide-Based Transparent Thin-Film Transistors: A transparent high mobility, n-type transparent thin-film transistor (TTFT) with a zinc indium oxide (ZIO) channel layer is reported. Such devices are highly transparent with ~85% optical transmission in the visible portion of the electromagnetic spectrum. ZIO TTFTs annealed at 600 °C operate in depletion-mode with threshold voltages ~ -20 V to -10 V and turn-on voltages ~3 V less than the threshold voltage. These devices have excellent drain current saturation, peak incremental channel mobilities of ~45 to 55 $cm^2V^{-1}s^{-1}$ drain current on-to-off ratios of ~10^6, and inverse subthreshold slopes of ~0.8 V/decade. In contrast, ZIO TTFTs annealed at 300 °C typically operate in enhancement-mode with threshold voltages of ~300 °C devices exhibit excellent drain-current saturation, peak incremental channel mobilities of ~10 to 30 $cm^2V^{-1}s^{-1}$ drain current on-to-off ratios of ~10^6, and inverse subthreshold slopes of ~0.3 V/decade. ZIO TTFTs with the channel layer deposited near room temperature are also demonstrated. X-ray diffraction analysis indicates the channel layers of ZIO TTFTs to be amorphous for annealing temperatures up to 500 °C and polycrystalline at 600 °C. Low temperature processed ZIO is an example of a class of high performance TTFT channel materials involving amorphous oxides composed of heavy-metal cations with $(n-1)d^{10}ns^0$ ($n \geq 4$) electronic configurations.
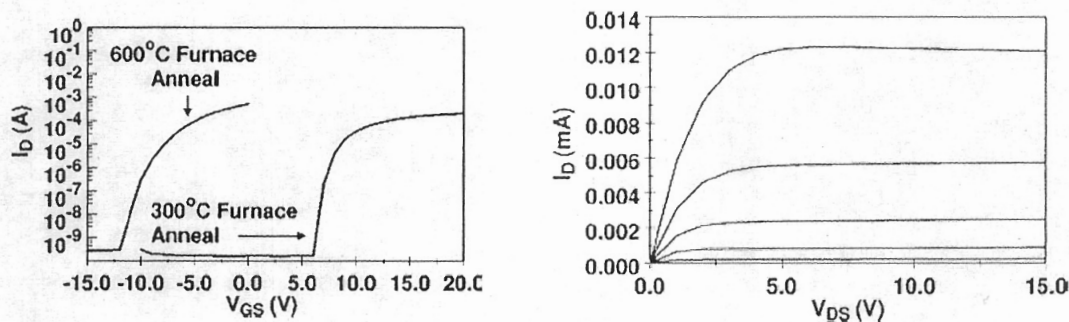
Figure 5. A zinc indium oxide-based transparent transistor. Log(I_D)-V_{GS} characteristics (V_{DS} = 20 V) of TTFTs in which the ZIO channel layer is subjected to either a 600°C or a 300°C post-deposition furnace anneal (**left**). The high temperature 600°C processed device is clearly depletion-mode, with a turn-on voltage of -12 V, a threshold voltage (extracted from linear extrapolation of an I_D -V_{GS} curve) of -9 V, a drain current on-to-off ratio of ~10^6, and an inverse subthreshold slope of 0.8 V/decade. Similar values for the low temperature 300°C processed enhancement-mode device are +6 V, +7 V, ~10^6, and 0.3 V/decade, respectively. Drain current-drain voltage (I_D - V_{DS}) characteristics of a TTFT in which the ZIO channel layer is not subjected to a post-deposition anneal (**right**). V_{GS} is decreased from 10 V (top curve, showing maximum current) to 0 V in 1 V steps. This TTFT is enhancement-mode. [N. L. Dehuff et al., J. Appl. Phys. 97, 97064505 (2005)]

VII. <u>Transparent Integrated Circuits</u>: Highly transparent ring oscillators, exhibiting ~85% optical transmittance in the visible portion of the electromagnetic spectrum, are fabricated using indium gallium oxide as the active channel material and standard photolithography techniques. The n-channel indium gallium oxide transparent thin-film transistors (TTFTs) exhibit a peak incremental mobility of ~7 $cm^2V^{-1}s^{-1}$ and turn-on voltage of ~2 V. A five-stage ring oscillator circuit (which does not employ level-shifting) exhibits an oscillation frequency of ~2.2 kHz when the gate and drain of the load transistor are biased at 30 V; the maximum frequency of oscillation observed is ~9.5 kHz, with the gate and drain of the load transistor biased at ~80 V.
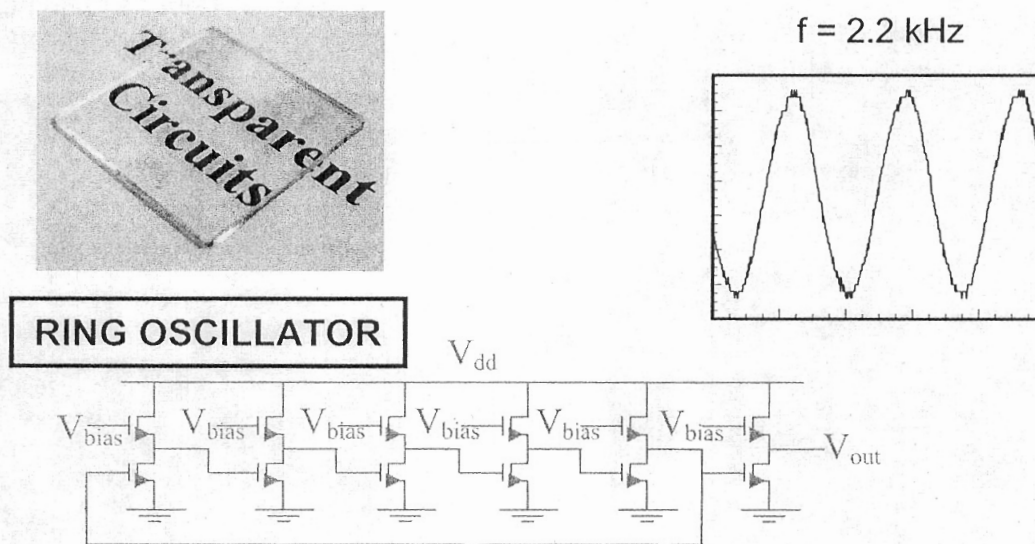
Figure 6. Transparent integrated circuits. (upper left) Glass substrate containing two ring oscillators, three inverters, and several discrete transistors resting atop the label "Transparent Circuits." **(bottom)** Circuit diagram of a five-stage ring oscillator. A ring oscillator consists of an odd number of inverters connected in series, with the output of the last stage fed back into the input of the first stage. An additional inverter at the output serves as an output buffer. **(upper right)** Output characteristics for the ring oscillator when $V_{DD} = V_{load} = 30$ V, yielding an oscillation frequency of 2.8 kHz. [R. E. Presley et al., Solid-State Electron. 50, 500-503 (2006)]

VIII. **Electrical Modeling of Thin-film Transistor Modeling**: An overview of device physics-oriented electrical modeling of thin-film transistors (TFTs) is presented. Four specific models are considered: (i) square-law, (ii) 3-layer, (iii) comprehensive depletion-mode, and (iv) discrete trap. For each model, a functional assessment of model equations is undertaken in terms of independent & dependent variables, model parameters, physical operating parameters, and constraining inequalities in order to facilitate mapping of model equations into a corresponding equivalent circuit. Channel mobility and 'subthreshold' current trends are elucidated. Finally, a conductance integral equation based on Shockley's gradual channel approximation is introduced and is employed in model development and device assessment.
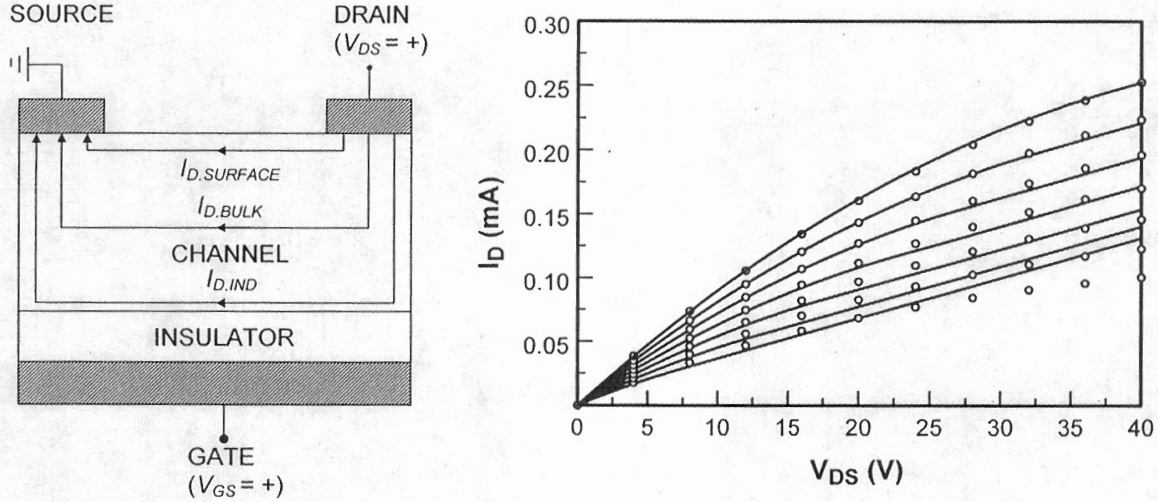
Figure 7. Thin-film transistor three-layer model. (left) A schematic of the 3-layer model for a simplified bottom-gate TFT with an n-type channel. **(right)** Measured I_D-V_{DS} curves (open circles) for a poorly operating SnO_2 TTFT with a fit to the data (continuous lines) using the 3-layer model. V_{GS} is decreased from 20 V (top curve, showing maximum current) to -10 V in 5 V increments. The poor drain current saturation characteristics are a consequence of having a low bulk layer resistance. [D. Hong et al., Critical Reviews in Solid State and Materials Sciences, (2006)]
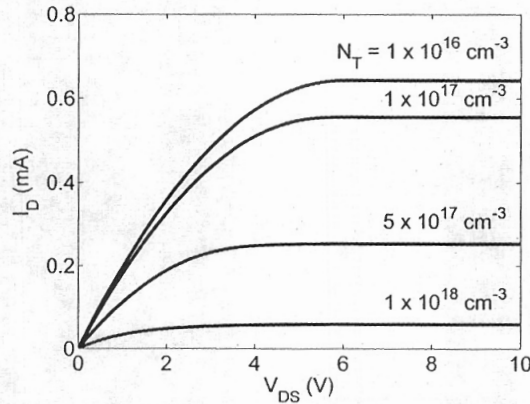
Figure 8. Thin-film transistor discrete trap model. Simulated drain current-drain voltage (I_D-V_{DS}) characteristics for an n-channel TFT corresponding to a gate voltage of 6 V and a trap depth of $E_C - E_T = 0.15$ eV below the conduction band minimum. An increase in the trap density significantly reduced the TFT drain current. [D. Hong et al., Critical Reviews in Solid State and Materials Sciences, (2006)]

IX. **Ba$_2$Cu$_2$S as a p-type Conductor**: BaCu$_2$S$_2$ is identified as a novel p-type conductor having materials properties appropriate for thin film solar cell applications. BaCu$_2$S$_2$ crystallizes in a low-temperature orthorhombic phase (α) and a high-temperature tetragonal form (β). We have prepared thin films of both of these phases. The α-BaCu$_2$S$_2$ films exhibit a bandgap of 2.3 eV, a conductivity of 17 S/cm, a hole mobility of ~3.5 cm^2 V^{-1} s^{-1}, and a carrier concentration of 10^{19} cm^{-3}. These properties, coupled with the robust chemical/physical nature of BaCu$_2$S$_2$ thin films motivated us to explore applying these films as p-type contacts to CuIn$_x$Ga$_{1-x}$Se$_2$ thin film solar cells with world-record efficiency. We are currently collaborating with the National Renewal Energy Laboratory (NREL), Golden, CO to pursue this application. Additionally, we have synthesized β-BaCu$_2$S$_2$ thin films and have found the bandgap to be 1.8 eV with a conductivity of 8 S/cm. This reduction in bandgap suggests that β-BaCu$_2$S$_2$ may be a useful absorber material for next-generation thin-film solar cell applications.

X. **MCuQF (M = Ca, Sr, Ba; Q = S, Se, Te)**: The materials MCuQF have been identified as a new family of p-type transparent conductors. Effort has been directed to developing the processing chemistry and materials properties of this family largely on the basis of powder techniques. This effort has quickly allowed the demonstration of simultaneously large band gaps and high electrical conductivity, while also providing means for observing and controlling optical-emission properties. Saturated red and green emission has been observed at room temperature, while saturated blue emission has been observed at 77 K. Efforts are being made to understand the defect chemistry of the blue emission, so that it can be stabilized at room temperature. Realization of this blue emission at room temperature would allow generation of an RGB triplet for display applications with a single phosphor host. The small work functions and high conductivities of the materials provide unique opportunities for charge injection and realization of efficient, solid-state light sources. High-conductivity thin films of BaCuQF have also been produced. BaCuTeF films are easy to process, with smooth, strongly c-axis oriented films on MgO being formed in-situ in the deposition chamber. These films have high p-type conductivity (100 S/cm), and are very smooth (see Fig. 10 for a similarly smooth film on Si). The thin-film morphology and electrical conductivity of BaCuSF is more difficult to control. Ex-situ post-deposition annealing is necessary, with higher temperatures (400 °C) necessary to stabilize the BaCuSF phase, which result in polycrystalline semi-insulators. These polycrystalline semi-insulators may be useful as channel materials in TTFTs if the crystallite size can be reduced to produce smoother surfaces.

200nm ZEISS ESB Grid = 1300 V Mag = 46.95 K X File Name = BCTF-14-2b.tif

Figure 9. PLD-deposited thin film of BaCuTeF on Si
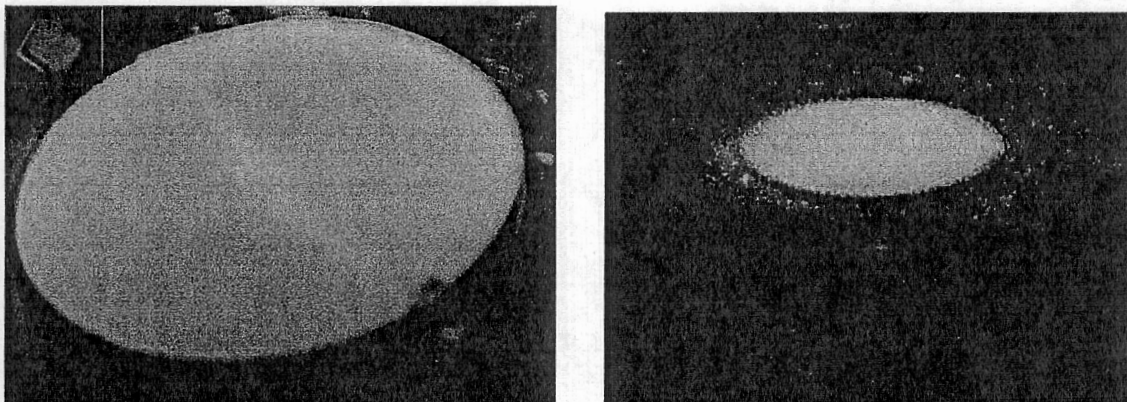
Figure 10. Photoluminescence from BaCuSF. (Left) Photograph of luminescent 6.5-cm sputtering target of BaCuSF. Upper left) saturated red emission from thin film of BaCuSF. (Right) Saturated green emission from BaCuSF.

XI. **PLD-deposited Transparent Thin-Film Transistors**: A pulsed laser deposition (PLD) process for deposition of transparent thin film transistors is described, and a zinc tin oxide-based transparent transistor (ZTO TTFT) is used for illustration. PLD processing has the capability to faithfully reproduce target stoichiometry in ablated films. This is useful if TTFT characteristics depend sensitively on composition or doping. Multi-layer capability, ultra-thin layer capability and high ambient gas pressure tolerance add to the usefulness of the tool. An amorphous ZTO channel layer is deposited by PLD and subsequently annealed at 600 °C in air. TTFT characteristics are reported that approach those produced by the optimized sputtering process described in III.
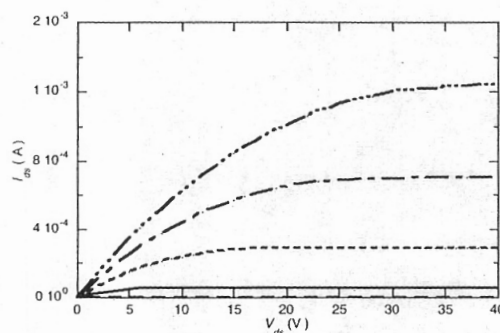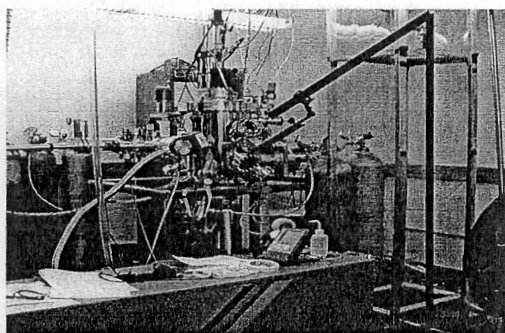
Figure 11. PLD-processed TTFTs. (**left**) The OSU PLD facility is based on an in-house design, and features a UHV chamber with a load lock and a 6-target capability. (**right**) Drain current-drain voltage (I_D - V_{DS}) characteristics of an enhancement-mode ZTO TTFT produced by PLD. Curves correspond to gate voltages of 0, 10, 20, 30, 40 V from the bottom upwards. Hard saturation is achieved, drain currents reach 1 mA at 30V drain voltage and 40 V gate voltage. Field-effect mobilities are of order 10 cm^2/Vs.

XII. <u>Processing Issues in Transparent Thin-Film Transistors</u>: TTFTs produced by several different methods sometimes exhibit properties that vary on the time scale of days and weeks after storage in ambient conditions. The main feature is loss of hard saturation and an increase in drain current for a given source-drain voltage and gate voltage. This behavior can be reversed by a short low-temperature (100 °C) annealing in air, and indicates that capping of the TTFTs will be a desirable process step in fabrication of devices. The presumed mechanism of the observed behavior is the modulation of the channel conductivity by adsorbed surface gases, which draw carriers from the channel layer.

XIII. <u>High Mobility n-type Transparent Conductors</u>: Doping of In_2O_3 with refractory metals is shown to produce n-type conductivity with a carrier Hall mobility of 112 cm^2/Vs, a factor of about 4 greater than the carrier mobility in nominally undoped or lightly-doped In_2O_3. This best case mobility is demonstrated for oriented films deposited on single-crystal YSZ at 650 °C, but even polycrystalline films deposited on amorphous SiO_2 at the moderate temperature of 400 °C display a Hall mobility > 65 cm^2/Vs.
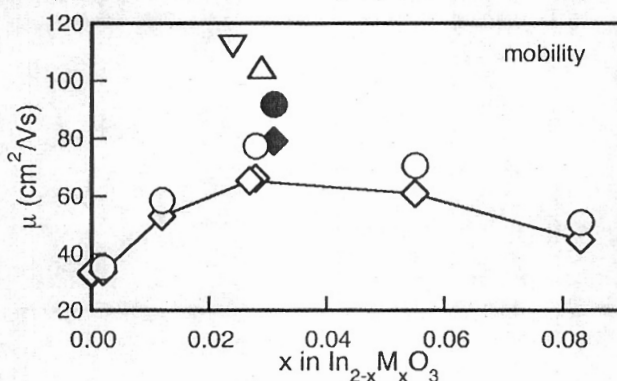
Figure 12. High Hall mobility in refractory-metal-doped In_2O_3. The open diamonds and circles are for films deposited on amorphous SiO_2 deposited at 400°C and 1 mTorr. The closed diamonds and circles are for optimized films on SiO_2. The triangles are for films on single-crystal YSZ. Mobilities represented by diamonds and the upright triangle are measured at room temperature, while those represented by circles and the inverted triangle are measured at liquid nitrogen temperature.

PUBLICATIONS:

1. S. Park, D. A. Keszler, M. M. Valencia, R. L. Hoffman, and J. F. Wager, "p-Type $BaCu_2S_2$ Films," Appl. Phys. Lett. 80, 4393-4394 (2002).
2. S. Park, B. L. Clark, D. A. Keszler, J. P. Bender, J. F. Wager, T. A. Reynolds, and G. Herman, "Low-Temperature Thin-Film Deposition and Crystallization," Science 297, 65 (2002).
3. J. Tate, M. K. Jayaraj, A. D. Draeske, T. Ulbrich, A. W. Sleight, K. A. Vanaja, R. Ragarajan, J. F. Wager and R. L. Hoffman, "p-Type Oxides for use in Transparent Diodes," Thin Solid Films 411, 119-124 (2002).
4. S. Park, J. P. Bender, J. F. Wager, and D. A. Keszler, "Low-temperature oxide thin-film deposition and crystallization," Abstracts of Papers, IONR-246, 224th ACS National Meeting, Boston, MA, United States, August 18-22, (2002).

5. H. Yanagi, J. Tate, S. Park, C.-H. Park, and D. A. Keszler, "p-type Conductivity in Wide Bandgap BaCuQF (Q =S, Se)," Appl. Phys. Lett. 82, 2814-2816 (2003).
6. H. Yanagi, S. Park, A. D. Draeseke, D. A. Keszler, and J. Tate, "P-type Conductivity in Transparent Oxides and Sulfide Fluorides," J. Solid State Chem. 175, 34-38 (2003).
7. R. L. Hoffman, B. J. Norris, and J. F. Wager, "ZnO-Based Transparent Thin-Film Transistors," Appl. Phys. Lett. 82, 733-735 (2003).
8. J. F. Wager, "Transparent Electronics," Science 300, 1245-1246 (2003).
9. R. L. Hoffman and J. F. Wager, "Energy Band Alignment of Injector/Insulator Heterojunctions," Thin Solid Films 436, 286-291 (2003).
10. S. Park, D. A. Keszler, "Synthesis of 3-R CuMO2+□ (M = Ga, In, Sc)", J. Solid State Chem. 173, 355-358 (2003).
11. J. F. Wager, M. M. Valencia, J. P. Bender, B. J. Norris, H. Q. Chiang, D. Hong, L. N. Norris, T. V. Harman, S. Park, J. Anderson, C.-H. Park and D. A. Keszler, J. Tate, H. Yanagi, M. Price, and R. L. Hoffman, "Transparent Electronics and Prospects for Transparent Displays," Proceedings of SPIE (Vol. 5080 Cockpit Displays X), D. G. Hopper (ed), pgs. 330-339 (2003).
12. D. Hong, N. Dehuff, R. L. Hoffman, B. J. Norris, H. Q. Chiang, J. P. Bender, J. T. Anderson, J. F. Wager, D. A. Keszler, "Transparent Transistor Development," Materials Research Society Symposium Proceedings (2004), 796 (Critical Interfacial Issues in Thin-Film Optoelectronic and Energy Conversion Devices), 99-104 (2003).
13. B. J. Norris, J. Anderson, J. F. Wager, and D. A. Keszler, "Spin-Coated Zinc Oxide Transparent Transistors," J. Phys. D. 36, L105-L107 (2003).
14. C.-H. Park, D. A. Keszler, H. Yanagi, and J. Tate, "Gap modulation in MCu[$Q_{1-x}Q'_x$]F (M = Ba, Sr; Q, Q' = S, Se, Te) and related materials," Thin Solid Films 445(2), 288-293 (2003).
15. "Crystalline oxide-silicon heterostructures and oxide optoelectronics", edited by D. Ginley, S. Guha, S. Carter, S. A. Chambers, R. Droopad, H. Hosono, D. C. Paine, D. G. Schlom, and J. Tate, Materials Research Society Symposium Proceedings, Vol 747, Materials Research Society, PA (2003).
16. R. E. Presley, C. L. Munsee, C.-H. Park, D. Hong, J. F. Wager, and D. A. Keszler, "Transparent Tin Oxide Thin-Film Transistors," J. Phys. D. 37, 2810-2813 (2004).
17. R. Kykyneshi, B. C. Nielsen, J. Tate, J. Li, and A. W. Sleight, "Structural and transport properties of $CuSc_{1-x}Mg_xO_{2+y}$ delafossites," J. Appl. Phys. 96, 6188-6194 (2004).
18. H. Q. Chiang, R. L. Hoffman, J.-Y. Jeong, J. F. Wager, and D. A. Keszler, "High Mobility Transparent Thin-film Transistors with a Zinc Tin Oxide Channel Layer," Appl. Phys. Lett. 86, 013503-013505 (2005).
19. N. L. DeHuff, E. S. Kettenring, D. Hong, C.-H. Park, H. Q. Chiang, R. L. Hoffman, and J. F. Wager, and D. A. Keszler, "Transparent Thin-Film Transistor with a Zinc Indium Oxide Channel Layer," J. Appl. Phys. 97, 064505:1-5 (2005).
20. J. F. Wager, "ZnO Transparent Thin-Film Transistor Device Physics," NATO Science Series, II: Mathematics, Physics and Chemistry (2005), 194(Zinc Oxide), 217-224 (2005).

21. P. F. Newhouse, C.-H. Park, D. A. Keszler, J. Tate, P. S. Nyholm, "High electron mobility W-doped In_2O_3 thin films by pulsed laser deposition," Appl. Phys. Lett. 87(11), 112108/1-112108/3 (2005).
22. D. Hong and J. F. Wager, and "Passivation of Zinc Tin Oxide Thin-Film Transistors," J. Vac. Sci. Technol. B, 23, L25-L27 (2005).
23. R. E. Presley, D. Hong, H. Q. Chiang, C. M. Hung, R. L. Hoffman, and J. F. Wager, "Transparent Ring Oscillator based on Indium Gallium Oxide Thin-Film Transistors," Solid-State Electron. 50, 500-503 (2006).
24. D. Hong, G, Yerubandi, H. Q. Chiang, M. Spiegelberg, and J. F. Wager, "Electrical Modeling of Thin-Film Transistors," Critical Reviews in Solid State and Materials Sciences, (2006).

PATENTS:

1. R. L. Hoffman and J. F. Wager, "Transparent transistors," provisional patent application (2002).
2. R. L. Hoffman and J. F. Wager, "Transistor Device having a Delafossite Material," United States Patent 7,026,713, April 11, 2006.
3. J. T. Anderson, D. A. Keszler, B. J. Norris, "High Quality Spin-Coated ZnO," invention disclosure filed (2003).
4. H. Q. Chiang, J. F. Wager, and R. L. Hoffman, "Transparent Thin-Film Transistor with a Zinc Tin Oxide Channel Layer," invention disclosure filed (2003).
5. H. Q. Chiang, R. L. Hoffman, N. L. DeHuff, D. Hong, and J. F. Wager, and "Transparent Thin-Film Transistor with a Zinc Indium Oxide Channel Layer," invention disclosure filed (2003).
6. R. L. Hoffman, J. F. Wager D. Hong, and H. Q. Chiang, "Passivation of oxide semiconductor channel thin-film transistors," invention disclosure filed (2004).

MURI Intelligent Luminescence for Communication, Display, and Identification
Presentations, Publications, Patents, Students
J. F. Wager, D. A. Keszler, and J. Tate
Oregon State University
Corvallis, OR 97331-3211
17 July 2006

PRESENTATIONS:

1. J. F. Wager, "Transparent Electronics and Optoelectronics: Where We Are Now and Where We Want To Go," OSU Physics Solid State Seminar, Corvallis, OR, November 1, 2001 (Invited)

2. J. F. Wager, "Transparent Electronics and Optoelectronics," Hewlett-Packard Seminar, Corvallis, OR, November 7, 2001. (Invited)

3. D. A. Keszler, "New optical and electro-optical materials," Montana State University, Department of Physics, April 2002. (Invited)

4. J. F. Wager, "Transparent Electronics and Optoelectronics," Arizona State University Solid State Seminar, Tempe, AZ, April 12, 2002 (Invited)

5. D. A. Keszler, "Ionic Borates and Electrooptically Relevant Systems," Northwestern University, May 2002. (Invited)

6. J. F. Wager, "Transparent Electronics and Optoelectronics: Prospects and Progress," Portland State University PASSS Seminar, Portland, OR, May 3, 2002. (Invited)

7. J. Tate, "P-type conductivity in transparent oxides and sulfide fluorides," American Chemical Society Meeting, August 2002. (Invited)

8. D. A. Keszler, "New Optical and Electrooptical Materials," Gordon Research Conference, August 2002. (Invited)

9. D. A. Keszler, "Low-Temperature Deposition and Crystallization of Oxide Thin Films," National Meeting of the American Chemical Society, August 2002. (Invited)

10. D. A. Keszler, "Growth and Characterization of NLO Crystals and Electrooptic Films," International Conference on Solid-State Crystals, October 2002. (Invited)

11. H. Yanagi, S. M. Park, D. A. Keszler and J. Tate, "P-type conductivity in transparent oxides and sulfide fluorides," National Meeting of the American Chemical Society, August 2002. (Contributed)

12. J. Tate, H. Yanagi, C.-H. Park, and D. A. Keszler "Bandgap engineering in BaCuSF," International Symposium on Transparent Oxide Thin Films for Electronics and Optics, Tokyo, Japan, April 10-11, 2003. (Invited)

13. J. F. Wager, "Transparent Electronics and Prospects for Transparent Displays," Pacific Northwest Chapter, Society for Information Display Meeting, Beaverton, Oregon, April 30, 2003,(Invited)

14. J. F. Wager, M. M. Valencia, J. P. Bender, B. J. Norris, H. Q. Chiang, D. Hong, L. N. Norris, T. V. Harman, S. Park, J. Anderson, C.-H. Park and D. A. Keszler, J. Tate, H. Yanagi, M. Price, and R. L. Hoffman, "Transparent Electronics and Prospects for Transparent Displays," SPIE Aerosense/Defense Symposium, Orlando, FL, 21-25 April 21-25, 2003. (Invited)

15. J. F. Wager, H. Q. Chiang, D. Hong, B. J. Norris, J. P. Bender, M. M. Valencia, C.-H. Park, J. Anderson, J. –Y. Jeong, D. A. Keszler, H. Yanagi, M. Price, J. Tate, and R. L. Hoffman, "Transparent Electronics: Materials, Devices, and Applications," AVS 50th International Symposium, Baltimore, MD, Nov. 2 - 7, 2003. (Invited)

16. D. Hong, N. DeHuff, R. L. Hoffman, B. J. Norris, H. Q. Chiang, J. P. Bender, J. T. Anderson, J. F. Wager, D. A. Keszler, "Transparent Transistor Development," MRS Fall Meeting, Boston, MA, Dec. 1-3, (2003).

17. J. F. Wager, "Transparent Electronics," University of Oregon Seminar, Eugene, OR, January 30, 2004. (Invited)

18. J. F. Wager, "ZnO Transparent Thin-Film Transistor Device Physics," NATO Advanced Research Workshop on "ZnO as a Material for Micro- and Optoelectronic Applications, St. Petersburg, Russia, June 23-25, 2004. (Invited)

19. J. F. Wager, "Transparent Thin-Film Transistors," 3rd Brazil MRS Meeting," Foz de Iguacu, Brazil, October 10-13, 2004. (Invited)

20. J. F. Wager, "Transparent Electronics: An Update," Pacific Northwest Chapter, Society for Information Display Meeting, Beaverton, Oregon, March 9, 2005. (Invited)

21. J. F. Wager, "A New Class of Electronic Materials for Printed Electronics," Printed Electronics 2005, Cambridge, UK, April 19-21, 2005. (Invited)

22. J. F. Wager, "Transparent Thin-Film Transistors with Amorphous Channel Layers," IMCAT 2005 & IUMRS-ICAM 2005, Singapore, July 3-8, 2005. (Invited)

23. J. Tate, "Oxide and sulfide transparent p-type conductors" University of Oregon Materials Science Seminar, Eugene, OR (June, 2004)

24. J. Tate, "What's strange about transparent conductors?", Oregon State University ASE Midsummer Conference (July, 2004) (outreach to high schools)

25. J. Tate, "A rediscovery of transparent conductors", Physics Colloquium, Reed College, 6 October, 2004.

26. D. A. Keszler, "Solution-based, low-temperature deposition of oxide thin films for electronics," International Conference on Digital Fabrication, September 2005. (Invited)

27. J. Tate, Symposium convener, "Materials for Transparent Electronics," MRS Fall Meeting, Boston, MA, November 28 – December 2, 2005.

28. J. F. Wager, "Amorphous Multicomponent Heavy Metal Cation Oxides for Transparent Thin-Film Transistor Applications," MRS Fall Meeting, Boston, MA, November 28 – December 2, 2005. (Selected as one of 'Top 5 Hot Talks/Cool Papers')

29. D. Hong, H. Q. Chiang, J. F. Wager, R. L. Hoffman, C. H. Park, and D. A. Keszler, "Zinc Tin Oxide-Based Transparent Thin-Film Transistors," in "Materials for Transparent Electronics," MRS Fall Meeting, Boston, MA, November 28 – December 2, 2005.

30. H. Q. Chiang, N. L. Dehuff, D. Hong, E. S. Kettenring, J. F. Wager, R. L. Hoffman, C. H. Park, and D. A. Keszler, "Amorphous Zinc Indium Oxide for Transparent Thin-Film Transistors," in "Materials for Transparent Electronics," MRS Fall Meeting, Boston, MA, November 28 – December 2, 2005.

31. J. F. Wager, Symposium convener, "Transparent Electronics," European Materials Research Spring Meeting & the International Conference on Electronic Materials (ICEM), May 2006.

32. H. Q. Chiang, R. E. Presley, D. Hong, C. M. Hung, J. F. Wager, and R. L. Hoffman, "Transparent Electronics: Inverters and Ring Oscillators," in "Advances in Transparent Electronics: from Materials to Devices," European Materials Research Spring Meeting & the International Conference on Electronic Materials (ICEM), May 29 - June 2, 2006.

33. D. Hong, H. Q. Chiang, R. E. Presley, N. L. Dehuff, J. P. Bender, J. F. Wager, C. H. Park, and D. A. Keszler, "Materials Exploration for Wide Band Gap Thin-Film Transistors via Sequential Layering Method of Binary Compounds," in "Advances in Transparent Electronics: from Materials to Devices," European Materials Research Spring Meeting & the International Conference on Electronic Materials (ICEM), May 29 - June 2, 2006.

34. J. F. Wager, "Transparent Electronics: TCOs go Active,"1st International Symposium on Transparent Oxides, Heraklion, Crete, October 22-25, 2006. (Invited)

PUBLICATIONS:

1. S. Park, D. A. Keszler, M. M. Valencia, R. L. Hoffman, and J. F. Wager, "p-Type $BaCu_2S_2$ Films," Appl. Phys. Lett. 80, 4393-4394 (2002).

2. S. Park, B. L. Clark, D. A. Keszler, J. P. Bender, J. F. Wager, T. A. Reynolds, and G. Herman, "Low-Temperature Thin-Film Deposition and Crystallization," Science 297, 65 (2002).

3. J. Tate, M. K. Jayaraj, A. D. Draeske, T. Ulbrich, A. W. Sleight, K. A. Vanaja, R. Ragarajan, J. F. Wager and R. L. Hoffman, "p-Type Oxides for use in Transparent Diodes," Thin Solid Films 411, 119-124 (2002).

4. S. Park, J. P. Bender, J. F. Wager, and D. A. Keszler, "Low-temperature oxide thin-film deposition and crystallization," Abstracts of Papers, IONR-246, 224th ACS National Meeting, Boston, MA, United States, August 18-22, 2002.

5. H. Yanagi, J. Tate, S. Park, C.-H. Park, and D. A. Keszler, "p-type Conductivity in Wide Bandgap BaCuQF (Q =S, Se)," Appl. Phys. Lett. 82, 2814-2816 (2003).

6. H. Yanagi, S. Park, A. D. Draeseke, D. A. Keszler, and J. Tate, "P-type Conductivity in Transparent Oxides and Sulfide Fluorides," J. Solid State Chem. 175, 34-38 (2003).

7. R. L. Hoffman, B. J. Norris, and J. F. Wager, "ZnO-Based Transparent Thin-Film Transistors," Appl. Phys. Lett. 82, 733-735 (2003).

8. J. F. Wager, "Transparent Electronics," Science 300, 1245-1246 (2003).

9. R. L. Hoffman and J. F. Wager, "Energy Band Alignment of Injector/Insulator Heterojunctions," Thin Solid Films 436, 286-291 (2003).

10. S. Park, D. A. Keszler, "Synthesis of 3-R CuMO2+□ (M = Ga, In, Sc)", J. Solid State Chem. 173, 355-358 (2003).

11. J. F. Wager, M. M. Valencia, J. P. Bender, B. J. Norris, H. Q. Chiang, D. Hong, L. N. Norris, T. V. Harman, S. Park, J. Anderson, C.-H. Park and D. A. Keszler, J. Tate, H. Yanagi, M. Price, and R. L. Hoffman, "Transparent Electronics and Prospects for Transparent Displays," Proceedings of SPIE (Vol. 5080 Cockpit Displays X), D. G. Hopper (ed), pgs. 330-339 (2003).

12. D. Hong, N. Dehuff, R. L. Hoffman, B. J. Norris, H. Q. Chiang, J. P. Bender, J. T. Anderson, J. F. Wager, D. A. Keszler, "Transparent Transistor Development," Materials Research Society Symposium Proceedings (2004), 796 (Critical Interfacial Issues in Thin-Film Optoelectronic and Energy Conversion Devices), 99-104 (2003).

4

13. B. J. Norris, J. Anderson, J. F. Wager, and D. A. Keszler, "Spin-Coated Zinc Oxide Transparent Transistors," J. Phys. D. 36, L105-L107 (2003).

14. C.-H. Park, D. A. Keszler, H. Yanagi, and J. Tate, "Gap modulation in MCu[$Q_{1-x}Q'_x$]F (M = Ba, Sr; Q, Q' = S, Se, Te) and related materials," *Thin Solid Films* 445, 288-293 (2003).

15. "Crystalline oxide-silicon heterostructures and oxide optoelectronics", edited by D. Ginley, S. Guha, S. Carter, S. A. Chambers, R. Droopad, H. Hosono, D. C. Paine, D. G. Schlom, and J. Tate, Materials Research Society Symposium Proceedings, Vol 747, Materials Research Society, PA (2003).

16. R. E. Presley, C. L. Munsee, C.-H. Park, D. Hong, J. F. Wager, and D. A. Keszler, "Transparent Tin Oxide Thin-Film Transistors," J. Phys. D. 37, 2810-2813 (2004).

17. R. Kykyneshi, B. C. Nielsen, J. Tate, J. Li, and A. W. Sleight, "Structural and transport properties of $CuSc_{1-x}Mg_xO_{2+y}$ delafossites," *Journal of Applied Physics* 96, 6188-6194 (2004).

18. H. Q. Chiang, R. L. Hoffman, J.-Y. Jeong, J. F. Wager, and D. A. Keszler, "High Mobility Transparent Thin-film Transistors with a Zinc Tin Oxide Channel Layer," Appl. Phys. Lett. 86, 013503-013505 (2005).

19. N. L. DeHuff, E. S. Kettenring, D. Hong, C.-H. Park, H. Q. Chiang, R. L. Hoffman, and J. F. Wager, and D. A. Keszler, "Transparent Thin-Film Transistor with a Zinc Indium Oxide Channel Layer," J. Appl. Phys. 97, 064505:1-5 (2005).

20. J. F. Wager, "ZnO Transparent Thin-Film Transistor Device Physics," NATO Science Series, II: Mathematics, Physics and Chemistry (2005), 194(Zinc Oxide), 217-224 (2005).

21. D. Hong, G, Yerubandi, H. Q. Chiang, M. Spiegelberg, and J. F. Wager, "Electrical Modeling of Thin-Film Transistors," Critical Reviews in Solid State and Materials Sciences, (2006).

22. D. Hong and J. F. Wager, and "Passivation of Zinc Tin Oxide Thin-Film Transistors," J. Vac. Sci. Technol. B, 23, L25-L27 (2005).

23. R. E. Presley, D. Hong, H. Q. Chiang, C. M. Hung, R. L. Hoffman, and J. F. Wager, "Transparent Ring Oscillator based on Indium Gallium Oxide Thin-Film Transistors," Solid-State Electron. 50, 500-503. (2006).

24. H. Q. Chiang, D. Hong, C. M. Hung, R. E. Presley, J. F. Wager, C.-H. Park, D. A. Keszler and G. S. Herman, "Thin-film Transistors with Amorphous Indium Gallium Oxide Channel," J. Vac. Sci. Technol. (submitted).

25. J. F. Wager, "Transparent Electronics: Schottky Barrier and Heterojunction Considerations," Thin Solid Films (submitted)

PATENTS:

1. R. L. Hoffman and J. F. Wager, "Transparent transistors," provisional patent application (2002).

2. R. L. Hoffman and J. F. Wager, "Transistor Device having a Delafossite Material," United States Patent 7,026,713, April 11, 2006.

3. J. T. Anderson, D. A. Keszler, B. J. Norris, "High Quality Spin-Coated ZnO," invention disclosure filed (2003).

4. H. Q. Chiang, J. F. Wager, and R. L. Hoffman, "Transparent Thin-Film Transistor with a Zinc Tin Oxide Channel Layer," invention disclosure filed (2003).

5. H. Q. Chiang, R. L. Hoffman, N. L. DeHuff, D. Hong, and J. F. Wager, and "Transparent Thin-Film Transistor with a Zinc Indium Oxide Channel Layer," invention disclosure filed (2003).

6. R. L. Hoffman, J. F. Wager D. Hong, and H. Q. Chiang, "Passivation of oxide semiconductor channel thin-film transistors," invention disclosure filed (2004).

STUDENTS:

1. Randy L. Hoffman, M. S., 2002   (MURI FUNDING = 75%)
   a. Citizenship: US
   b. Thesis title: "Development, Fabrication, and Characterization of Transparent Electronic Devices"
   c. Employment: Hewlett-Packard, Corvallis, OR
   d. Graduate Scholarship Assistant (OSU ECE award for selected incoming graduate students)
   e. Outstanding Graduate Research Assistant Award, OSU College of Engineering

2. Benjamin J. Norris, Ph. D., 2003 (MURI FUNDING = 75%)
   a. Citizenship: US
   b. Thesis Title: "Low-Cost Deposition Methods for Transparent Thin-Film Transistors"
   c. Employment: Intel, Hillsboro, OR

3. Hai Q. Chiang, M. S., 2003 (MURI FUNDING = 75%)
   a. Citizenship: US

b. Thesis Title: "Development of Novel Transparent Thin-Film Transistors"
c. Employment: Hewlett-Packard, Corvallis, OR (2003-2004)
d. Further study: Ph. D., School of EECS, Oregon State University, Corvallis, OR

4. Melinda Valencia, M. S., 2003 (MURI FUNDING = 25%)
   a. Citizenship: US
   b. Thesis Title: "p-Type Transparent Electronics"
   c. Employment: Hewlett-Packard, Corvallis, OR
   d. Graduate Scholarship Assistant (OSU ECE award for selected incoming graduate students)

5. Taran V. Harman, M. S., 2003 (MURI FUNDING = 25%)
   a. Citizenship: US
   b. Thesis Title: "Ferroelectric Thin Film Development"
   c. Employment: Wafertech, Camas, WA
   d. Graduate Scholarship Assistant (OSU ECE award for selected incoming graduate students)

6. Matthew Price, M.S., 2006 (MURI FUNDING = 25%)
   a. Citizenship: US
   b. Project Title: "Hall measurements of transparent conductors and a study of magnesium tin oxide"
   c. Further study: Ph. D. Science Education, Oregon State University, Corvallis, OR

7. Cheol-Hee Park, Ph.D. 2005 (MURI FUNDING = 25%)
   a. Citizenship: Korea
   b. Thesis title: "Synthesis and study of transparent p- and n-type semiconductors and luminescent materials"
   c. Employment: LG Chemical

8. Ganesh Yerubandi, M. S., 2005 (MURI FUNDING = 25%)
   a. Citizenship: India
   b. Thesis title: "Discrete Interface Trap Modeling of Thin-Film Transistors"
   c. Employment: Wafertech, Camas, WA

9. Jeremy Anderson, Ph. D., expected 2006 (MURI FUNDING = 25%)
   a. Citizenship: US
   b. Project title: Synthesis and study of dielectics and wide band-gap semicondutors for solution-processed devices

10. Nicci DeHuff, Ph. D., no longer pursuing degree (MURI FUNDING = 50%)
    a. Citizenship: US
    b. Employment: Boeing, Kent, WA

11. David Hong, M. S., 2005 (MURI FUNDING = 75%)
    a. Citizenship: US

b. Thesis title: "Process Development and Modeling of Thin-Film Transistors"
c. Graduate Scholarship Assistant (OSU ECE award for selected incoming graduate students)
d. Further study: Ph. D., School of EECS, Oregon State University, Corvallis, OR

12. Rick Presley, M. S., 2006 (MURI FUNDING = 75%)
   a. Citizenship: US
      Thesis title: "Transparent Electronics: Thin-Film Transistors and Integrated Circuits"

13. Craig Munsee, M. S., 2005 (MURI FUNDING = 50%)
   a. Citizenship: US
      Thesis title: "Characterization of Solution-Based Inorganic Semiconductor and Dielectric Materials for Inkjet Printing"
   b. Employment: Hewlett-Packard, Corvallis, OR

14. James Osborne, M. S. 2004 (MURI FUNDING = 25%)
   a. Citizenship: U.S.
   b. Project Title: "Zinc tin oxide thin films by pulsed laser deposition for use as transparent thin film transistors"
   c. Employment: Microsoft, Redmond, WA.

15. Robert Kykyneshi, M. S. 2004 (MURI FUNDING = 25%)
   a. Citizenship: Ukrainian
   b. Project Title: "Transport properties of $CuSc_{1-x}Mg_xO_{2+y}$ and $BaCu_2S_2$ transparent semiconductors"
   c. Further study: Ph. D. Materials Science, Oregon State University

16. Matt Spiegelberg, M. S., 2005 (MURI FUNDING = 75%)
   a. Citizenship: US
   b. Thesis Title: "Modeling and Development of Thin-Film Transistors"
   c. Graduate Scholarship Assistant (OSU ECE award for selected incoming graduate students)
   d. Employment: National Instruments, Austin, Texas

17. Emma Kittenring, M. S. expected 2006 (MURI FUNDING = 25%)
   a. Citizenship: U.S.

18. Celia Hung, M. S. expected 2006 (MURI FUNDING = 75%)
   a. Citizenship: U.S.

19. Hai Q. Chiang, Ph. D. expected 2007 (MURI FUNDING = 25%)
   a. Citizenship: U.S.

20. Robert Kykyneshi, Ph. D.. expected 2006 (MURI FUNDING = 25%)
   a. Citizenship: Ukrainian

b. Project Title: "BaCuQF-based films and devices"

21. David Hong, Ph. D., Expected 2008 (MURI FUNDING = 25%)
Citizenship: US

University of Pennsylvania

Department of Electrical and Systems Engineering
The Moore School of Electrical Engineering
200 South 33rd Street
Philadelphia, PA 19104-6390

CORTICONIC NETWORKS: ALGORITHMS, SIMULATIONS, AND HARDWARE IMPLEMENTATIONS

Prepared by:
Nabil H. Farhat
e-mail: farhat@ee.upenn.edu
Tel: 215-898-5882

Contributors:
Ramin Pashie
Ning N. Song
George (Jie) Yuan

1

1. INTRODUCTION

It is generally agreed that brain tissue is the most complex self-organizing matter known to us in the universe. In particular this applies to the cortex and all subcortical centers like the thalamus and the hippocampus with which the cortex interacts to carry out higher-level brain functions such as perception, cognition, memory, language, control of complex motion, speech and perhaps even awareness and consciousness The thalamus interacts with the cortex to form internal representations of sensory data. Fig. 1 gives a block diagram of the thalamo-cortical complex. Inasmuch as the hippocampus is the gateway to memory we view its interaction with cortex to be responsible for the formation of associative memory. Understanding and creating models of how the cortex carries out such higher-level functions has far reaching implications for science, technology and medicine with the most obvious being the design of future machines with brain-like intelligence. This has been the goal of our efforts in this MURI.

To create a system of equations that models the cortex in fine detail, that is to model the cortex/brain on the <u>microscopic</u> scale of neurons, synapse, dendrites, axons and the dynamics of linear and nonlinear membrane patches with their voltage and chemically activated ionic channels, is daunting even with the impressive computational resources available today or promised to be available in the future.

For this reason we developed a macroscopic approach to modeling the cortex that is based on combining the tools of nonlinear dynamics and information theory with known salient organizational and anatomical features of the cortex and the way it interacts with the thalamus. This approach produced the following *cortical equations* which describe a parametrically coupled logistic-map network (PCLMN):

$$X_i(n+1) = \mu_i(n)X_i(n)(1 - X_i(n)) \qquad i = 1,2....N \tag{1}$$

$$\mu_i(n) = 4\left(X_i^s\right)^{C_i^s} e^{-\alpha n} + \left(1 - e^{-\alpha n}\right)\frac{1}{N_i}\sum_{j\varepsilon|N_i|} 4\left(X_j(n)\right)^{C_{ij}} \tag{2}$$

$$C_{ij}(m+1) = C_{ij}(m)(1 + \Delta C_{ij}(m)) \tag{3}$$

$$\Delta C_{ij}(m) = \delta \tanh \beta I_{ij} \tag{4}$$

$$I_{ij} = H_i + H_j - 2H_{ij} \tag{5}$$

where all quantities are defined in earlier papers and documents [1]-[4] which contain a progression of ideas that led to these equations and the way they are used to form a

PCLMN incorporating salient and plausible features of cortical organization and anatomy some of which are not found in current neural net and connectionist models.

Reference [1] and [2] describe how the elements of the coupling factors matrix of a PCLMN can be set in order that the network forms stimulus-specific attractors. Only dynamic stimulus-specific attractors could be found with the method described. By dynamic is meant that a convergent state-vector of the network consists of a mix of fixed-point, periodic (period-m) and/or chaotic orbits only for which the convergent values of the control parameter vector $\overline{\mu}(n)$ fall in all regions of the bifurcation diagram of the logistic map.

This was followed by the development of an MI driven adaptation process (see [3] and [4]) that utilizes chaos to enable a PCLMN to self-organize its coupling factors matrix such that the adapted or self-organized network exhibits stimulus-specific fixed-point attractors only, in addition to a host of other remarkable novel properties summarized below.

It is also expected that by modifying eq. (4) for adaptation, attractors of any single class or a mix of classes selected from fixed-point, period-m, or chaotic can be achieved. The modification would be

$$\Delta C_{ij}(m) = \delta \tanh \beta \left| I_{ij} - \gamma \right| \tag{6}$$

where the choice of the real constant γ enables the components of $\overline{\mu}(n)$ to converge to values distributed in any desired part of the μ_i axis in the well known bifurcation diagram of the logistic map.

2. SIGNIFICANT PROPERTIES OF THE PCLMN

The PCLMN has several unique properties described in [3] and [4] and also to a lesser level in [1] and [2]. The most intriguing of these is the immense number of stimulus-specific attractor an adapted (self-organized) PCLMN has. The number is astronomical being $N_a = L^N$ where N is the size of the network and L is the number of levels over which the state variable $X_i(n), i = 1,2...N$ of the i-th element in the network is measured or discerned. We have strong evidence supporting the validity of this property. One comes from convergence considerations of the adapted PCLMN [5] that resemble the convergence of a class of neural network known as the Andersen Brain-State-In-a-Box network [6]-[9] and from extensive numerical simulations in which the adapted PCLMN was probed by 100 distinct input patterns, followed by examining the histogram of the Euclidean distances between the convergent states (attractors).

Examples of the ability of the PCLMN to classify (stimulus input) patterns with stimulus-specific attractors are shown in Figs. (2-4). The stimulus patterns used in these numerical simulation examples are four sound spectrograms (see Fig. 2). Time evolution

3

of the network for various inputs showing initial bursts into "chaotic" activity followed by gradual MI (mutual information) driven annealing are shown in Figs. 2 and 3.

There are other significant properties of the PCLMN. We mention here (a) ability to accept both dynamic or static input (stimulus) patterns and represent them by fixed-point attractors, (b) guaranteed convergence to an attractor via information driven annealing and self-organization occurring within a finite number of iterations (time steps) in numerical simulations and, (c) nearest-neighbor connections architecture which facilitates mixed (-digital analog) VLSI and photonic implementations of PCLMNs.

3. LABELING OF ATTRACTORS

The benefits of the availability of an enormous number of coexisting stimulus-specific attractors that can be used to represent inputs to the network cannot be enjoyed without a way to identify or associate the attractors with the inputs that spawned them. To this end we found that a combination of a PCLMN with one of the standard associative memory networks produces what we call a *cortical-module* with unique properties. A cortical-module consisting of a heteroassociative network with a capacity of C associations would be able to label C attractors of the PCLMN and therefore the C input patterns that spawned them. An array of N_h such heteroassociative memories (each of which modeling a patch of the association cortex) can label or identify $N_h C$ inputs. Another unique potential property of the cortical-module however is its ability to produce a sequence of associations or labels triggered by the application of an input to the PCLMN. This remarkable property can be achieved by feeding back the output label of the associative network as new input to the PCLMN after the original input has vanished. (Recall that the effective input to the PCLMN decays exponentially in time see eq. 2 and references [1]-[4]). The sequence of associations realized in this manner is chosen by proper pairing of PCLMN attractors with specified output labels of the associative net. This capability means that for the first time we have available a way for producing prescribed trajectories in the state-space of a network. This is significant because it explains how trains of thought might occur in the brain/cortex and opens the way for realizing complex motor control and motor function which is important for speech synthesis, locomotion, and phase-array antenna control to mention a few applications.

4. HARDWARE IMPLEMENTATIONS OF THE PCLMN

Hardware implementations of PCLMNs is required for many applications where speed and low power consumption are important. To this end we have developed a method for analog synthesis of arbitrary one-dimensional maps including the logistic map and the sine-circle map which is described in [10]. This development was important because it opened the way for building PCLMNs in analog or mixed digital/analog hardware including optoelectronic enabling technologies such as fast spatial light modulators and sensor arrays,. In this section we briefly summarize our work on the

implementation of a mixed-signal silicon Cort-X chip and a photonic Cort-X whose design and implementation were informed by the Silicon Cort-X.

The Silicon Cort-X:

Two silicon Cort-X chips were designed and fabricated through MOSIS. Die photos of the two chips are shown in Fig. 6. The Cort-X I, was designed and fabricated in a $0.6\,\mu m$ 5V CMOS process. Cort-X I was designed to evaluate the processing element design. It included 8 processing elements. An individual processing element of the network consists of an IRON and a nonlinear local connection module. A self-calibration technique was developed to overcome the process variation of the nonlinear analog circuits. Each designed element covered a die area of 0.55 mm^2, and consumed $240\,mW$ power. Good nonlinear coupling was demonstated. However high power consumption and an error in the IRON layout prevented complete characterization of this chip and prompted the design of Cort-X II.

The Cort-X II chip was designed for large-volume integration. Open-loop circuits and new structures were used to reduce power consumption. A self-calibration technique was developed to compensate for the fabrication process variation, which is an important issue for open-loop circuits. A Cort-X II chip was fabricated in a 0.25 μm 2.5V CMOS process. It included 16 processing elements. Each element consumes $12\,mW$ power, which is 20 times less than in Cort-X I. Testing results showed that the nonlinear connection module implements acceptable nonlinear transfer function with fast settling. Noticeable phase noise was however evident in the bifurcation diagrams of the fabricated IRONs in this chip (see Fig. 8). A major part of the noise was traced to the testing environment and inadequate shielding in the multilayer (6 layered) testing board. A low-power testing board with better shielding between its layers is being considered to suppress the noise and is expected to suppress environmental noise to a level that will make it possible to address any other sources of noise that might be present on the chip level. This will eliminate the noise evident in the bifurcation diagram of the chip operating in a logistic map mode or the sine-circle map mode (see Fig. 8). It is seen that with noise suppression the bifurcation diagrams will get closer to both the H-spice simulations and to the theoretical plots shown in Fig. 8.

Both chips were designed to operate at 1 MHz, that is 10^6 iterations per second which amounts to 1μsec iteration time. To this one needs to add the time needed to compute the mutual information matrix by the computer/controller from the state vector history $\overline{X}(n)$ stored over about 100 iterations in order to anneal the network by adapting the coupling matrix to reach convergence to a stimulus-specific fixed point attractor. Both chips provide good nonlinear coupling as shown in Fig. 7.

Photonic Cort-X

A conceptual diagram of an exploratory photonic Cort-X arrangement is shown in Fig. 9. This arrangement was hurriedly put together for proof of concept and a demo at

the forthcoming MURI Wrap Up Meeting. The digital micromirror device (DMD) is a MEMs (microelectromechanical system) typically consisting of 1024 x 768 micromirrors rapidly and individually switched by means of an external electronic digital control board. As a mirror is switched it throws light from a beam illuminating the device either into or out of the pupil of an imaging lens to create a short-duration controlled burst of light pulses that give precise digital control of the irradiance pattern on a screen or exposure pattern of a photographic plate or a CCD (charge coupled device) sensor array. The optical switching time, the rise-time as the light enters the pupil of the lens, is $\sim 2\mu\sec$. The mechanical switching time, including the time for the mirror to electromechanically latch in the switched position is $20\mu\sec$. This rapid mirror switching enables projecting $9.7 \ 10^3$ digitally loaded binary patterns per second. A newer version of the DMD has a binary frame rate of $16.3 \ 10^3$ full binary frames per second. This amounts to a data stream of 12.8 Gbit/sec offering unique capabilities in spatial light modulation. Light patterns giving $\mu_i(n)$ produced by the DMD can be multiplied by a logistic map mask with logistic reflectance function $4X_i(1 - X_i)$ $X_i\varepsilon[0,1]$ to form $X_i(n+1) = 4\mu_i(n) \ X_i(1 - X_i)$ i=1,2,...N with the product measured (or imaged) by a CCD or line scan camera: An illustration of this process is given in Fig. 10.

An example of the promise of the photonic Cort-X is shown in Fig. 11 where the arrangement in Fig. 9 was used to produce the bifurcation diagram of the logistic map which is seen to compare very well with the computed bifurcation diagram.

Work on the photonic Cort-X is continuing as we write and we hope to demonstrate its operation at our forthcoming wrap-up meeting together with the Silicon Cort-X.

5. Publications: Specific or Relevant to Program

1. G. Lee and N. Farhat, "The Bifurcation Network I", Neural Networks, vol. 14, pp. 115-131, (2001).

2. N. Farhat, "Dynamic Brain State-In-A-Box", Optical Memory and Neural Networks, vol. 10, pp. 203-209, (2001).

3. G. Lee and N. Farhat, "The Bifurcating Neuron Network 2: An Analog Associative Memory", Neural Networks, vol. 15, pp. 69-84, (2002).

4. G. Lee and N. Farhat, "Parametrically Coupled Sine Map Networks", International Journal of Bifurcation and Chaos, vol. 11, pp. 1815-1834, (2001).

5. G. Lee and N. Farhat, "The Double Queue Method: A Numerical Method for Integrate-and-Fire Neuron Networks", Neural Networks, vol. 14, pp. 921-932, (2001).

6. Emilio Del Moral Hernandez, Geehyuk Lee and Nabil H. Farhat, "Analog Realization of Arbitrary One-Dimensional Maps", IEEE Transactions on Circuits and Systems I, vol. 50, pp. 1538-1547, Dec. 2003.

7. N. Farhat, "Corticonic Networks for Higher-Level Processing", IAESTED NCT'04, Feb. 23, 2004, Gridelwald, Switzerland, (Invited). Published in Conf. Proc. by ACTA Press, ISBN: 0-88986-389-1, Feb. 2004.

8. J. Yuan, N. Farhat and J. Van der Spiegel, "GBOPCAD: A Synthesis Tool for High-Performance Gain-Boosted OPAMP Design", IEEE Transactions on Circuits and Systems I, vol. 52, pp. 1535-1544, Aug. 2005.

9. J. Yuan, N. Farhat and J. Van der Spiegel, "A 50 MS/s 12-bit CMOS Pipeline A/D Converter with Nonlinear Background Calibration", 2005 IEEE Custom Integrated Circuits Conference, San Jose, CA, Sept. 18-22, 2005.

10. J. Yuan, N. Farhat and J. Van der Spiegel, "Cort-X: A Biologically-Inspired Corticonic System – Theory and CMOS Implementation", IEEE Trans. on Circuits and Systems I: regular paper, submitted.

11. J. Yuan, N. Farhat and J. Van der Spiegel, "A Continuous-Time Nonlinear Interconnection Module for a CMOS Corticonic System: Cort-X", IEEE Trans. on Circuits and Systems I: regular paper, submitted.

12. J. Yuan, N. Farhat and J. Van der Spiegel, "Background Calibration of Nonlinear Errors for a 50 MS/s 12-bit CMOS Pipeline A/D Converter", IEEE Journal of Solid-State circuits, submitted.

Invited Presentations:

1. N. Farhat, "Dynamic Pattern Recognition", ONR Surface and Aerospace Surveillance Technology Gathering, Naval Research Laboratory, Washington, D.C., April 17, 2002.

2. N. Farhat, "Corticonics: A Mesoscopic Dynamical Approach to Modeling the Cortex", Georgia Institute of Technology, Atlanta, GA, Sept. 20, 2001.

3. N. Farhat, "Nonlinear Dynamical Modeling of Higher Level Brain Function", University of Pennsylvania, Office of the Provost for Research, Visit of Staff Members of the Senate and Armed Services Committee, Jan. 7, 2002. (Five Presentations pre-selected by Senate Staffers made by A.G. MacDiarmid, D. Luzzi, K. Winey, J. Vohs and N. Farhat).

4. N. Farhat, "Corticonics and the Modeling of Intelligence", University of Florida, Gainesville, Fla., Feb. 28, 2002.

5. N. Farhat, "Corticonics: A Mesocopic Dynamical Brain Theory", Neurosurgery Grand Rounds Lecture, HUP, June 20, 2002.

6. N. Farhat, "Dynamic Brain State….", SPIE Annual Meeting, Seattle, July, 2002 (Invited).

7. N. Farhat, "Modeling the Cortex", Army Research Laboratory, Adelphi, Maryland, Sept. 10, 2002.

8. N. Farhat, "Parametrically-Coupled Map Networks as Macroscopic Models of Cortical Function", Vision Seminar, Dept. of Psychology, University of Pennsylvania, Feb. 9, 2004.

9. N. Farhat, "Corticonics: Towards Designing Machines with Brain-Like Intelligence", Wright-Patterson AFB, Dayton, Ohio, July, 2005.

10. R. Pashaie and N. Farhat, "Equilibrium-State Emission of Electron Trapping Thin-Film Material for Applications in Nonlinear Dynamics", Presented at the 32nd Northeast Bioengineering Conference, April 2006, Easton, PA.

Conference papers in preparation or submitted:

"A CMOS Monolithic Implementation of a Nonlinear Interconnection Module for a Corticonic Network", J. Yuan, N. Farhat and J. Van der Spiegel, 2006 International Symposium on Circuits and Systems, Kos Island, May 23-26, 2006.

"A CMOS Monolithic Implementation of a Nonlinear Element for Arbitrary Bifurcation Map Generation", J. Yuan, N. Farhat and J. Van der Spiegel, 2006 International Symposium on Circuits and Systems, Kos Island, May 23-26, 2006.

Patents:

- Dynamical Brain Model for use in Data Processing Applications, US 2004/0073415 A1, April 15, 2004 (publication).

- Cort-X Dynamic Brain Model, UPenn Reference, UOP-4-4US, May 2005 (application).

6. Corticonics Research Group
N. Farhat (PI)

Ph.D. Students supported in part by MURI*	Topic	Graduation Date
1. Ramin Pashaie	Photonic Cort-X	Fall 2007

2. Ning Song	Cort-X Machine (Silicon) Cort-X + Massive Associative Memory) for perceptual categorization and cognitive applications	Summer 2007
3. George Yuan	Silicon Cort-X	August 2006
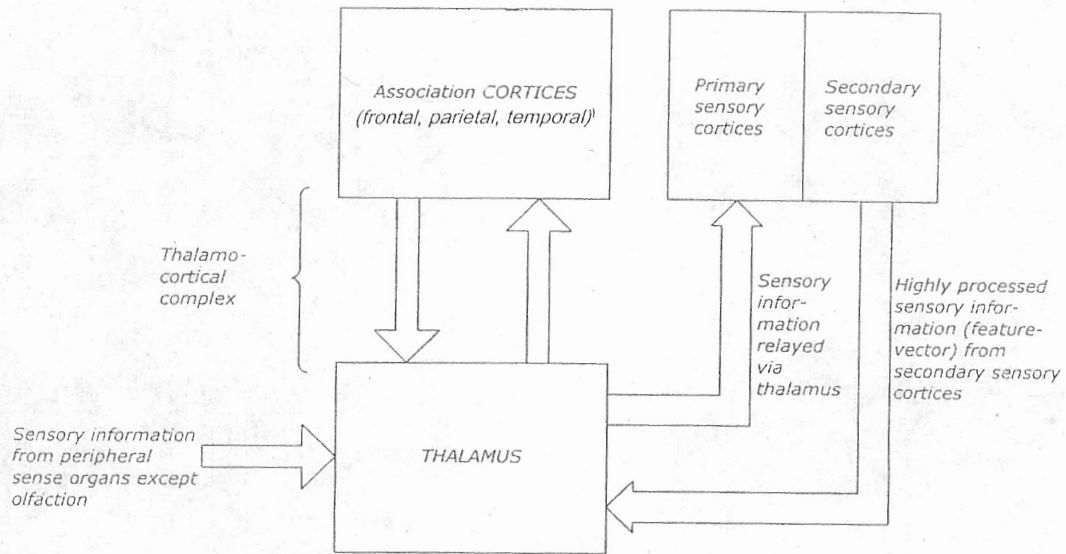
Fig. 1. Organization of cortico-thalamo-cortical projections
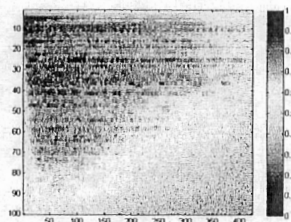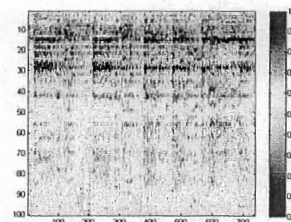
(a)   (b)
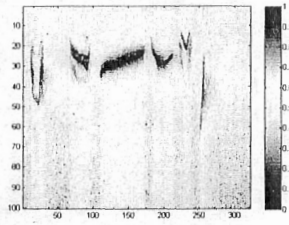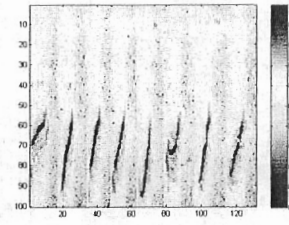
(c)   (d)

Figure 2 . Sound Spectrograms, Frequency v.s. time (in arbitrary units) with color coded normalized intensity. (a) gong, (b) Handel music, (c) and (d) bird songs.
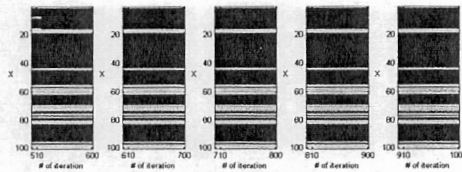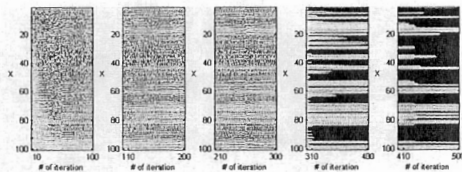
Bird song
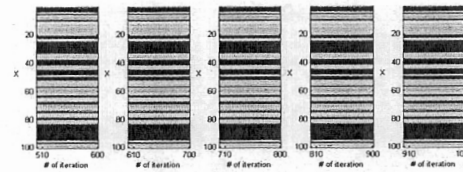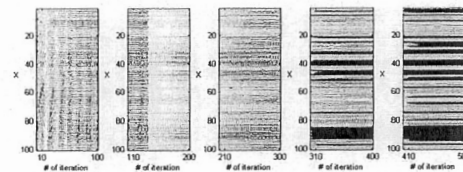
Gong
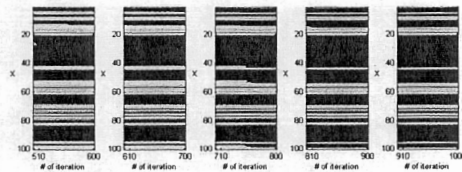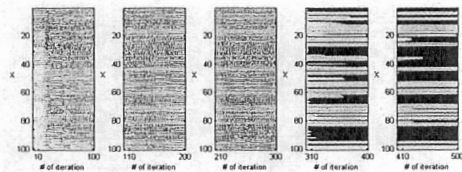
Bird song
Figure 3: Convergence of sound spectrograms spectrograms of two distinct songs
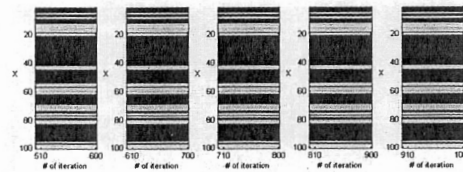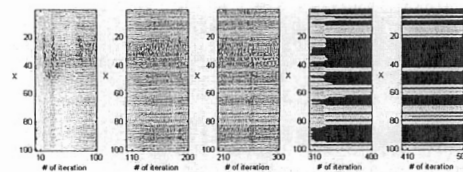
Handel music
Figure 4: Convergence of sound of gong and music
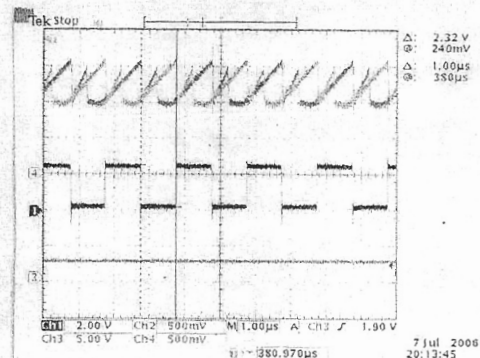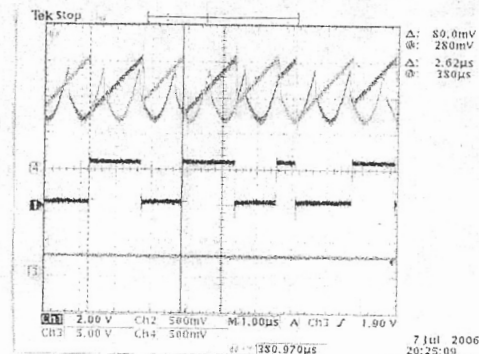
(a)   (b)

Fig. 5.   Dynamics of the bifurcation processing element of the silicon Cort-X chip implemented with an Integrated Circuit Relaxation Oscillator Neuron (IRON) under different periodic resting potentials. The IRON is designed with two charging branches to reduce the power consumption and remove the refractory period. The refractory period evolved in biology to give the neurons an opportunity to recover after each firing of an action potential to limit the maximum firing frequency of a biological neuron and to conserve energy. This of course is not a constraint in electronic implementations where firing frequency can be in the MHz range as compared to few hundred Hz in the biological neuron. The top traces show the membrane potential of the IRON building up at a constant rate from the quadratic resting potential waveform needed for realizing a logistic map, until it reaches the threshold voltage when a spike is fired. The bottom trace gives the phase of the periodic signal at the instants of firing. The normalized modulu 2π phase values of the periodic quadratic waveform at the up and down transitions of the bottom trace give the values of the state variable X of the IRON. In (a) the resting potential of the IRON is modulated by a periodic (quadratic) signal of low amplitude giving rise to a two valued phase sequence (period-2 attractor). In (b) the amplitude of the periodic resting potential is increased to show a chaotic sequence of phase values.
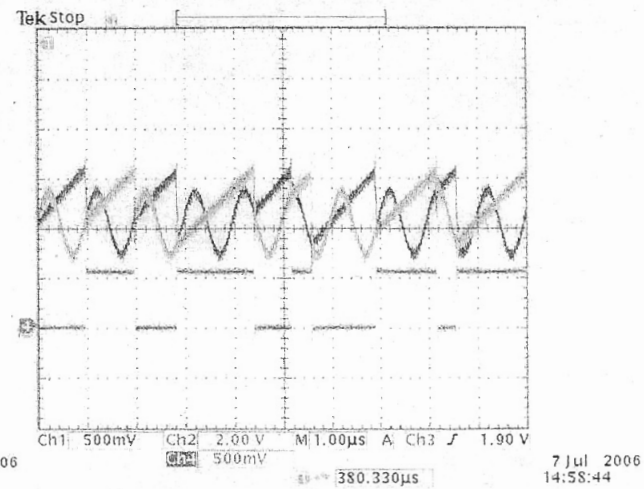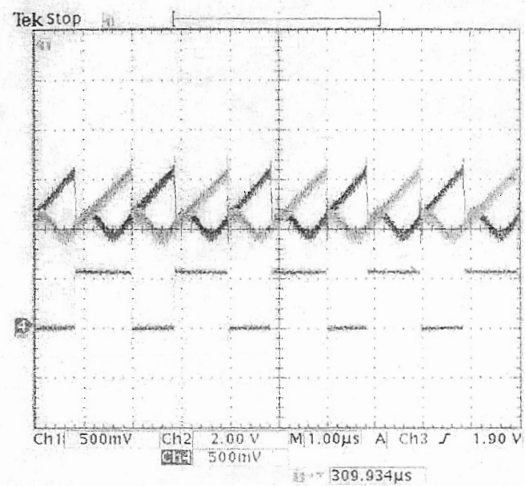
Fig. 5. (cont'd) Same as in Figure 5 but for cosinusoidal resting potential that gives rise to phase sequence of a sine-circle map. Bottom traces are phase sequences corresponding to period-2 attractor (left), and to chaotic attractor (right).
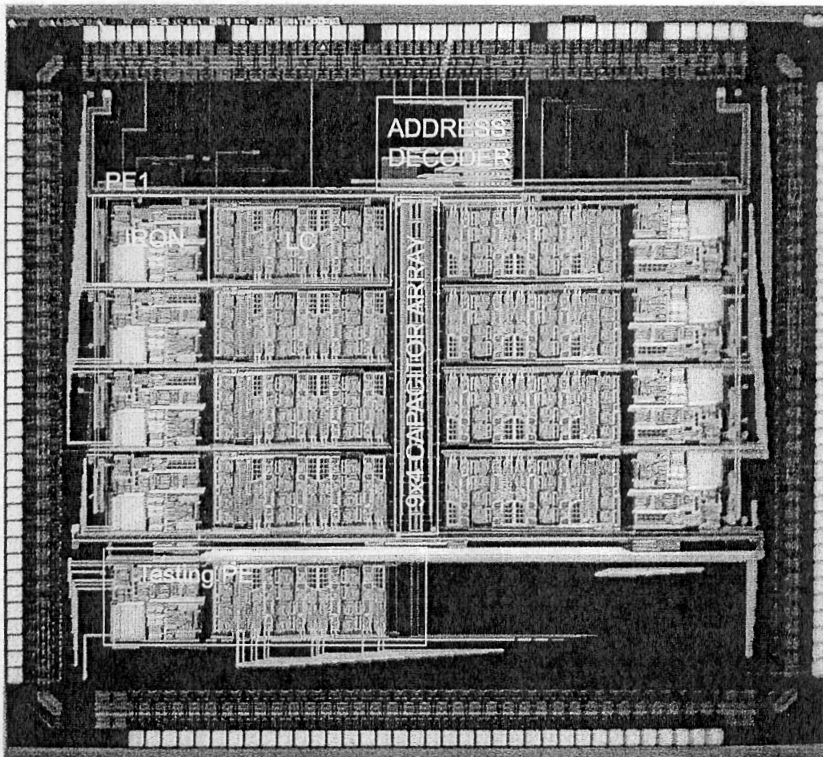
1. 0.6um, 5V CMOS
2. 8 PEs, 1 testing PE
3. PE=LC1+IRON1
4. 0.55mm^2/PE, 240mW/PE
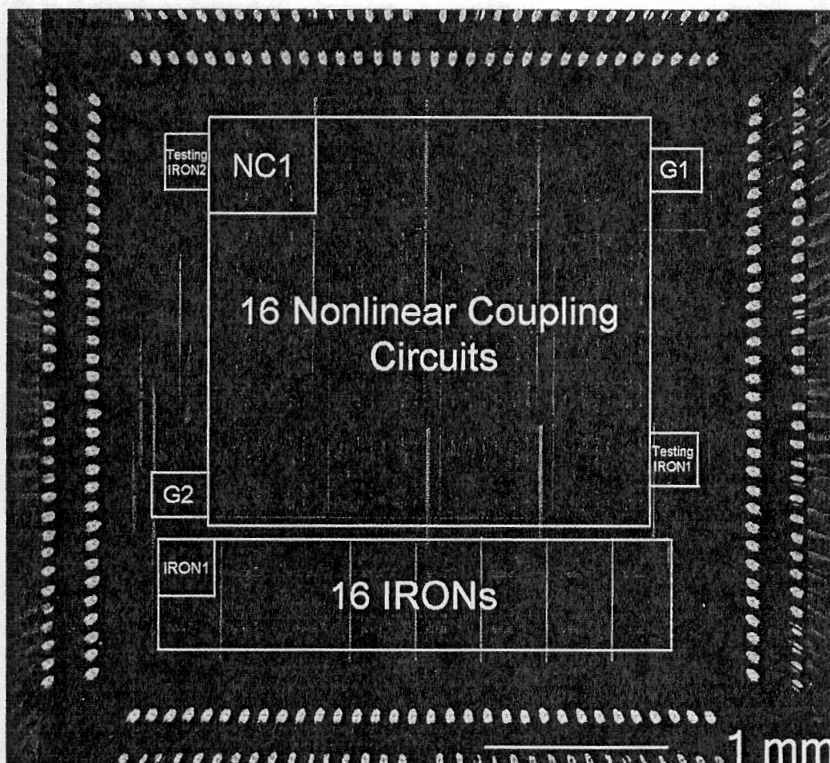
1. 0.25um, 2.5V CMOS
2. 16 PEs
3. PE=LC2+IRON2
4. 0.22mm^2/PE, 12mW/PE

Fig. 6 :Die Photos of Cort-X I (top), Cort-X II (bottom)

14

CHARACTERISTICS OF SILICON CORT-X
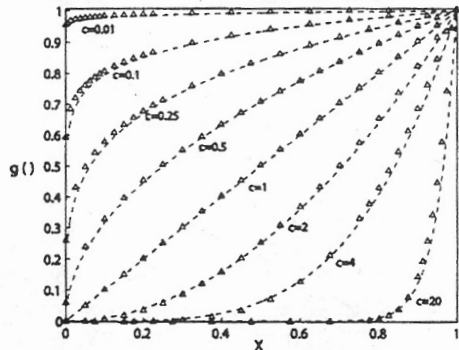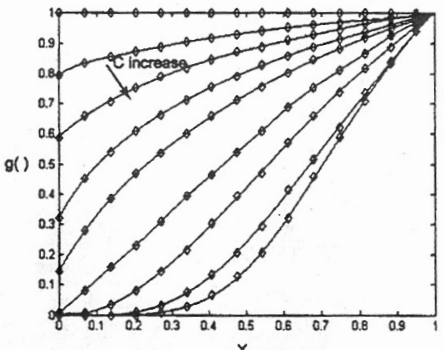
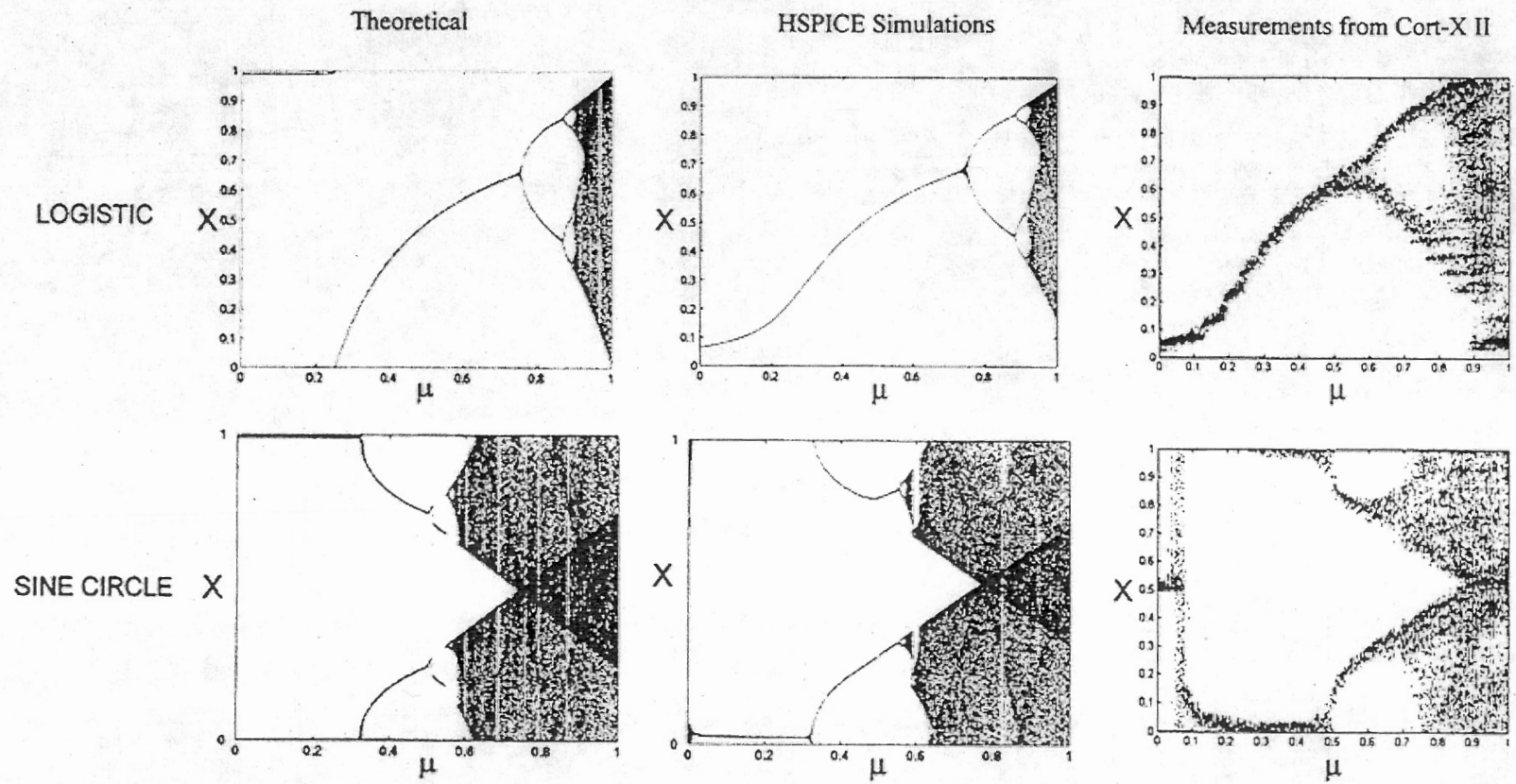|	Cort-X I	Cort-X II
Fabrication technology	0.6 μ m 5V CMOS process	0.25 μ m 2.5 V CMOS process
Number of elements	8	16
Iteration speed	1 MHz	1 MHz
Size	0.55 mm^2	0.22 mm^2
Power consumption/element	240mW	12mW
Nonlinear function		
IRON shortcomings	Power consumption, reliability	Noise (solvable)

Figure 7

Fig 8: Bifurcation diagram of the logistic (top) and the sine-circle maps (bottom).
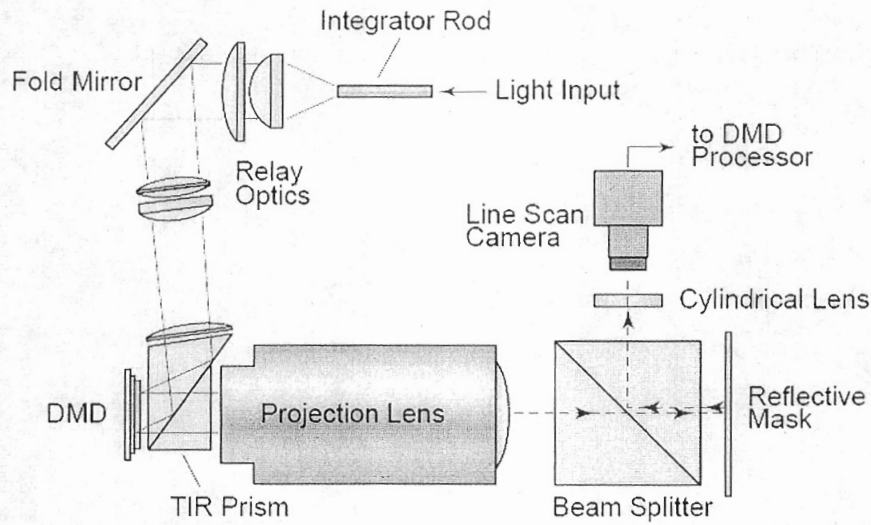Theoretical (left), Spice simulation (middle), measurements (right)

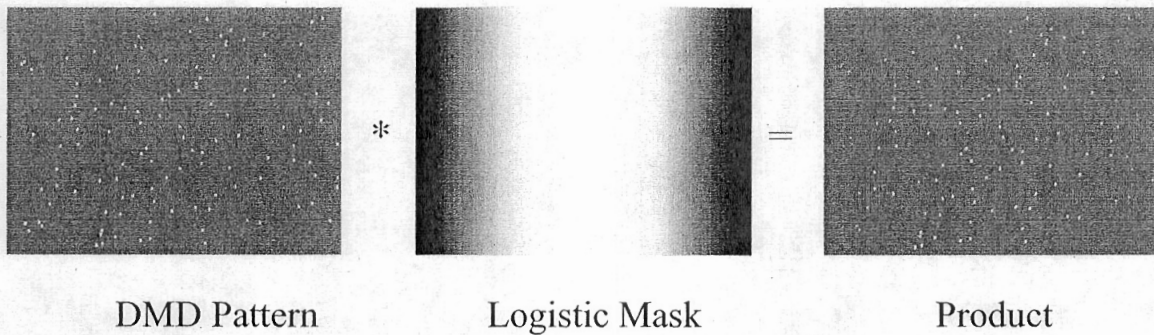Fig. 9. Preliminary prototype of the photonic cortex

DMD Pattern   Logistic Mask   Product

Fig. 10. The DMD and a mask with logistic reflectance function $4x_i(n)(1-x_i(n))$, $x_i \in [0,1]$ can be used to form the product operation in the logistic maps $4\mu_i(n) \, x_i(n) \, (1-x_i(n)) = x_i(n+1)$, $i = 1,2,\ldots,N$. The value of $\mu_i \in [0,1]$ is formed by the DMD and the product is measured by a CCD camera and fed back to the DMD and the process is repeated to iterated a network of N logistic maps.
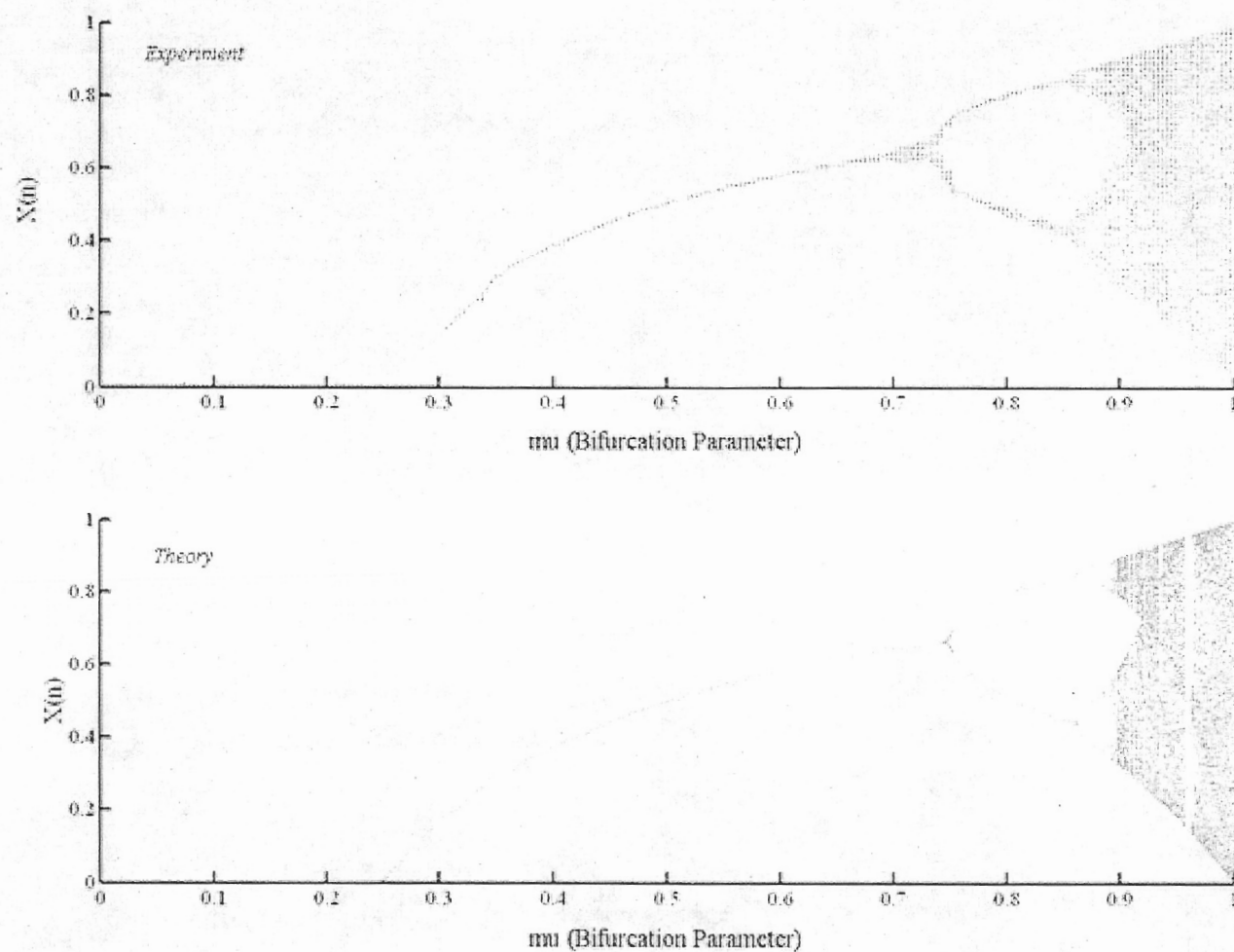
17

Fig. 11. Bifurcation diagram of a single logistic map produced by the photonic cort-x (top). Computed diagram is given for comparison (bottom).

7. REFERENCES

1. N. Farhat, G.H. Lee, and X. Ling, "Dynamical Networks for ATR", in NATO/RTO Meeting Proceedings 6, Non-Cooperative Air Target Identification Using Radar, Published by NATO/RTO, BP25, 7 Rue Ancelle, F-92001, Neuilly-Sur-Seine, CEDEX, FRANCE, Nov. 1998, pp. D-1 to D-10.

2. N. Farhat, "Corticonic Systems for Higher-Level Processing and Radar Target Identification", in NATO/RTO Meeting Proceedings 40, High-Resolution Radar Techniques, Published by NATO/RTO, BP25, 7 Rue Ancelle, F-92001, Neuilly-Sur-Seine, CEDEX, FRANCE, November 1999, pp. 71-1 to 71-9.

3. N. Farhat, "Corticonics: The Way to Designing Machines with Brain-Like Intelligence", in Critical Technologies For the Future of Computing, S. Bains and L.J. Irakliotis (Eds.), Proc. Of SPIE, Vol. 4109, SPIE, Bellingham, WA, 2000, pp. 103-109.

4. N. Farhat, "Corticonic Systems and Algorithms For Dynamical Pattern Recognition", White Paper/Proposal Submitted to US Army Research Office, March 2000.

5. N. Farhat, "Dynamic Brain-State-in-a-Box", Optical Memory and Neural Networks, vol. 10, no. 4, pp. 203-209 (2001). (Issue published in 2002.)

6. J. Anderson, et. al., "The BSB; A Simple Nonlinear Autoassociative Neural Network", in Associative Neural Memory, M. Hassoun, (Ed.), pp. 77-103, Oxford Univ. Press, 1993, Oxford.

7. H.G. Greenberg, "Equilibria of the Brain State in a Box", Neural Networks, vol. 1, pp. 323-324, 1988.

8. A. Kawamoto and J. Anderson, "A Neural Network Model of Multistable Perceptron", Acta Psychologica, vol. 59, pp. 35-65.

9. S. Haykin, Neural Networks – A Comprehensive Foundation, MacMillan, New York (1994), pp. 571-577.

10. E. Del Moral Hernandez, Geehyuk Lee and Nabil Farhat, "Analog Realization of Arbitrary One-Dimensional Maps", IEEE Trans. On Circuits and Systems I, vol. 50, pp. 1538-1547, Dec. 2003.